Spectral Fingerprinting and Chemical Mapping of Plant-Based Meat Analogues using Portable Hyperspectral Imaging System and Multivariate Analysis

by

Logesh Dhanapal

A Thesis submitted to the Faculty of Graduate Studies of
the University of Manitoba
in the partial fulfillment of the requirements of the degree of

MASTER OF SCIENCE

Department of Biosystems Engineering

University of Manitoba

Winnipeg, Canada

THESIS ABSTRACT

The ultra-processed nature and multiple ingredients of plant-based meat analogues cause excessive-quality variation during storage suggesting the need for real-time quality monitoring and chemical mapping techniques. This research utilizes a non-destructive portable hyperspectral imaging technique in the visible and near-infrared ranges (400–1000 nm) to predict the quality (CIE- *L**, *a**, *b**, moisture, texture) of plant-based meat burger patties followed by mapping of the quality distribution attributed to major ingredients and color variations over the storage period.

Firstly, the study analyzed the effect of 10-30% textured vegetable protein (TVP), 5-25% pea protein (PP), and storage time (14 days) on quality using conventional quality assessment approaches, revealing the instability of overall quality even over a short storage period. Principal Components Analysis (PCA) applied to HSI data indicated that the primary variance stems from discoloration and moisture loss due to storage days, TVP, and PP. This variance is associated with the spectral variations at 500–650nm and 950–980 nm. Developed Partial Least Square Regression (PLSR) models possessed good prediction accuracies for *a**, *b**, moisture, and hardness. Pixel-by-pixel prediction maps highlighted the non-uniform component distribution.

Secondly, the study examines the role of HSI in addressing the color instability of PBMB by visualizing color evolution during a 10-day storage period, influenced by TVP, PP, fava bean protein, and fat mimic. Simplified PLSR prediction models with improved accuracies were developed with interval-PLS (iPLS), recursive-PLS (rPLS), and genetic algorithm (GAs). Prediction maps showed the patterns of color deterioration. Findings highlighted that color evaluation of heterogenous plant-based food formulations using single-point colorimeters is insufficient to represent the whole sample.

This research illustrated that spectral fingerprinting could visualize component distribution in complex food formulations, aiding in formulation optimization and understanding ingredient interactions. The findings are crucial for informed decisions on grading, labeling, and storage. Overall, VNIR-HSI in combination with multivariate analysis proves to be a valuable analytical tool for real-time quality inspection in plant-based food production, highlighting the potential of digital technologies in promoting sustainable foods.

Keywords: *Meat alternatives, Food quality, Non-destructive food testing, Smart sensing, Hyperspectral imaging, Chemometrics, Plant proteins*

ACKNOWLEDGEMENTS

First and foremost, I would like to express my deep sense of gratitude to my beloved guide Dr. Chyngyz Erkinbaev, for accepting me as his student and providing exemplary guidance and encouragement throughout my M.Sc. program. I would like to express my humble thanks to Dr. Maneka Malalgoda and Dr. Nandika Bandara for their valuable suggestions and for serving on my thesis committee. I take this opportunity to thank Dr. Jitendra Paliwal for providing motivation and encouragement. I extend my deepest gratitude to Dr. Jeyan Arthur Moses for his trust and guidance through this academic journey. My heartfelt thanks to my parents and family members for making my studies abroad possible. Special thanks to Abhinav Tiwari, Kavi Mughil, and Dasinija Karikalan for their never-ending support. Acknowledgements are extended to Dr. Chyngyz Erkinbaev and the University of Manitoba Graduate Studies Faculty (UMGF) for their financial support. Sincere thanks to my colleagues Maheshi, Angshuman, and Inka. I express my gratitude to my friends Chitra, Tulasi, David, Anashwar, Anukiruthika, Bhagya, Harshini, Vijay, and Subi.

RESULTS DISSEMINATION

Publications

The major original contribution from the experimental work carried out in the frame of this thesis is published as 2 research papers.

1. **Dhanapal, L**., & Erkinbaev, C. **(2024)**. Portable hyperspectral imaging coupled with multivariate analysis for real-time prediction of plant-based meat analogues quality. Journal of Food Composition and Analysis, 126, 105840. https://doi.org/10.1016/j.jfca.2023.105840.

2. **Dhanapal, L.**, & Erkinbaev, C. **(2024)**. Non-invasive characterization of color variation in plant-based meat burgers using portable hyperspectral imaging device and multivariate image analysis. Future Foods, 9, 100293. https://doi.org/10.1016/j.fufo.2023.100293

Conference presentations

The conference presentations during the initial and later stages of the experimental works are outlined below.

1. **Logesh Dhanapal*** and Chyngyz Erkinbaev **(2023)**, Portable Hyperspectral Imaging for Non-invasive and Real- time Prediction of Plant-based Meat Quality, EFFoST International Conference, Valencia, Spain, 6-8 Nov.

2. **Logesh Dhanapal*** and Chyngyz Erkinbaev **(2023)**, Real-time Prediction of Quality of Plant-based Meat Analogues Using Portable Hyperspectral Imaging System and Multivariate Analysis, Canadian Society for Bioengineering (CSBE) Conference, Lethbridge, Alberta, 23-26 July.

3. **Logesh Dhanapal*** and Chyngyz Erkinbaev **(2023)**, Non-Destructive Testing and Chemical Mapping of Plant- Based Meat Quality Using Portable Hyperspectral Imaging, CIFST National Conference, London, Ontario, 8 June.

TABLE OF CONTENT

THESIS ABSTRACT **2**
ACKNOWLEDGEMENTS **3**
RESULTS DISSEMINATION **4**
TABLE OF CONTENT **5**
LIST OF FIGURES **9**
LIST OF TABLES **11**

CHAPTER 1 ..... **12**

INTRODUCTION **12**
1.1 Research background 12
1.2 Thesis objectives 15
1.3 Thesis organization 16
1.4 References 17

CHAPTER 2 ..... **20**

THEORETICAL BACKGROUND OF HYPERSPECTRAL IMAGING AND MULTIVARIATE ANALYSIS **20**
2.1 Electromagnetic spectrum and VNIR spectroscopy 20
2.2 Relation between digital image, spectroscopy, and hyperspectral Imaging 21
2.3 Structure and components of hyperspectral imaging 22
2.4 Chemometrics 24
2.5 Image pre-processing 24
2.5.1 Image calibration 24
2.5.2 Image Segmentation 25
2.6 Data extraction and treatment 25
2.7 Multivariate modelling 25
2.7.1 Data Exploration: Principal component analysis 25
2.7.1.1 Process of decomposing the original data into scores and loadings 26
2.7.1.2 Interpreting PCA 26
2.7.2 Prediction: Partial least square regression modelling 27

2.8 Multivariate image analysis 28
2.8.1 Exploration of Images: PCA 28
2.8.2 Pixel-by-pixel Prediction 29
2.9 References 30

CHAPTER 3 32

PORTABLE HYPERSPECTRAL IMAGING COUPLED WITH MULTIVARIATE ANALYSIS FOR REAL-TIME PREDICTION OF PLANT-BASED MEAT ANALOGUES QUALITY 32
3.1 Abstract 32
3.2 Introduction 32
3.3 Materials and Methods 35
3.3.1 Sample preparation 35
3.3.2 Quality attributes determination 36
3.3.3 Hyperspectral imaging acquisition 36
3.3.4 Multivariate analysis 37
3.3.4.1 Principal component analysis 37
3.3.4.2 Partial least square regression modeling 37
3.3.4.3 Statistical analysis 38
3.4 Results and Discussion 38
3.4.1 Effect of storage period and protein type on quality 38
3.4.1.1 Color analysis 38
3.4.1.2 pH value 40
3.4.1.3 Moisture content and water activity 40
3.4.1.4 Texture 43
3.4.2 Principal component analysis on measured (PCA-M) quality variables 43
3.4.3 Characteristics of VNIR spectra 45
3.4.4 PCA-S based unsupervised classification 47
3.4.4.1 Discrimination based on the storage period 47
3.4.4.2 Discrimination based on plant-protein concentration 49
3.4.5 PLSR Prediction models 50
3.4.5.1 Prediction of color and hardness 53

3.4.5.2 Prediction of moisture, pH, and water activity 55
3.4.6 Variables of importance and regression coefficients 55
3.4.7 Pixel-by-pixel prediction 57
3.5 Conclusion 59
3.6 References 60

CHAPTER 4 64

NON-INVASIVE CHARACTERIZATION OF COLOR VARIATION IN PLANT-BASED MEAT BURGERS USING PORTABLE HYPERSPECTRAL IMAGING DEVICE AND MULTIVARIATE IMAGE ANALYSIS 64
4.1 Abstract 64
4.2 Introduction 64
4.3 Materials and Methods 68
4.3.1 Sample formulation and preparation 68
4.3.2 Measurement and statistical analysis of color values 69
4.3.3 Hyperspectral image acquisition 70
4.3.4 Principal component analysis 70
4.3.5 Spectral pre-processing 70
4.3.6 Partial least square regression modeling 71
4.3.7 Optimization of simplified PLSR models 72
4.3.8 Evaluation of model performance 72
4.3.9 Multivariate exploration of images 73
4.4 Results and Discussion 73
4.4.1 Effect of treatments and storage stages on color 73
4.4.2 An overview of spectral characteristics of PB samples 75
4.4.3 Full wavelength PLSR modeling for color prediction 78
4.4.4 Feature wavelength extraction in simplified PLSR models 82
4.4.5 Exploration of PCA Score Surface Images 87
4.4.6 Visualization of pixel-by-pixel prediction using PLSR 90
4.5 Conclusion 92
4.6 References 93

CHAPTER 5 98

THESIS SUMMARY AND OVERALL CONCLUSION 98

5.1 General conclusions 98

5.2 Future recommendations 99

APPENDIX 100

AUTHOR CONTRIBUTIONS 1006

LIST OF FIGURES

Figure 2.1 Concept of digital image: From grayscale to RGB 21

Figure 2.2 Structure of a Hypercube, with each pixel representing a spectrum and each voxel representing a wavelength in the spectrum 22

Figure 2.3 Components of a Hyperspectral Imaging System 23

Figure 2.4 Illustration of PCA application on hypercubes 28

Figure 2.5 Illustration of PLSR application on hypercubes 29

Figure 3.1 Images of (a) prepared control PBMB; (b) beef burger patty; (c) PBMB purchased from local market. *PBMB- Plant-based meat burger 39

Figure 3.2 Principal Component Analysis biplot on measured quality variables of 10 different plant-based meat burger formulations. TVP – Textured Vegetable Protein proportion, PP-Pea Protein proportion 44

Figure 3.3 Overview of spectral changes in the VNIR range of plant-based meat burgers (PBMB): a) mean spectra extracted from samples of day 1, b) mean spectra extracted from day 1 to day 14 of the control PBMB, c) 1st derivative pre-processed spectra of control PBMB, d) spectra response in ~ 550 nm, e), spectra response ~ 920 nm. * Control PBMB – 25% Textured Vegetable Protein proportion. 46

Figure 3.4 Principal component analysis scores plot: a) 140 PBMB samples during 14 days of the storage period, b) 70 Textured vegetable protein based PBMB samples; c) 70 Pea protein based PBMB samples. *PBMB- Plant-based meat burger 48

Figure 3.5 Principal component analysis loadings plot: a) 140 PBMB stored samples b) 70 Textured vegetable protein based PBMB samples, c)70 Pea protein based-PBMB samples PBMB samples. *PBMB- Plant-based meat burger 49

Figure 3.6 Comparison of the performance of prediction models based on preprocessing methods: a) redness (a*) value, b) yellowness (b* value), c) moisture content, d) hardness. Model 1 - raw spectra, Model 2 - 1st derivative, Model 3 – mean centering, Model 4 – 1st derivative mean centering, Model 5 – smoothing. 51

Figure 3.7 Calibration plots for the prediction of quality parameters: a) redness (a*) value), b) moisture content, c) yellowness (b* value), d) hardness 53

Figure 3.8 Significant data covariance explained by latent variables of PLSR models: a) LV1 of redness, b) LV2 for yellowness, c) LV3 of moisture, d) LV4 of hardness. 54

Figure 3.9 Regression coefficients of the PLSR models 55
Figure 3.10 Pixel-by-pixel prediction quality distribution in plant-based meat burgers 57

Figure 4.1 Digital images of plant-based meat burger samples – (a) Control, 15% textured vegetable protein (w/w); (b) T-3, 40% fat emulsion (w/w); (c) T-1, 35% textured vegetable protein (w/w); (d) T-2, 15% pea protein (w/w); (e) T-4, 17.5% fava bean protein (w/w); and (f) beef burger patty 69

Figure 4.2 Spectral profiling of plant-based meat burgers in the VNIR range – (a) mean spectra and (b) Sav-Gol-SD pre-processed spectra of PB samples from 5 treatments; (c) PCA score plot and (d) loading plot for pre-processed meant spectra. *Sav-Gol-SD, second derivative; PCA, Principal Component Analysis 76

Figure 4.3 Principal Component Analysis carried out on hypercube image of Control PB sample – (a) PCA score plot of PC1 versus PC2 for all pixels in the hypercube image, (b) false color RGB image with scores of PC1-PC4 concinnated, (c-e) score-surfaces, and (f-h) loading plots. *Control, 15% textured vegetable protein (w/w)..... 87

Figure 4.4 Principal Component Analysis carried out on hypercube images of D1-PB samples – (a-b) score-surfaces of PC1 and PC2, and (c-d) corresponding loading plots. *D1- day1..... 89

Figure 4.5 Color distribution maps of (a) redness evolution in plant-based meat burgers of T-2 and T-3 treatments, (b) yellowness evolution in plant-based meat burgers of T-1 and T-4 PB treatments. *T-1, 35% textured vegetable protein (w/w); T-2, 15% pea protein (w/w); T-3, 40% fat emulsion (w/w); T-4, 17.5% fava bean protein 91

LIST OF TABLES

Table 3.1 Summary of variations in quality traits of the prepared plant-based meat burgers 39

Table 3.2 Effect of ingredient composition on the quality traits of plant-based meat burgers (PBMB)..... 41

Table 3.3 Effect of storage period on the quality parameters of Control PBMB formulation 42

Table 3.4 Summary of full wavelength PLSR prediction modeling results 52

Table 4.1 Colour evaluation across treatments and storage stages of plant-based meat burger patties 73

Table 4.2 Comparison of the performance of prediction models based on full wavelengths..... 79

Table 4.3 Comparison of the performance of simplified prediction models based on feature wavelengths..... 85

CHAPTER 1
INTRODUCTION

1.1 Research background

Trends in the plant-based meat sector

The anticipated global population rise to 10 billion by 2050 is expected to increase food demand between 59 to 98%. To meet the associated protein demand of 943.5 million metric tons, there is a significant need for a 50–73 % rise in meat production (Agri-food Innovation Council, 2019)(Henchion et al., 2017). However, the challenges associated with traditional meat production systems such as environmental sustainability, animal welfare, and health concerns have intensified the focus on plant-based meat analogues (PBMA) on a global scale. Reports from (Springmann, Clark, et al., 2018) emphasize that a 75% reduction in red meat consumption globally is crucial to eliminate the environmental consequences caused by the livestock industry's extensive use of resources, including 14.5% of greenhouse gas emissions, 0% of arable land, 29% of agricultural freshwater, 36% of crop calories, respectively (Mottet et al., 2017). (Scarborough et al., 2014) reported that high meat product diets yielded more than double the CO_2 equivalent emissions, reaching 7.19 kg CO_2 e/day, compared to the significantly lower emissions of 2.89 kg CO_2 e/day associated with plant-based diets. Further, the increased consumption of red and processed meat is estimated to incur health costs of approximately $285 billion (U.S.) (Springmann, Mason-D'Croz, et al., 2018). In response to these growing stresses, PBMA has emerged as a sustainable meat alternative with significant interest among consumers, researchers, product developers, and investors.

Plant-based meat burgers: A dominant PBMA format

Texturization of plant proteins through structuring techniques like low-moisture extrusion results in extrudates with agglomerated structures and voids. Upon hydration, these structures form typical fibrillar-like structures with a chewy characteristic (Samard et al., 2019). With further traditional meat processing technologies, these extrudates have been widely transformed into PBMA formats, including plant-based meat burger patties (PBMB), nuggets, and tenders (Saerens et al., 2021). However, only PBMB has witnessed significant commercialization. According to the Good Food Institute (GFI), a nonprofit organization, PBMB patties dominate the sales at 43 % of the total PBMA formats, followed by sausage links, tenders, nuggets, and wings (Good Food

Institute, 2022) . And in terms of animal type, plant-based beef remains the largest subcategory (32%) by dollar sales.

Challenges and knowledge gap

As per GFI's (Good Food Institute, 2023), refrigerated PBMB has been a key growth driver for PBMA, as it has been increasingly shelved in the meat case. After years of rapid distribution growth, currently, refrigerated PBMB distribution as measured by TDP (total distribution points) has declined by 14%. The rate of sales in terms of velocity (units/TDP) has declined compared to pre-pandemic years for both frozen and refrigerated PBMB. As per recent consumer reports (Good Food Institute, 2023)(Li et al., 2023), one of the top barriers to consumer acceptance was "didn't meet expectations" during repeated consumption which can be aligned with (i) quality variations within PBMB products and (ii) a gap to resemble the meat products. As outlined by these reports, reasons why consumers tried once or twice but didn't continue were due to but not limited to appearance, texture, flavor, mouthfeel, and cost. In the context of quality, "Food Quality" is commonly defined as the sum of attributes predominantly associated with the texture, appearance, taste, stability, smell, and nutritional value of food, which must be ensured up to consumer standards. Thus, quality changes in a stored product hinder the palatability and acceptance of PBMB.

The reason for quality variations is their ultra-processed nature, as by definition the "ultra-processed foods", PBMB is manufactured with little or no whole foods, and with processed ingredients that are extracted or refined from whole foods. The numerous plant-derived ingredients in PBMB, each with distinct physicochemical properties, distinct structure-function relationships of specific plant proteins in solubility, hydration, and the presence of associated antinutritional factors, collectively contribute to variations in quality parameters such as color, moisture content, and textural properties during storage (De Marchi et al., 2021)(McClements et al., 2021a). To alleviate these problems, substantial studies have been reported on the effect of new raw materials and novel structuring techniques on the nutritional properties (Smetana et al., 2021), physicochemical properties (Bakhsh et al., 2021), microbial attributes (Tóth et al., 2021), and volatile composition changes of PB products (De Marchi et al., 2021).

However, studies focusing on standardized methods for monitoring and evaluating PBMB quality are very limited (McClements et al., 2021b). Firstly, in the context of quality variations from an industrial perspective, the rising food recalls and declining sales increase the need for real-

time quality monitoring techniques for enhanced/stable food quality. Existing quality monitoring techniques are targeted, destructive, labor-intensive, and primarily rely on traditional wet chemistry methods which require extensive sample preparation making them unsuitable for integration in processing and packaging facilities thereby hindering routine quality control processes. Thus, the demand for accurate, rapid, and non-contact photonics-based quality assessment techniques has risen.

Secondly, in the context of the evaluation of new-product/formulations perspective, existing research to evaluate the PBMA visual appearance has primarily relied on contact-based single-point colorimeters. Measuring color at single points, without considering the whole surface of complex formulations, limits or hinders the acceptance of research outcomes and their comparability to traditional meat products. In this context, the demand for chemical mapping tools to visualize how the color of PB responds to different ingredients, storage, or treatment has risen.

Hyperspectral imaging and chemometrics

Hyperspectral imaging (HSI), a non-destructive process analytical tool (PAT) has been successfully applied for quality assessment of meat and agricultural commodities in the past few years. HSI captures spatial images of a sample across series of contiguous wavelengths, generating a unique "***spectral fingerprint***" or signature for each pixel. Spectral fingerprint represents the pattern of electromagnetic energy reflected, absorbed, or transmitted at specific wavelengths, reflecting the material's distinct chemical, physical, and biological properties. The main difference of a hyperspectral image to other imaging techniques is that for each pixel, a whole spectrum is obtained. Visible and near-infrared (VNIR) spectral signals from hyperspectral images (HSI) have proved to be an effective method for predicting and mapping desired quality parameters in both meat (Hasan et al., 2022) and non-meat (grains, flour) (Erkinbaev et al., 2022)(Mundhada et al., 2022). Chemometrics, a discipline that uses mathematical and statistical approaches, plays a fundamental role in extracting useful information from spectral data of food. Among these, Principal Component Analysis (PCA) and Partial Least Square Regression (PLSR) have been widely accepted for qualitative and quantitative predictions (Roussel Sylvieand Preys, 2014). Coupling these techniques with HSI enables "***chemical mapping***", visualizing the spatial distribution of chemical components within a sample based on its spectral characteristics (Amigo et al., 2013).

Smart-portable hyperspectral devices

While numerous HSI studies have been reported on food quality, these have largely remained exploratory, exemplifying proof of concept through lab setups with slow acquisition rates. Such setups necessitate fast computers, sensitive detectors, extensive data storage, and complex data analysis, rendering them unsuitable for high-throughput commercial applications. On the other hand, accelerated digitalization in the food sector has brought the concept of "Food Quality 4.0", where spectral fingerprinting techniques meet and need Industry 4.0 capabilities, resulting in their evolution towards miniaturized and smart field devices (Hassoun, Aït-Kaddour, et al., 2023). Portable, miniaturized, and hand-held hyperspectral imaging devices could be conveniently employed for real-time analysis by translating the results obtained from multivariate prediction models. (Hassoun, Jagtap, et al., 2023)

Motivation and problem statement

Taking into consideration the ultra-processed nature, associated quality concerns, and lack of standardized quality assessment methods, it is extremely important for real-time quality monitoring and chemical mapping of plant-based meat products. A comprehensive literature review shows that it's important to understand the effect of major ingredients (textured protein, non-textured proteins, fat mimic) on the quality parameters (color, moisture, texture, pH, aW) of PBMB during their storage under retail packaging conditions. Furthermore, the color of PBMB decides the major factor in the purchase decision, given the color variation/instability during the storage period, it is important to explore the mapping of color values across the sample surface. To this end, the current study investigates the potentiality of non-destructive portable hyperspectral imaging techniques in the visible and near-infrared ranges coupled with multivariate data and image analysis for the prediction of plant-based burger quality parameters and visualize their distribution.

1.2 Thesis objectives

- To utilize spectral signals in the visible and near-infrared ranges (400-1000 nm) to develop prediction models for the non-destructive prediction of plant-based meat burger quality using a portable hyperspectral imaging device.
    - To formulate PBMB and characterize the effect of protein types (textured, and non-textured protein) and storage time on their quality.

- To extract spectral and spatial information from the hypercube images and develop multivariate statistical models for the prediction of selected quality parameters.
- To develop pixel-by-pixel prediction models for visualizing the effect of major protein ingredients (textured, and non-textured protein) on quality distribution.

- To develop simplified prediction models with feature wavelengths for investigating the color changes in plant-based meat burgers occurring pixel-by-pixel.
  - To characterize the effect of major ingredients (textured, non-textured proteins, fat mimic) and storage time on PBMB color values
  - To develop simplified prediction models by extracting the feature wavelengths
  - To explore the spectral feature variation on HSI images
  - To visualize the color changes with respect to ingredients and storage time via prediction maps.

1.3 Thesis organization

This thesis is comprised of 5 chapters and is structured as follows:

Chapter 1 presents the general introduction to this research and its objectives.

Chapter 2 presents an overview of the theoretical background of hyperspectral imaging and multivariate analysis, providing readers comprehensive understanding of how to apply essential chemometric techniques to analyze hyperspectral data. The chapter carefully selects key techniques and steps used in the current study.

"The experimental work conducted in the frame of this thesis is comprised in Chapter 3 and Chapter 4 as manuscript-based formats."

Chapter 3 titled "Portable Hyperspectral Imaging Coupled with Multivariate Analysis for Real-time Prediction of Plant-based Meat Analogues Quality" was published in the Journal of Food Composition and Analysis. This chapter aims to explore the spectral signals in the visible and near-infrared ranges to create predictive models for assessing the quality of plant-based meat burgers. It involves formulating PBMB prototypes, examining how different protein types, concentrations, and storage time affect their quality. These PBMB protypes aim to replicate the physio-chemical properties of beef patties, without undergoing sensory or nutritional analysis. As this study represents the first instance of simultaneously detecting quality parameters in PBMB

using a completely non-invasive technique, this chapter primarily investigates the feasibility of spectral data to qualitatively explain PBMB characteristics, focusing on spectral shifts and validating them with conventional instrument-based quality measurements. Furthermore, the chapter explores the extent of spectral data to quantitatively define the quality parameters through prediction models. Finally, it examines the feasibility of extending to pixel-by-pixel prediction models using fundamental variable selection technique.

Chapter 4 titled "Non-invasive characterization of color variation in plant-based meat burgers using portable hyperspectral imaging device and multivariate image analysis" is published in Future Foods. Chapter 4 is dedicated to the development of simplified prediction models focusing on feature wavelengths to analyze pixel-by-pixel color changes in PBMB. Following the findings from Chapter 3, which signify the importance of examining color variations during storage and VNIR HSI's ability to predict color values more accurately, Chapter 4 sets to explore the potential of HSI as a tool for color characterization. This chapter mainly focuses on the image analysis and extent of HSI to capture information at individual image level. Additionally, it focuses on improving the pixel-by-pixel prediction capacities by investigating advanced variable selection algorithms. This study extends to assessing the impact of major ingredients on the color of PBMB.

Chapter 5: outlines an overall conclusion and future recommendations.

1.4 References

Agri-food Innovation Council, 2019. (n.d.). *PLANT- BASED PROTEIN MARKET GLOBAL AND CANADIAN MARKET ANALYS IS*.

Amigo, J. M., Martí, I., & Gowen, A. (2013). Chapter 9 - Hyperspectral Imaging and Chemometrics: A Perfect Combination for the Analysis of Food Structure, Composition and Quality. In F. Marini (Ed.), *Chemometrics in Food Chemistry* (Vol. 28, pp. 343–370). Elsevier. https://doi.org/https://doi.org/10.1016/B978-0-444-59528-7.00009-0

Bakhsh, A., Lee, S.-J., Lee, E.-Y., Hwang, Y.-H., & Joo, S.-T. (2021). Evaluation of Rheological and Sensory Characteristics of Plant-Based Meat Analog with Comparison to Beef and Pork. *Food Science of Animal Resources*, *41*(6), 983–996. https://doi.org/10.5851/kosfa.2021.e50

De Marchi, M., Costa, A., Pozza, M., Goi, A., & Manuelian, C. L. (2021). Detailed characterization of plant-based burgers. *Scientific Reports*, *11*(1), 2049. https://doi.org/10.1038/s41598-021-81684-9

Erkinbaev, C., Nadimi, M., & Paliwal, J. (2022). A unified heuristic approach to simultaneously detect fusarium and ergot damage in wheat. *Measurement: Food*, *7*, 100043. https://doi.org/https://doi.org/10.1016/j.meafoo.2022.100043

Good Food Insititute. (2023). *2023 outlook: The state of the plant-based meat category*.

Good Food Institute. (2022). *2022-Plant-Based-State-of-the-Industry-Report*.

Hasan, M. M., Chaudhry, M. M. A., Erkinbaev, C., Paliwal, J., Suman, S. P., & Rodas-Gonzalez, A. (2022). Application of Vis-NIR and SWIR spectroscopy for the segregation of bison muscles based on their color stability. *Meat Science*, *188*, 108774. https://doi.org/https://doi.org/10.1016/j.meatsci.2022.108774

Hassoun, A., Aït-Kaddour, A., Abu-Mahfouz, A. M., Rathod, N. B., Bader, F., Barba, F. J., Biancolillo, A., Cropotova, J., Galanakis, C. M., Jambrak, A. R., Lorenzo, J. M., Måge, I., Ozogul, F., & Regenstein, J. (2023). The fourth industrial revolution in the food industry—Part I: Industry 4.0 technologies. *Critical Reviews in Food Science and Nutrition*, *63*(23), 6547–6563. https://doi.org/10.1080/10408398.2022.2034735

Hassoun, A., Jagtap, S., Garcia-Garcia, G., Trollman, H., Pateiro, M., Lorenzo, J. M., Trif, M., Rusu, A. V., Aadil, R. M., Šimat, V., Cropotova, J., & Câmara, J. S. (2023). Food quality 4.0: From traditional approaches to digitalized automated analysis. *Journal of Food Engineering*, *337*, 111216. https://doi.org/https://doi.org/10.1016/j.jfoodeng.2022.111216

Henchion, M., Hayes, M., Mullen, A. M., Fenelon, M., & Tiwari, B. (2017). Future Protein Supply and Demand: Strategies and Factors Influencing a Sustainable Equilibrium. *Foods (Basel, Switzerland)*, *6*(7). https://doi.org/10.3390/foods6070053

Li, J., Silver, C., Gómez, M. I., Milstein, M., & Sogari, G. (2023). Factors influencing consumer purchase intent for meat and meat substitutes. *Future Foods*, *7*, 100236. https://doi.org/https://doi.org/10.1016/j.fufo.2023.100236

McClements, D. J., Weiss, J., Kinchla, A. J., Nolden, A. A., & Grossmann, L. (2021a). Methods for Testing the Quality Attributes of Plant-Based Foods: Meat- and Processed-Meat Analogs. *Foods*, *10*(2). https://doi.org/10.3390/foods10020260

McClements, D. J., Weiss, J., Kinchla, A. J., Nolden, A. A., & Grossmann, L. (2021b). Methods for Testing the Quality Attributes of Plant-Based Foods: Meat- and Processed-Meat Analogs. *Foods*, *10*(2). https://doi.org/10.3390/foods10020260

Mottet, A., de Haan, C., Falcucci, A., Tempio, G., Opio, C., & Gerber, P. (2017). Livestock: On our plates or eating at our table? A new analysis of the feed/food debate. *Global Food Security*, *14*, 1–8. https://doi.org/https://doi.org/10.1016/j.gfs.2017.01.001

Mundhada, S., Chaudhry, M., Erkinbaev, C., & Paliwal, J. (2022). Non-Destructive Quality Monitoring of Flaxseed During Storage. *Journal of Food Measurement and Characterization*, *16*, 1–11. https://doi.org/10.1007/s11694-022-01464-5

Roussel Sylvie and Preys, S. and C. F. and L. J. (2014). Multivariate Data Analysis (Chemometrics). In C. and C. P. J. O'Donnell Colm P. and Fagan (Ed.), *Process Analytical Technology for the Food Industry* (pp. 7–59). Springer New York. https://doi.org/10.1007/978-1-4939-0311-5_2

Saerens, W., Smetana, S., Van Campenhout, L., Lammers, V., & Heinz, V. (2021). Life cycle assessment of burger patties produced with extruded meat substitutes. *Journal of Cleaner Production*, *306*, 127177. https://doi.org/https://doi.org/10.1016/j.jclepro.2021.127177

Samard, S., Gu, B., & Ryu, G.-H. (2019). Effects of extrusion types, screw speed and wheat gluten addition on physicochemical characteristics and cooking stability of meat analogues. *Journal of the Science of Food and Agriculture*, *99*. https://doi.org/10.1002/jsfa.9722

Scarborough, P., Appleby, P., Mizdrak, A., Briggs, A., Travis, R., Bradbury, K., & Key, T. (2014). Dietary greenhouse gas emissions of meat-eaters, fish-eaters, vegetarians and vegans in the UK. *Climatic Change*, *125*. https://doi.org/10.1007/s10584-014-1169-1

Smetana, S., Profeta, A., Voigt, R., Kircher, C., & Heinz, V. (2021). Meat substitution in burgers: nutritional scoring, sensorial testing, and Life Cycle Assessment. *Future Foods*, *4*, 100042. https://doi.org/https://doi.org/10.1016/j.fufo.2021.100042

Springmann, M., Clark, M., Mason-D'Croz, D., Wiebe, K., Bodirsky, B., Lassaletta, L., Vries, W., Vermeulen, S., Herrero, M., Carlson, K., Jonell, M., Troell, M., Declerck, F., Gordon, L., Zurayk, R., Scarborough, P., Rayner, M., Loken, B., Fanzo, J., & Willett, W. (2018). Options for keeping the food system within environmental limits. *Nature*, *562*. https://doi.org/10.1038/s41586-018-0594-0

Springmann, M., Mason-D'Croz, D., Robinson, S., Wiebe, K., Godfray, C., Rayner, M., & Scarborough, P. (2018). Health-motivated taxes on red and processed meat: A modelling study on optimal tax levels and associated health impacts. *PLOS ONE*, *13*, e0204139. https://doi.org/10.1371/journal.pone.0204139

Tóth, A. J., Dunay, A., Battay, M., Illés, C. B., Bittsánszky, A., & Süth, M. (2021). Microbial Spoilage of Plant-Based Meat Analogues. *Applied Sciences*, *11*(18). https://doi.org/10.3390/app11188309

CHAPTER 2

THEORETICAL BACKGROUND OF HYPERSPECTRAL IMAGING AND MULTIVARIATE ANALYSIS

2.1 Electromagnetic spectrum and VNIR spectroscopy

Electromagnetic spectrum constitutes of electromagnetic radiation, energy released or absorbed by charged particles in the form of waves. Electromagnetic radiation, comprised of electrical and magnetic waves that oscillate on perpendicular planes, exhibits characteristic *wavelengths* (distance between two adjacent troughs/crests). The electromagnetic spectrum encompasses a wide range of wavelengths, frequencies, and photon energies, reflecting the diverse nature of electromagnetic radiation including gamma rays, X-rays, ultraviolet radiation, visible light, infrared radiation (divided into near-infrared, mid-infrared, and far-infrared), microwaves, and radio waves (Britannica, 2024). The subrange spanning from 400 to 700 nm is designated as the visible region or “light”, as it is visible to the human eye. Beyond the visible spectrum lies the infrared range, where wavelengths extend from 700 nm to approximately 2500 nm.

The interaction between light photons and molecules of the materials of interest is the basis for food material analysis through spectroscopy (Adriana S. Franca, 2017). Upon contact, the light energy gets absorbed by the material due to atomic and molecular interactions. Within the visible region, electrons absorb energy, transitioning from lower to higher orbits. In the mid-infrared region, energy absorption occurs at resonant frequencies, causing bounded molecules to vibrate in various directions through movements such as stretching, bending, and rotation (ElMasry & Sun, 2010). The radiation that is not absorbed by the sample is either reflected or transmitted.

Vis-NIR spectroscopy is considered the simplest non-destructive and non-targeted technique, requiring no prior sample preparation while enabling the simultaneous measurement of multiple constituents (Wang, 2019). Changes in spectral characteristics occur as irradiation passes through the sample, reflecting its structure, moisture content, particle size, temperature, and chemical composition (Chaudhry M, 2019). The resulting absorption spectrum acts as a unique "fingerprint" containing information about the sample's physical and chemical composition.

2.2 Relation between digital image, spectroscopy, and hyperspectral Imaging

An image is a 2D array of pixels (picture elements), with each pixel assigned a numeric value representing its gray level or color intensity (Gonzalez & Faisal, 2019). Grayscale images are typically regarded as univariate images that represent intensity across a single band of the electromagnetic spectrum, with color values typically ranging from 0 to 255.

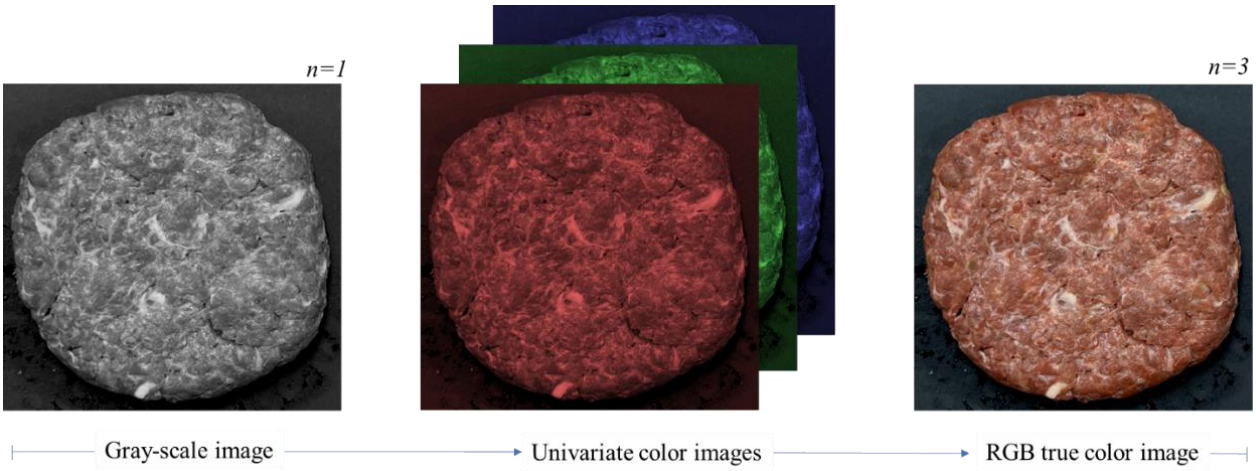

Figure 2.1 Concept of digital image: From grayscale to RGB

While color images are typically composed of 3 univariate images each representing intensity across the red, green, and blue bands of the electromagnetic spectrum (Zheng et al., 2016). **Fig. 2.1** illustrates this concept. In simpler terms variable (wavelength, n) n=1 is univariate image, n is between 1 and 20 it is multivariate image, and images beyond n=10 is termed as "hyperspectral". Whereas hyperspectral images consist of multiple continuous bands across various wavelengths. In Fig 2.1 it is evident that the information about a subject intensified from n=1 to n=3. Subsequently, hyperspectral image carries substantial amount of information, necessitating the use of range of mathematical tools for analysis (Gallagher & Lawrence, 2020).

Hyperspectral images comprise a series of images of the same object across numerous contiguous wavebands for each spatial position (Chen et al., 2002). Each pixel of the image holds its spectra **(Fig. 2.2)**, which enables the characterization of specific positions' composition, while spatial images offer surface feature information. Spectral measurements reveal "what" is present in the food sample, while spatial dimensions visualize the location of specific chemical

compounds. Integration of spectral and spatial dimensions offers a comprehensive understanding of both "what" and "where" within the food sample (Wu & Sun, 2013a).

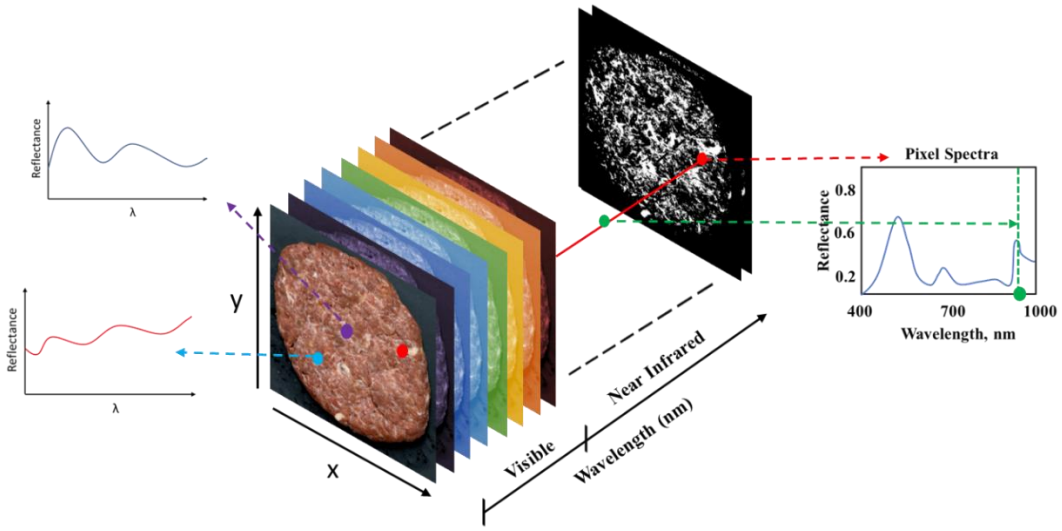

Figure 2.2 Structure of a hypercube, with each pixel representing a spectrum and each voxel representing a wavelength in the spectrum

2.3 Structure and Components of Hyperspectral Imaging

Data Structure: HSI results in a three-dimensional data structure, known as a hyperspectral data cube or hypercube **(Fig. 2.2)**, which can be conceptualized as a three-dimensional array L with dimensions (X x Y x λ), where each pixel (defined by its x-y coordinate), represents a spectrum across λ wavelengths.

Acquisition mode: Hyperspectral imaging (HSI) acquisition involves three primary modes: Line Scan, Point Scan, and Area Scan. Line-scan mode is particularly useful for applications requiring high-resolution spectral information, where HSI systems capture spectral and spatial information line by line. This mode involves scanning a target object along a single line, with each line representing a unique spatial position **(Fig. 2.3)**. As the scanning progresses, spectral data is collected for each line, enabling comprehensive analysis of both spectral and spatial characteristics of the target (Wu & Sun, 2013b).

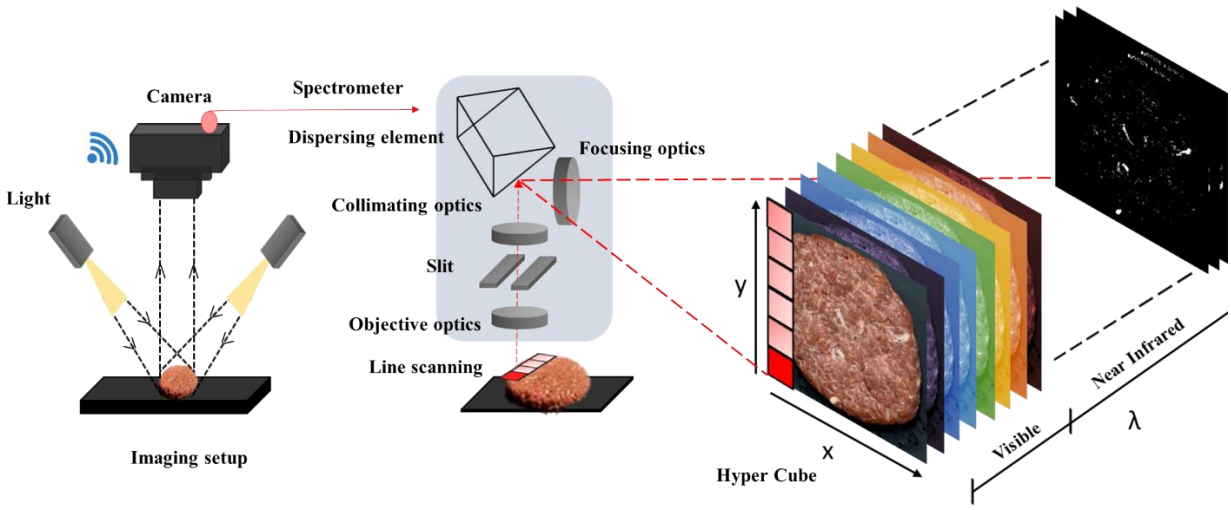

Figure 2.3 Components of a Hyperspectral Imaging System

Components and working:

(I) A ***light source*** to illuminate the target. Typically, halogen lights provide broadband illumination across the visible and near-infrared spectral ranges for reflectance imaging (Wu & Sun, 2013b).

(II) A ***wavelength dispersion device***, such as an imaging spectrograph, disperses the received light signal into different wavelengths without moving parts. This spectrograph comprises an input slit, collimating optics, a dispersive unit, and a focusing lens. The objective of the HSI camera projects the target image onto the input slit, restricting incoming information to a single line. Collimating optics direct the light to the dispersive unit, where it spreads into spectra, and a focusing lens projects the dispersed light onto area detectors (Sun, 2010).

(III) ***Area detectors*** quantify the intensity of the acquired light by converting incident photons into electrons. Commonly used are CMOS photodiodes, or complementary metal-oxide-semiconductor solid-state area detectors. CMOS image sensors contain a photodetector coupled with a readout amplifier within each pixel, enabling fast signal transfer and making them suitable for online industrial inspection applications. A proper selection of spectral imaging mode, optimization of the acquisition mode, and components based on the target material of interest enable precise capture for high-resolution imaging and spectral characterization (Qin, 2010).

2.4 Chemometrics

Chemometrics, also known as multivariate data analysis, involves the application of advanced mathematical and statistical techniques to process extensive data from process analytical technology (PAT) instruments (O'Donnell et al., 2014). Its primary objective is to extract meaningful chemical information from these big datasets. Chemometrics plays a crucial role in managing the large datasets produced by hyperspectral imaging (HSI) by reducing dimensionality while preserving essential spectral details, thus enabling the development of quantification or classification models (Amigo et al., 2013). The primary objective of HSI is to assess essential quality attributes of food samples from real-time spectral (multivariate) measurements. This involves developing multivariate calibration models (predictive modelling) that establish a relationship between spectral data and quality parameters determined through reference methods (Roussel Sylvieand Preys, 2014). Initially, mathematical pre-treatments are applied to separate chemical information from physical variations in spectral signals. Principal Component Analysis (PCA) is a key technique within chemometrics, condensing complex datasets into fewer variables called principal components (PCs), which capture the maximum variability in the data. This aids in sample distribution analysis and outlier detection. Partial Least Squares (PLS) regression extracts key underlying factors contributing significantly to response variation, thereby simplifying the regression model to focus on essential variables.

2.5 Image pre-processing

To mitigate noise, artifacts, and unwanted signals in raw images due to environmental factors, image pre-processing methods are essential. Spatial and/or spectral pre-processing techniques are utilized to remove these undesirable artifacts from the image, ensuring that the data used for subsequent analysis is of high quality and reliability.

2.5.1 Image calibration

The raw HSI image obtained represents the detector signal intensity. To convert this raw intensity image into a reflectance image, a reflectance calibration process is essential, utilizing black and white reference images. The reflectance calibration involves correcting the raw HSI images using **Eq. 2.1**.

$$R = \frac{I_S - I_D}{I_W - I_D} \qquad \textit{(Eq 2.1)}$$

Where R denotes the corrected HSI image; I_S represents the raw HSI image, I_D signifies the black reference image, and I_W indicates the white reference image (Mendoza & Lu, 2015).

2.5.2 Image Segmentation

Image segmentation in HSI aims to partition an image into distinct regions, identifying areas of interest (ROI) for further analysis (Vidal & Amigo, 2012). Typically, hyperspectral images are square, and it's crucial to exclude any areas outside the sample as they often contain noisy spectra. Determining and segmenting ROIs is often complex and depends on the particular objective or issue being addressed. ***Manual ROI selection*** involves outlining ROIs manually but is time-consuming and subjective. Whereas ***Thresholding*** methods simplify images by converting multilevel images into binary images, where background pixels are assigned as 0 and object pixels (ROI) as 1, based on a predetermined threshold value T. This value is often determined by comparing intensities or color values. This threshold can be established using scores from a PCA model.

2.6 Data extraction and treatment

Extracting mean reflectance spectra from the ROI within the raw HSI data cube is a crucial step for subsequent analysis and model development. Prior to modelling, data preprocessing techniques are frequently employed on the mean spectra to minimize noise and unwanted fluctuations in the spectral signal. Identifying the most suitable technique depends on the specific conditions encountered, and it's essential to compare different methods to determine the optimal combination for a particular dataset (Rinnan et al., 2009). Please refer to the Chapter 4 (Section 4.5) for more information.

2.7 Multivariate modelling

2.7.1 Data Exploration: Principal component analysis

PCA is a dimensionality reduction technique used to transform high-dimensional datasets into a lower-dimensional space while retaining the essential information within the original data (Roussel Sylvieand Preys, 2014). PCA involves the projection of the original sample coordinates onto a new set of axes, referred to as principal components (PCs). By capturing the variance and correlations among variables, PCA shows the essential structure of the data, resulting in easier visualization and interpretation. The primary equation of PCA **Eq. 2.2**, decomposes the original data matrix X into score matrix (T), loading matrix (P), and residual matrix (E).

$$\boldsymbol{X = TP^T + E} \qquad \textit{(Eq 2.2)}$$

Scores represent transformed data points in the lower-dimensional space, capturing the essential information from the original dataset. Loadings define the directions of maximum variance in the original dataset and indicate the contribution of each variable to the principal components. Residuals account for unexplained variance in the data that cannot be captured by the principal components.

2.7.1.1 Process of decomposing the original data into scores and loadings

PCs are determined by decomposing the variance-covariance matrix $V(p,p)$, which is calculated using the **Eq. 2.3.**

$$V(p,p) = \frac{1}{n-1}\, X^T X \qquad \textit{(Eq 2.3.)}$$

where X represents the data matrix with dimensions $n \times p$ (n is the number of observations and p is the number of variables) and X^T represents the transpose. PCA diagonalizes this matrix to compute its eigenvalues (T) and eigenvectors (P). The eigenvalues represent the amount of variance explained by each principal component, and the eigenvectors represent the directions of maximum variance. Once the eigenvectors (P) are sorted in descending order based on their corresponding eigenvalues, the original data matrix X can be decomposed into the score matrix $\boldsymbol{T}$ and the loading matrix $\boldsymbol{P}^T$ as **Eq. 2.4**:

$$X(n,p) = \boldsymbol{T}\,(n,k)\,\boldsymbol{P}^T(k,p) + E(n,p) \qquad \textit{(Eq 2.4.)}$$

Where, T represent the score matrix, with $n \times k$ dimensions. $\boldsymbol{P}^T$ is the loading matrix, representing the weights of each original variable in constructing the principal components, with dimensions $k \times p$. E is the residual matrix representing unexplained variance, with dimensions $n \times p$ and k is the number of principal components chosen.

2.7.1.2 Interpreting PCA

It involves various visualizations to understand the relationship between samples and variables (Wise et al., 2005). **Score Plot,** samples with close scores have similar behaviour and levels in the original variables. **Loading Plot, v**ariables are depicted as vectors, each with distinct weights along PC directions. Close directions indicate strong correlation, and higher loading weights signify significant contribution to the PC axis, aiding in variable selection.

2.7.2 Prediction: Partial least square regression modelling

Partial Least Squares Regression (PLSR) is a multivariate linear predictive modelling method used to establish correlations between an explanatory variable X (mean spectra) and parameters of interest Y (quality parameters). Like any prediction model, in PLSR, the relationship between X and Y is captured through the **Eq. 2.5**.

$$\hat{\boldsymbol{y}} = \boldsymbol{f}(\boldsymbol{X}) \qquad (Eq\ 2.5.)$$

where $\hat{y}$ denotes the predicted value of y. The determination of function f involves reducing the error between the actual y values and their corresponding predicted $\hat{y}$ values. The calibration or training set, comprising both X and Y data are primarily used to build and optimize PLSR models. These models once optimized, applied to predict the parameters of interest for unknown samples.

In PLSR, datasets X and Y undergo decomposition into their latent structures, which captures the essential information and underlying patterns within the data (Roussel Sylvieand Preys, 2014). After which a regression model is iteratively established between the scores of the X and Y blocks. This iterative process involves both outer and inner relations, with the outer relations denoting individual blocks (X and Y) and the inner relations link the two blocks together (Wise et al., 2005).

(i)**The outer relation** within X and Y is expressed using equations **Eq. 2.6** and **2.7**,

$$X = TP^T + E = \Sigma t_r p_r^T + E \qquad (Eq\ 2.6.)$$

$$Y = UQ^T + F = \Sigma u_r q_r^T + F \qquad (Eq\ 2.7.)$$

These equations represent the decomposition of X and Y into score matrices (T and U), loading matrices (P and Q), and residual matrices (E and F). The score matrices T and U capture the underlying patterns in the data, while the loading matrices P and Q describe the relationship between the original variables and the scores.

(ii) **The inner relation** within X and Y is established by plotting the scores of the X block and the scores of the Y block for each component. This inner relation is expressed by **Eq. 2.8**

$$\hat{u} = \Sigma b_r t_r \qquad (Eq\ 2.8.)$$

$\hat{u}$ represents the predicted scores of Y, b_r represents the regression coefficient, and t_r is the score vector for X. Conclusively, the relationship between X and Y is expressed as **Eq. 2.9**

$$Y{=}TBQ'{+}Ft_r \qquad (Eq\ 2.9.)$$

This equation demonstrates how the latent structures captured from both X and Y contribute to predicting the relationship between the two datasets. For further insights into PLSR, refer (Geladi & Kowalski, 1986).

2.8 Multivariate image analysis

2.8.1 Exploration of Images: PCA

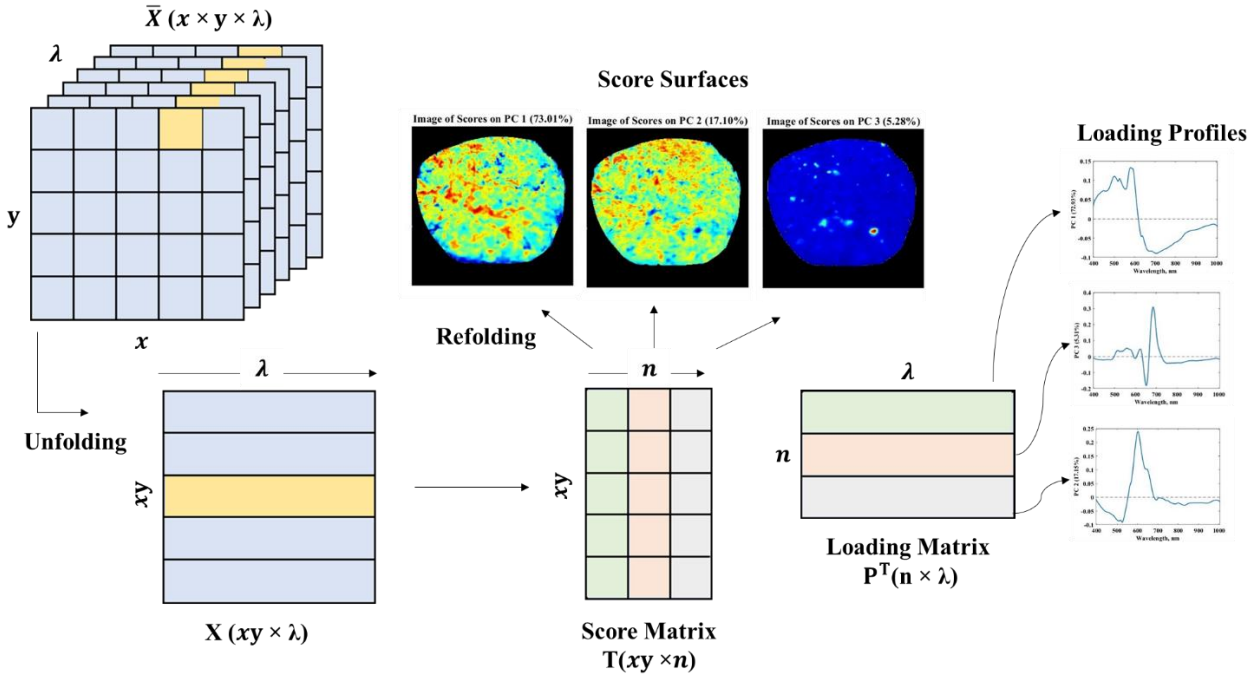

Figure 2.4 Illustration of PCA application on hypercubes

PCA is a fundamental technique applied to hypercubes for identifying key factors of variability and analyse the spatial distribution of constituents in a single image qualitatively. In this process, the data cube $\bar{\boldsymbol{X}}$ **(**$\boldsymbol{x}$ × **y** × **λ)** is initially unfolded into a matrix **X (**$\boldsymbol{xy}$ × **λ)**. As depicted in **Eq.2.2**., this unfolded matrix is then decomposed using PCA into a score's matrix $\boldsymbol{T}$ (**xy** ×$\boldsymbol{n}$) and loadings matrix $\boldsymbol{P^T}$**(**$\boldsymbol{n}$ × **λ)** where $\boldsymbol{n}$ represents the number of principal components selected. The scores matrix captures the variation in pixel concentrations while the loadings contain the associated spectral variability. Subsequently, the scores are re-folded to generate score images, which provide spatial visualization of the distribution of components across the original hypercube. For further insights refer (Gallagher & Lawrence, 2020)

2.8.2 Pixel-by-pixel Prediction

Pixel-by-pixel prediction using PLSR provides a detailed understanding of spatial variations of predicted quality parameter within samples. First, the spectra in each hypercube image are averaged to obtain mean spectra representing each sample. These mean spectra are then grouped together to form a matrix known as the X Block. Further, the measured quality parameter values corresponding to each sample are organized into a Y Block matrix. PLSR regression is applied to the X Block and Y Block matrices, which establishes a predictive model that relates the spectral data (X) to the quality parameters (Y). The regression process involves selecting appropriate model parameters, such as the number of LVs, through techniques like cross-validation. The resulting regression coefficients capture the relationship between the spectral features and the quality parameters. Further, to predict quality parameters for each pixel in the image, hypercube of a prediction sample is considered, which is unfolded to create a vector representation of the pixel spectra. This unfolded hypercube vector is then multiplied by the regression coefficients to obtain a prediction vector. The prediction vector is refolded to reconstruct a prediction image, which provides pixel-by-pixel predictions of the quality parameters across the sample. For further insights refer (Elmasry & Nakauchi, 2016)

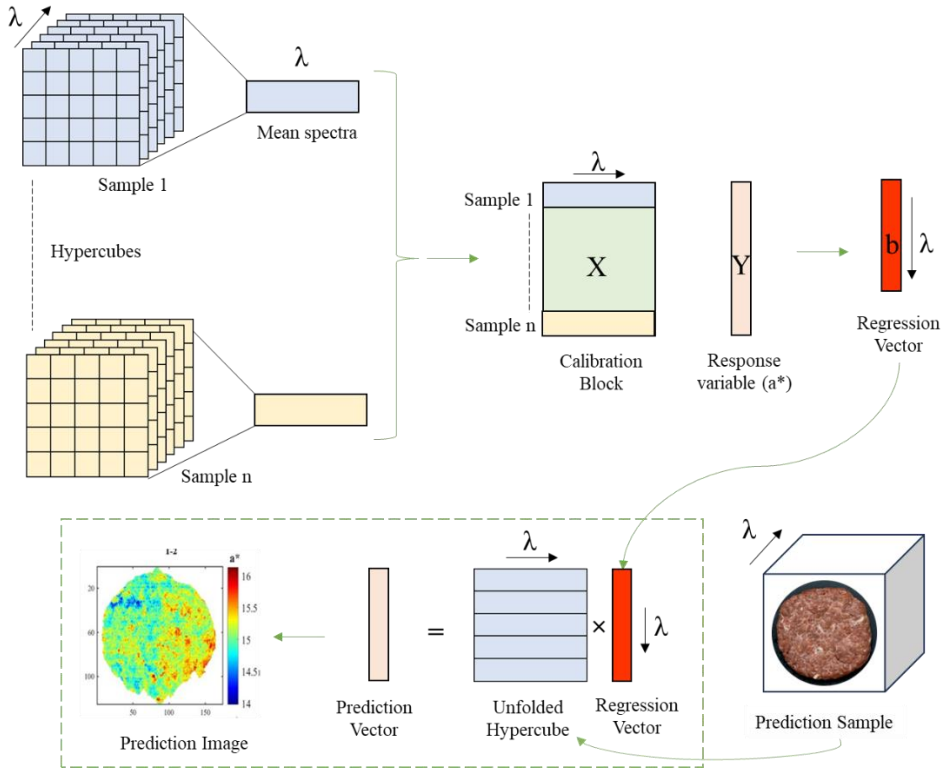

Figure 2.5 Illustration of PLSR application on hypercubes

2.9 References

Adriana S. Franca, L. M. L. N. (2017). *Spectroscopic Methods in Food Analysis*.

Amigo, J. M., Martí, I., & Gowen, A. (2013). Chapter 9 - Hyperspectral Imaging and Chemometrics: A Perfect Combination for the Analysis of Food Structure, Composition and Quality. In F. Marini (Ed.), *Chemometrics in Food Chemistry* (Vol. 28, pp. 343–370). Elsevier. https://doi.org/https://doi.org/10.1016/B978-0-444-59528-7.00009-0

Britannica, T. E. of E. (2024). *Electromagnetic spectrum*.

CHAUDHRY, M. M. A. (2019). *Innovative and non-destructive technologies to evaluate quality of rocket leaves for ready to eat salads*.

Chen, Y.-R., Chao, K., & Kim, M. S. (2002). Machine vision technology for agricultural applications. *Computers and Electronics in Agriculture*, *36*, 173–191. https://api.semanticscholar.org/CorpusID:15179648

Elmasry, G., & Nakauchi, S. (2016). Image analysis operations applied to hyperspectral images for non-invasive sensing of food quality – A comprehensive review. *Biosystems Engineering*, *142*, 53–82. https://doi.org/10.1016/j.biosystemseng.2015.11.009

ElMasry, G., & Sun, D.-W. (2010). CHAPTER 1 - Principles of Hyperspectral Imaging Technology. In D.-W. Sun (Ed.), *Hyperspectral Imaging for Food Quality Analysis and Control* (pp. 3–43). Academic Press. https://doi.org/https://doi.org/10.1016/B978-0-12-374753-2.10001-2

Gallagher, N., & Lawrence, L. (2020). *Introduction to Hyperspectral and Multivariate Image Analysis and Principal Components Analysis for Multivariate Images*.

Geladi, P., & Kowalski, B. (1986). Partial Least-Squares Regression: A Tutorial. *Analytica Chimica Acta*, *185*, 1–17. https://doi.org/10.1016/0003-2670(86)80028-9

Gonzalez, R., & Faisal, Z. (2019). *Digital Image Processing Second Edition*.

Mendoza, F., & Lu, R. (2015). Basics of Image Analysis. In *Food Engineering Series* (pp. 9–56). https://doi.org/10.1007/978-1-4939-2836-1_2

O'Donnell, C., Fagan, C., & Cullen, P. J. (2014). *Process Analytical Technology for the Food Industry*. https://doi.org/10.1007/978-1-4939-0311-5

Qin, J. (2010). CHAPTER 5 - Hyperspectral Imaging Instruments. In D.-W. Sun (Ed.), *Hyperspectral Imaging for Food Quality Analysis and Control* (pp. 129–172). Academic Press. https://doi.org/https://doi.org/10.1016/B978-0-12-374753-2.10005-X

Rinnan, Å., van den Berg, F., & Engelsen, S. B. (2009). Review of the most common pre-processing techniques for near-infrared spectra. *TrAC Trends in Analytical Chemistry*, *28*(10), 1201–1222. https://doi.org/https://doi.org/10.1016/j.trac.2009.07.007

Roussel Sylvie and Preys, S. and C. F. and L. J. (2014). Multivariate Data Analysis (Chemometrics). In C. and C. P. J. O'Donnell Colm P. and Fagan (Ed.), *Process Analytical Technology for the Food Industry* (pp. 7–59). Springer New York. https://doi.org/10.1007/978-1-4939-0311-5_2

Sun, D.-W. (2010). *Hyperspectral Imaging for Food Quality Analysis and Control*. https://doi.org/10.1016/C2009-0-01853-4

Vidal, M., & Amigo, J. (2012). Pre-processing of hyperspectral images. Essential steps before image analysis. *Chemometrics and Intelligent Laboratory Systems*, *117*, 138–148. https://doi.org/10.1016/j.chemolab.2012.05.009

Wang, X. (2019). 7 - Near-infrared spectroscopy for food quality evaluation. In J. Zhong & X. Wang (Eds.), *Evaluation Technologies for Food Quality* (pp. 105–118). Woodhead Publishing. https://doi.org/https://doi.org/10.1016/B978-0-12-814217-2.00007-X

Wise, B., Gallagher, N., Bro, R., Shaver, J., Windig, W., & Koch, R. (2005). User's Manual PLS_Toolbox 3.5 for use with Matlab TM, Eigenvector Research. *Manson*.

Wu, D., & Sun, D. (2013a). Advanced applications of hyperspectral imaging technology for food quality and safety analysis and assessment: A review — Part II: Applications. *Innovative Food Science and Emerging Technologies*, *19*, 15–28. https://api.semanticscholar.org/CorpusID:51829477

Wu, D., & Sun, D.-W. (2013b). Advanced applications of hyperspectral imaging technology for food quality and safety analysis and assessment: A review - Part I: Fundamentals. *Innovative Food Science & Emerging Technologies*, *19*, 1–14. https://doi.org/10.1016/j.ifset.2013.04.014

Zheng, C., He, H.-J., & Sun, D.-W. (2016). Chapter 3 - Object Measurement Methods. In D.-W. Sun (Ed.), *Computer Vision Technology for Food Quality Evaluation (Second Edition)* (Second Edition, pp. 65–85). Academic Press. https://doi.org/https://doi.org/10.1016/B978-0-12-802232-0.00003-7

CHAPTER 3

PORTABLE HYPERSPECTRAL IMAGING COUPLED WITH MULTIVARIATE ANALYSIS FOR REAL-TIME PREDICTION OF PLANT-BASED MEAT ANALOGUES QUALITY

Logesh Dhanapal and Chyngyz Erkinbaev*

3.1 Abstract

Growing demand for plant-based meat analogues and their quality changes during storage necessitates real-time quality monitoring and chemical mapping. This study reports the use of portable hyperspectral imaging in the visible-near-infrared (VNIR) range (400–1000 nm) coupled with multivariate analysis for the prediction of quality traits (color, moisture, pH, and hardness) in plant-based meat burgers (PBMB) of different formulations ranging from 10–30% textured vegetable protein (TVP) and 5–25% pea protein (PP) during a 14-day storage period and map the quality distribution on each pixel. PCA was applied to explore both spectral (PCA-S) and measured quality data (PCA-M), while PLSR was applied for prediction modeling. ANOVA and PCA-M results showed the instability of PBMB quality even over a short storage period. PCA-S showed successful spatial separation of PBMB samples based on storage days, TVP, and PP concentrations. The PLSR models possessed good prediction accuracies for redness (R^2_P = 0.92, RMSEP = 0.74), yellowness (R^2_P = 0.93, RMSEP = 0.44), moisture (R^2_P = 0.90, RMSEP = 0.81 % Wb), and hardness (R^2_P = 0.81, RMSEP = 0.87 N). Overall, the prediction results and distribution maps unravel the feasibility of VNIR-HSI coupled with chemometrics for real-time quality inspection in plant-based food production.

Keywords: Meat alternatives, Smart sensing, Chemometrics, Non-destructive analysis, Food quality, Plant proteins,

3.2 Introduction

The rising global population necessitates a 50–73 % upsurge in meat production to meet the protein demand of 943.5 million metric tons (Henchion et al., 2017). In response to the growing stress on resource-intensive traditional meat production systems, plant-based meat analogues (PBMA) have emerged as sustainable alternatives (Vallikkadan et al., 2023a). Among various PBMA options, plant-based meat burger (PBMB) patties displayed immense market potential, attracting significant research interest, and witnessing large-scale commercialization. PBMB are

simulated meat products fabricated from texturized and non-texturized plant proteins, fat mimics, binding, coloring, and flavoring agents to mimic the characteristics of lean meat patties (Kyriakopoulou et al., 2019). According to (Future Market Insights, 2023), the PBMB market is expected to experience exponential growth with an estimated Compound Annual Growth Rate exceeding 22% between 2020 and 2030.

However, persistent variations in PBMB quality characteristics continue to pose an unresolved challenge (McClements et al., 2021a). The numerous plant-derived ingredients in PBMB, each with distinct physicochemical properties, distinct structure-function relationships of specific plant proteins in solubility, hydration, and the presence of associated antinutritional factors, collectively contribute to variations in quality parameters such as color, moisture content, and textural properties during storage (De Marchi et al., 2021)(McClements et al., 2021a). Quality changes during storage, including appearance, texture, flavor, and mouthfeel, can hinder the palatability, acceptance, and commercialization of PBMB (Li et al. 2023). Extensive research studies have reported the role of novel ingredients in the physicochemical attributes, microbial characteristics, nutritional properties, and changes in the volatile composition of PBMB products (Tóth et al., 2021)(Sakai et al., 2022a)(Zhou et al., 2022)(Bakhsh, Lee, Lee, Sabikun, et al., 2021)(De Marchi et al., 2021). However, studies focusing on quality variations in PMBA and standardized methods for analyzing and evaluating PBMB quality are relatively limited.

Existing quality monitoring techniques are targeted, destructive, labor-intensive, and primarily rely on traditional wet chemistry methods which require extensive sample preparation making them unsuitable for integration in processing facilities thereby hindering routine quality control processes (McClements et al., 2021b). In this context, non-destructive spectral fingerprinting technologies have been extensively studied for on-line or at-line food quality monitoring.

Visible-near infrared (VNIR) spectroscopy measures the combination tones and overtones of molecular vibrations when light interacts with food samples. Conversely, hyperspectral imaging (HSI), integrates spectroscopy with computer vision technologies in a single system to provide spectral information at each pixel (Erkinbaev et al., 2022). VNIR-HSI yields a better representation of chemical characteristics in non-homogeneous food surfaces and their changes over time. Coupling chemometrics tools such as Principal Component Analysis (PCA) and Partial Least Square Regression (PLSR) could serve as an essential tool for extracting useful chemical information amidst the presence of unspecified signals, such as broad and overlapped peaks

resulting from heteroatomic bonds in complex food matrices (Ren & Sun, 2022) (Squeo et al., 2022).

VNIR-HSI coupled with chemometrics has found applications in predicting the quality attributes of both fibrous fresh, processed meat products and plant-based ingredients. In bison muscles, Hasan et al. (Hasan et al., 2022) predicted quality-associated physio-chemical properties, and Chaudhry et al. (Hasan et al., 2022) predicted pixel-by-pixel color variations during aging periods. Feng et al. (Feng & Makino, 2020) predicted the color evolution of sausages during storage. (Squeo et al., 2022) reported the prediction of proximate composition and alpha-galactosidase content of textured vegetable protein (TVP) using near-infrared (NIR)-HSI. The prediction of chemical composition, adulteration, quality, and microbial parameters in whole grains and milled flours has been reported (Mundhada et al., 2022), (Erkinbaev, Morrison, et al., 2017), (Erkinbaev et al., 2022). The collective findings demonstrate the potential of extending VNIR-HSI to the PBMA that constitutes the physiochemical attributes of processed meat and the functional nature of plant-based ingredients. McClements et al. (McClements et al., 2021), and Schreuders et al. (Schreuders et al., 2021) have described HSI as a potential tool for assessing the quality of meat alternatives.

The majority of current HSI analysis techniques utilize benchtop instruments in a laboratory setting rendering them unsuitable for real-time applications. With the advent of Food Quality 4.0, portable, miniaturized, and smart spectral fingerprinting devices have been studied for predicting food quality and the results obtained from multivariate prediction models have been exemplified as proof of concept for real-time analysis. However, to the best of our knowledge, such an approach for quality prediction of meat alternatives has not been explored.

A comprehensive review of the literature reveals a dearth of research on standardized methods for evaluating meat alternatives' quality. Considering the complex nature of PBMB with numerous plant-derived ingredients, there is a critical need to understand the role of major ingredients i.e., textured, and non-textured protein, and their effect on quality during the storage period. The real-time prediction and distribution maps of quality parameters generated by HSI may potentially meet this requirement. Therefore, this study aimed to investigate the feasibility of portable and hand-held hyperspectral imaging system in the VNIR (400–1000 nm) range, coupled with multivariate analysis for the prediction of major quality parameters of PBMB during the storage period. In this context, the objectives of the study were (i) to formulate plant-based meat burger patties and

characterize the effect of protein types and storage time on their quality, (ii) to extract spectral and spatial information from the hypercube images and develop multivariate statistical models for the prediction of selected quality parameters, (iii) to develop pixel-by-pixel prediction models for visualizing the quality changes, and iv) examine the feasibility of portable HSI for real-time measurements.

3.3 Materials and Methods

3.3.1 Sample preparation

The reference PBMB (control) was formulated on a mass basis (w/w), proportioned with 25% TVP, 10% pea protein powder (PP), 15% fava bean protein powder, 2% xanthan gum, 30% fat mimic, 10% potato starch, 1% soy lecithin, and 8% miscellaneous/ soluble taste components (natural flavorings, nutritional yeast, black strap molasses, beetroot powder, acetic acid, ascorbic acid, citrus extract). The PBMB fabrication process begins with the preparation of a coarse oil-in-water (o/w) fat emulsion from cacao butter, coconut oil, water, and xanthan gum using a homogenizer (X 120, Ingenieurbüro CAT, M. Zipperer GmbH) at 28.00 rpm for 20 minutes. Protein components were hydrated in the ratio of 1:2 (m/v) for 30 mins at room temperature. Subsequently, the mixture was blended with other dry ingredients and frozen fat emulsion using a lab scale mixer (KitchenAid®) to obtain a homogenous composite which was shaped into 2 cm thickness and 5 cm diameter. The physiochemical and optical properties of the control PBMB formulation were compared with commercially purchased PBMB and lean patty.

To create a diverse data set for predicting quality parameters, ten different formulations of PBMBs were developed by changing the proportions of major base components from the prepared control formulation. The stimulated PBMBs were categorized in 2 batches i.e., SET I, and SET II, having TVP, and PPC, as the base components respectively. Further, each set is divided into 5 formulations by varying the concentration of the respective base ingredients. Such, SET I consist of TVP 15%, 20%, 25%, 30%, and 35% (w/w); SET II consists of PPC 5%, 7.5%, 10%, 12.5%, and 15% (w/w). To stimulate handling and storage, the samples of each formulation from every set were packed in sealed plates, stored at a temperature of 5°C, and analyzed each day for 2 weeks.

A total of 140 stimulated PBMB samples (10 formulations × 14 storage time) were stored. After each corresponding storage time, they were scanned by the HSI-VNIR scanning and analyzed for their color, pH, water activity (a_w), moisture content, and texture (cohesiveness,

hardness, and stringiness). The values for each attribute for all tested samples were then used as reference values for calibrating the models for predicting these attributes.

3.3.2 Quality attributes determination

Using the standard AOAC method (AOAC, n.d.), the moisture content of the samples was obtained on a wet basis by drying the samples at 130 °C for 16 hours. The pH of the sample was determined using a digital pH meter (OAKTON pH 700, Cole-Parmer, Canada). Before the pH test, 3 grams of every sample set were homogenized in 20 mL of distilled water using (X 120, Ingenieurbüro CAT, M. Zipperer GmbH) (Bakhsh, Lee, Lee, Sabikun, et al., 2021). The color of the samples was measured and recorded using the (Chroma Meter CR–410, Konica Minolta, Japan). Upon calibration, CIE-L^* (lightness), a^* (redness) b^* (yellowness) were measured at three different locations across the sample surface. The values were then averaged for each color parameter. These values were used to calculate the color difference (ΔE) using the equation *(*Eq 3.1.),

$$\Delta E = \sqrt{(L - L_0)^2 + (a - a_0)^2 + (b - b_0)^2} \qquad (Eq\ 3.1.)$$

Where L, a, and b are color values of the sample of interest, and L_0, a_0, and b_0 are color values of either (i) day 1 samples, (ii) 15% TVP and 5% PP PBMB samples. The texture/mechanical strength of the sample was examined in terms of hardness, cohesiveness, and springiness using a texture profile analyzer (TPA) (LLOYD LS Materials Testing Machine) as reported by (Zhou et al., 2022). The software NEXYGENPlus™ was used to measure the parameters from the force versus time profile of the test samples. Samples were uniformly cut into 10×10×10 mm and then compressed to 75% of their original thickness at room temperature with a crosshead speed of 20 mm/s using a cylindrical probe with a diameter of 10 mm.

3.3.3 Hyperspectral imaging acquisition

VNIR hyperspectral images were obtained using the portable Specim IQ camera (Specim Inc., Finland) that employs a line scanning approach. Images were captured using diffuse reflectance mode and an integration time of 5 ms, obtaining data within the 400–1000 nm spectral range with 204 spectral bands; the camera also featured a spectral resolution of 7 nm. Images were obtained at a 22 cm distance from the samples. The setup was accompanied by a 575 W halogen-based lighting system with an incident angle of approximately 40° and supplemented with barn doors to direct and focus its illumination. The acquired images characterize data in a 3D hypercube of

dimensions X, Y, and Z at a resolution of 512 × 204 (spatial x spectral). The first two dimensions (X, Y) store spatial data forming a 2D image while the last dimension (Z) stores spectral data. Every pixel within the acquired image corresponds to a spectrum of reflectance against wavelengths. Specim IQ Studio, the accompanying software of the camera, was used to generate a library of spectra and create applications for the camera that allow it to identify components within an image in real time. To calibrate the captured images, the variation in sample illumination was corrected by incorporating a white reference panel within the image frame. The black reference is recorded as part of the data acquisition process of the camera. Further, the three-dimensional hypercubes of PBMB were analyzed using MATLAB (Mathworks Inc., Natick, MA). Regions of interest (ROI) of PBMB were selected and stored in a spectral library.

3.3.4 Multivariate analysis

3.3.4.1 Principal component analysis

Principal component analysis (PCA) was used as an unsupervised exploratory tool on spectral data (PCA-S) to examine the spectral features of stimulated PBMB samples and to inspect possible spatial separation of PBMB samples based on ingredient concentration and storage periods. PCA-S was carried out using MATLAB-compatible PLS Toolbox 8.6 (Eigenvector Technologies, Manson, MA). The mean reflectance spectra of each PMBM were first derived from the acquired hyperspectral images of PBMB by averaging regions of interest (ROI) for VNIR spectral ranges. VNIR spectra were pre-processed by Savitzky-Golay 1st Derivative (9-point window, polynomial order 2, 11-point window) and mean centering, which was optimized to provide the best results compared to raw, multiplicative scatter correction (MSC), and standard normal variate (SNV). PCA-S was then applied for spectral data compression which projects the selected spectral data into principal components (PCs). The PCA-S loadings were assessed to determine the probable association between variables. Further, PCA on measured quality variables (PCA-M) was carried out using OriginPro Software, version 8.5 (OriginLab Corporation, Northampton, USA), to visualize and quantify relations between the selected PBMB samples.

3.3.4.2 Partial least square regression modeling

PLS toolbox was used to implement the PLSR modeling for the prediction of quality characteristics including color values (a^*, b^*), textural properties (hardness), and physiochemical properties such as moisture, pH, and a_w. Similar to PCA, the spectral dimensionality was minimized by projecting the spectral data onto the latent variables (LV) in the PLSR approach. A

global data matrix of 140 × 204 (samples × vector of spectra) was split into a training/calibration set (80%) and a test/external validation set (20%). Venetian blinds cross-validation was conducted, involving 10 data splits with 1 sample per blind. Based on the lowest cross-validation error, the optimal number of LVs was selected. The selection of the optimal model was based on the highest coefficients of determination (R^2) and lowest root mean square errors (RMSE) in calibration (R^2_C, RMSEC), cross-validation (R^2_{cv}, RMSECV), and prediction (R^2_P, RMSEP). Five preprocessing conditions were evaluated with raw spectra (Model 1), Savitzky-Golay 1st derivative (Model 2) with a 9-point window, 2nd order polynomial, 11-point window, mean centering (Model 3), combination of 1st derivative with mean centering (Model 4), and smoothing (Model 5). These evaluations aimed to identify the most accurate model functions for predicting individual quality attributes.

3.3.4.3 Statistical analysis

OriginPro Software, version 8.5 (OriginLab Corporation, Northampton, USA) was used to perform one-way ANOVA, and Tukey pairwise comparison test to determine statistical significance among the quality traits of selected samples. A significance level of p-value < 0.05 was used to indicate statistical significance.

3.4 Results and Discussion

3.4.1 Effect of storage period and protein type on quality

The visual resemblance of the prepared control PBMB to commercial PBMB and the beef patty is depicted in **(Fig. 3.1)**. **Table 3.1** exhibits significant variations in quality traits for the prepared PBMB formulations. The wide range and a reasonable degree of variability within each quality trait would enhance the predictive model's robustness by encompassing a broad range of spectral features, enabling a more accurate quality prediction.

3.4.1.1 Color analysis

The magnitude of visual variation among the PBMBs on the first day of storage is indicated by the color coordinates presented in **Table 3.2**. In comparison to PP-based PBMBs, TVP-based PBMB samples exhibited significantly higher L^* and lower b^* values ($p < 0.05$), This is attributed to the greater hydration capacity of TVP and consequent dilution of the betalain pigment (Ryu et al., 2023).

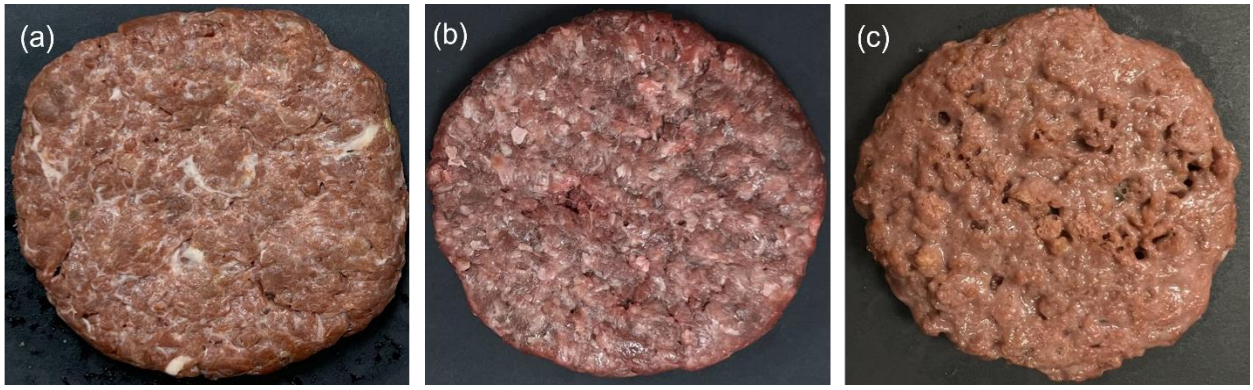

Figure 3.1 Images of (a) prepared control PBMB; (b) beef burger patty; (c) PBMB purchased from local market. *PBMB- Plant-based meat burger

Table 3.1 Summary of variations in quality traits of the prepared plant-based meat burgers

Quality trait	Minimum	Maximum	Mean	Standard Deviation
L*	44.91	61.60	53.90	3.79
a*	12.83	18.18	15.13	1.19
b*	10.49	16.75	14.04	1.49
Moisture (% Wb)	46.12	62.50	55.90	2.95
pH	5.98	6.65	6.37	0.14
a_w	0.94	0.97	0.96	0.01
Hardness (N)	7.16	21.12	11.28	2.69
Cohesiveness (N)	-4.45	0.38	-0.72	0.72
Stringiness (mm)	-120.46	-6.54	-55.97	13.85

The addition of TVP in PBMB formulations resulted in a significant decrease in *a** and *L** as TVP content increased from 15% to 35%. Specifically, *a** decreased from 16.52 ± 0.17 to 14.06 ± 0.13, while *L** decreased from 61.69 ± 0.65 to 52.66 ± 0.43. Conversely, *b** increased from 10.82 ± 0.14 to 13.15 ± 0.11, resulting in a darker and slightly less saturated reddish-brown hue compared to the 15% TVP sample. These findings align with prior research (Bakhsh et al, 2021), which also reported a decline in *L** and *a** values and an increase in *b** values with increasing TVP content in PBMB, both before and after cooking. Whereas the addition of PP in PBMB formulation from

5% to 15% resulted in increased *L** and *a** values ($p < 0.05$), and decreased *b** values, giving the samples a light brown color with a reddish hue compared to the 5% PP sample. This can be attributed to the smaller particle size and uniform distribution of PP, due to its strong water-binding capacity. Furthermore, the higher PP content in PBMB samples led to a significant increase in surface water content, suggesting a greater degree of light reflection. The quality degradation of a representative sample (TVP 25%) during the storage period is presented in **Table 3.3**. Until day 4, there were no statistically significant variations in the *L** and *a** values, suggesting a stable redness. From day 8, a decrease in *L** and *a** values of PBMB were observed ($p < 0.05$), indicating a darker color and reduced redness. Sakai et al. (2022) explained a similar change in the color of TVP-based PBMB. The *b** value exhibited a sharp increase from day 8 ($p < 0.05$), indicating a more pronounced shift towards a yellow color in PBMB. Similar findings regarding the effect of storage time on sausages were reported (C. H. Feng & Makino, 2020). The results obtained suggest that the stimulated PBMB formulations had been successful at accurately mimicking the light scattering and absorption behavior of the commercial PBMB and beef burger patties.

3.4.1.2 pH value

The pH values of the prepared PBMBs, as depicted in **Table3. 2**, ranged from 5.98 ± 0.02 to 6.65 ± 0.01, which are consistent with (Bakhsh, Lee, Lee, Sabikun, et al., 2021). An increase in pH was observed from 6.40 ± 0.01 to 6.65 ± 0.01 ($p < 0.05$) with an increase in TVP content from 15% to 35%, due to the slightly alkaline nature of TVP (pH 7.42–7.43) (De Marchi et al., 2021). The drop in pH values from day 8, as illustrated in **Table 3.3**, indicates a deterioration process during storage ($p < 0.05$) (Ardila et al., 2023). This is primarily attributed to the growth of molds, which metabolize the nutrients in the PBMB under reduced O_2 levels and produce lactic acid and other organic acids. These metabolic by-products contribute to the decrease in pH observed during storage (Ardila et al., 2023).

3.4.1.3 Moisture content and water activity

An increase in moisture contents ($p < 0.05$) of PBMBs, ranging from 57.49 to 59.79%, for 15–35% TVP, and 56.59 to 59.81% for 5–25% PP, is depicted in **Table 3.2**. (Bakhsh, Lee, Lee, Sabikun, et al., 2021) examined the effect of methylcellulose on different concentrations of TVP-based PBMB and reported a moisture increase from 48.32 to 57.43% with an increase in commercial TVP.

Table 3.2 Effect of ingredient composition on the quality traits of plant-based meat burgers (PBMB)

Ingredient	*L**	*a**	*b**	*ΔE*	pH	a_w	Moisture (%, Wb)	Cohesiveness (N)	Hardness (N)	Stringiness (mm)
TVP 15%	61.69±0.65^{a}	16.52±0.17^{b}	10.82±0.14^{f}	-	6.40±0.01^{c}	0.967	57.49^{cde}	-0.87±0.68^{a}	10.86±3.85^{ab}	-32.95±0.37^{a}
TVP 20%	59.45±0.37^{b}	16.21±0.14^{bc}	10.93±0.07^{f}	1.91±0.36^{d}	6.42±0.00^{c}	0.967	57.73^{bcd}	-0.30±0.06^{a}	8.54±6.49^{b}	-33.32±0.23^{a}
TVP 25%	58.84±0.63^{b}	14.86±0.14^{def}	11.91±0.12^{e}	3.16±0.53^{cd}	6.54±0.00^{b}	0.96	58.23^{bc}	-0.85±0.93^{a}	8.81±1.94^{b}	-33.24±0.23^{a}
TVP 30%	56.22±0.02^{c}	14.36±0.09^{ef}	12.43±0.11^{de}	5.75±0.08^{b}	6.56±0.01^{b}	0.964	58.33^{bc}	-0.44±0.00^{a}	7.86±0^{b}	-36.91±0.00^{a}
TVP 35%	52.66±0.43^{d}	14.06±0.13^{f}	13.15±0.11^{cd}	9.30±0.35^{a}	6.65±0.01^{a}	0.961	59.79^{a}	-0.40±0.04^{a}	10.91±5.44^{ab}	-31.91±0.27^{a}
PP 5%	46.22±0.76^{f}	15.10±0.99^{cdef}	15.37±0.42^{a}	-	5.98±0.02^{e}	0.955	56.59^{de}	-3.22±2.54^{a}	15.28±2.72	-120.47±0.86^{e}
PP 7.5%	49.31±0.31^{e}	15.76±0.46^{bcd}	15.61±0.44^{a}	4.07±0.55^{bc}	6.00±0.01^{e}	0.959	57.20^{e}	-1.30±0.27^{a}	18.28±4.10^{ab}	-55.04±17.47^{bc}
PP 10%	50.87±1.36^{de}	15.67±0.26^{bcd}	14.62±0.23^{b}	5.46±1.25^{b}	6.18±0.03^{d}	0.963	58.39^{bc}	-2.30±1.80^{a}	13.88±4.79^{ab}	-47.49±4.18^{ab}
PP 12.5%	51.08±0.25^{de}	15.56±0.49^{bcde}	14.49±0.22^{b}	5.63±0.36^{b}	6.42±0.01^{c}	0.964	58.53^{b}	-2.15±1.54^{a}	11.27±1.19^{ab}	-68.89±0.00^{cd}
PP 15%	52.43±0.62^{d}	17.77±0.46^{a}	13.45±0.26^{c}	7.87±70^{a}	6.50±0.04^{b}	0.965	59.81^{a}	-0.59±0.26^{a}	21.70±2.00^{a}	-78.65±0.00^{d}

Data are presented as mean values (n = 3) and data that do not share a lowercase superscripted letter in the same column are significantly different ($p < 0.05$). TVP - textured vegetable protein; PP - pea protein

Table 3.3 Effect of storage period on the quality parameters of Control PBMB formulation

Storage Period	*L**	*a**	*b**	pH	a_w	Moisture (%, Wb)	Cohesiveness (N)	Hardness (N)	Stringiness (mm)
Day 1	58.84±0.63^{a}	14.86±0.14^{a}	11.91±0.12^{c}	6.54±0.00^{a}	0.96	58.23^{a}	-0.85±0.93^{a}	8.81±1.94^{d}	-33.24±0.23^{a}
Day 4	58.02±0.79^{a}	14.20±0.27^{a}	13.15±0.20^{b}	6.52±0.01^{ab}	0.961	56.38^{b}	-0.8497^{a}	9.64±2.08^{cd}	-47.60±0.30^{ab}
Day 8	56.74±0.09^{b}	14.04±0.06^{b}	14.36±0.01^{a}	6.50±0.01^{bc}	0.952	55.48^{c}	-0.4005^{a}	11.29±2.51^{bc}	-57.31±0.00^{bc}
Day 12	55.25±0.03^{c}	13.66±0.04^{c}	13.95±0.01^{a}	6.48±0.01^{c}	0.954	54.06^{d}	-0.2404^{a}	12.19±5.69^{ab}	-60.03±0.75^{bc}
Day 14	55.22^{c}±0.09	13.04±0.05^{c}	14.46±0.09^{a}	6.48±0.00^{c}	0.948	53.52^{e}	-0.2124^{a}	14.28±9.11^{a}	-61.25±10.45^{c}

Data are presented as mean values (n = 3) and data that do not share a lowercase superscripted letter in same column are significantly different ($p < 0.05$). Control formulation = 25% textured vegetable protein (w/w)

As expected, PBMB samples stored for longer durations exhibited lower moisture content ($p < 0.05$) than the corresponding fresh samples. Moisture of the control PBMB formulation was recorded as 58.23% on day 1 and 53.52% on day 14. The loss of moisture can be attributed to migration or evaporation during the storage and handling of meat alternatives, as explained by (Vallikkadan et al., 2023b). Further, loss of free/surface water could be witnessed with the decrease in a_w ($p < 0.05$) as shown in **Table 3.3**. The observed a_w value exceeding 0.95 aligns with findings from (Ardila et al., 2023), indicating the susceptibility of PBMB to microbial activity, and highlighting the importance of appropriate storage conditions.

3.4.1.4 Texture

The effect of major protein ingredient type and composition on TPA parameters (hardness, cohesiveness, and springiness) obtained from force versus time curves of double compression tests, is shown in **Table 3.2.** The TPA ranges as mentioned in **Table 3.1** are in in-line with the results reported by (Dreher et al., 2021)(Bakhsh Allah AND Lee, 2021; Sakai et al., 2022). The TPA parameters of PBMBs containing PP as the major ingredient are significantly higher ($p < 0.05$) compared to those with TVP as the major ingredient. TVP addition decreased the TPA parameters of PBMB ($p < 0.05$). (Vallikkadan et al., 2023b) highlighted the specific impact of individual plant proteins on the textural characteristics of HMMA. These findings are consistent with (Bakhsh, Lee, Lee, Sabikun, et al., 2021), who reported that compression values increased when the proportion of TVP decreased, likely due to their binding property. However, marginal, or no significant difference in springiness values was observed with TVP or PP addition ($p > 0.05$). With storage time, the hardness, and cohesiveness of model PBMB increased ($p < 0.05$) due to the relative decrease in moisture content as described by previously mentioned studies. Whereas cohesiveness was lowered during storage ($p < 0.05$). (Zhou et al., 2022) described a similar effect in PBMB due to the reduced strength to withstand fracture in a patty.

3.4.2 Principal component analysis on measured (PCA-M) quality variables

To acquire a better understanding of the pattern captured by the measured quality variables, a data matrix of 10 PBMB formulations × 11 quality traits from the day 1 sample was used in PCA-M. PC1, responsible for 53.40% of the total variance, primarily explains the $L*$, pH, moisture, a_w, cohesiveness, and stringiness. PC2, accounting for 21.24% of the total variance, predominantly relates to $b*$, moisture content, and a_w. The scores of the biplot **(Fig. 3.2)**, explain the variation

among the PBMB formulations and the loadings explain the correlation between the quality traits of the PBMB.

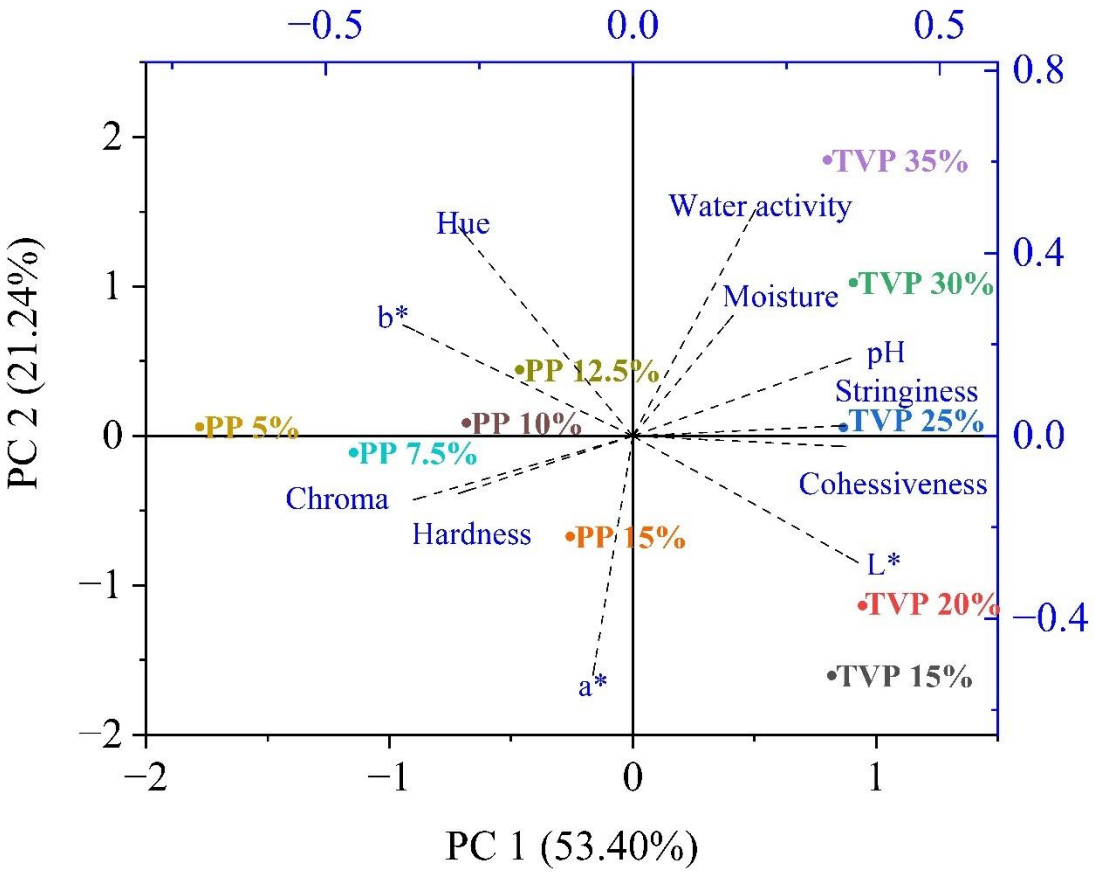

Figure 3.2 Principal Component Analysis biplot on measured quality variables of 10 different plant-based meat burger formulations. TVP – Textured Vegetable Protein proportion, PP-Pea Protein proportion

It can be observed that the scores of the samples on the first two principal components (PCs) plane effectively represented the pattern of increasing TVP and PP concentration. PC1 captured the main variability among the major ingredient types (TVP and PP), where the TVP-based samples had positive scores while PP-based samples had negative scores. Further, PC2 primarily reflected the variability associated with TVP concentration, where the samples with low TVP% had negative scores, with an increase in TVP% the scores were positive. Loadings of PC1 signify that the higher weights were for *a**, *L**, a_w, and moisture. Moreover, the loadings of the biplot **(Fig. 3.2)** signify that, (i) among TVP-based PBMBs, samples with 15% and 20% TVP are lighter, less yellowish, reddish, and have lower pH, moisture content, and water activity. Whereas samples

with 25–35% TVP are relatively darker lighter, slightly yellowish, pale red, and have higher pH, moisture content, and a_w; (ii) among PP-based PBMBs, as the concentration increases from 5–15% PP, yellowness reduced, lightness, reddishness, a_w, moisture, and pH relatively increased. The existence of complex correlations between the PBMB formulations and physio-chemical parameters was quantified and visualized through PCA-M. This outcome justifies the requirement for chemical mapping to ensure the quality of meat alternatives. Moreover, the deductions derived from **(Fig. 3.2)** are utilized to validate the unsupervised spectral characterization in the subsequent sections.

3.4.3 Characteristics of VNIR spectra

Fig. 3.3 illustrates the mean spectra derived from the region of interest in the selected PBMB samples, encompassing 204 wavelengths within the VNIR range (400–1000 nm). A similar spectral pattern, but significant distinction in the magnitudes of reflectance intensities could be observed as the protein type and concentrations are varied **(Fig. 3.3a)**, as well as over the storage period **(Fig. 3.3b)**. The observed spectral pattern was in good agreement with the results of Sakai et al. (2022), who investigated the objective color attributes and reflectance difference of the PBMB using a colorimeter. Sakai et al. (2022) reported a rapid increase in reflectance in PBMB made with beet pigments, featuring a prominent valley near 600 nm. Higher reflectance values are observed in PBMBs with higher PP%, lower TVP %, and fresh samples respectively **(Fig. 3.3a)**. The variations in the major chemical composition of the PBMB samples lead to variations in the internal absorption and scattering characteristics. The presence of noise and baseline drift within the raw mean spectra were minimized through spectral preprocessing, **Fig. 3.3c** shows the first-order derived spectral response. Clear spectral shifts with increasing storage days could be observed at ~550 nm **(Fig. 3.3d)** and ~900 nm **(Fig. 3.3e)**. A similar spectral trend in the VNIR range for sausages stuffed in different casings during the storage period was reported by (C. H. Feng & Makino, 2020). According to the relevant literature on meat muscles (Hasan et al., 2022) (Elmasry et al., 2013) (Chaudhry et al., 2021), slopes at 500–650 nm are correlated to the pigments are responsible for the color and redness of meats. A wide peak detected near 950–980 nm is attributed to the third and second overtones of O-H stretching, respectively.

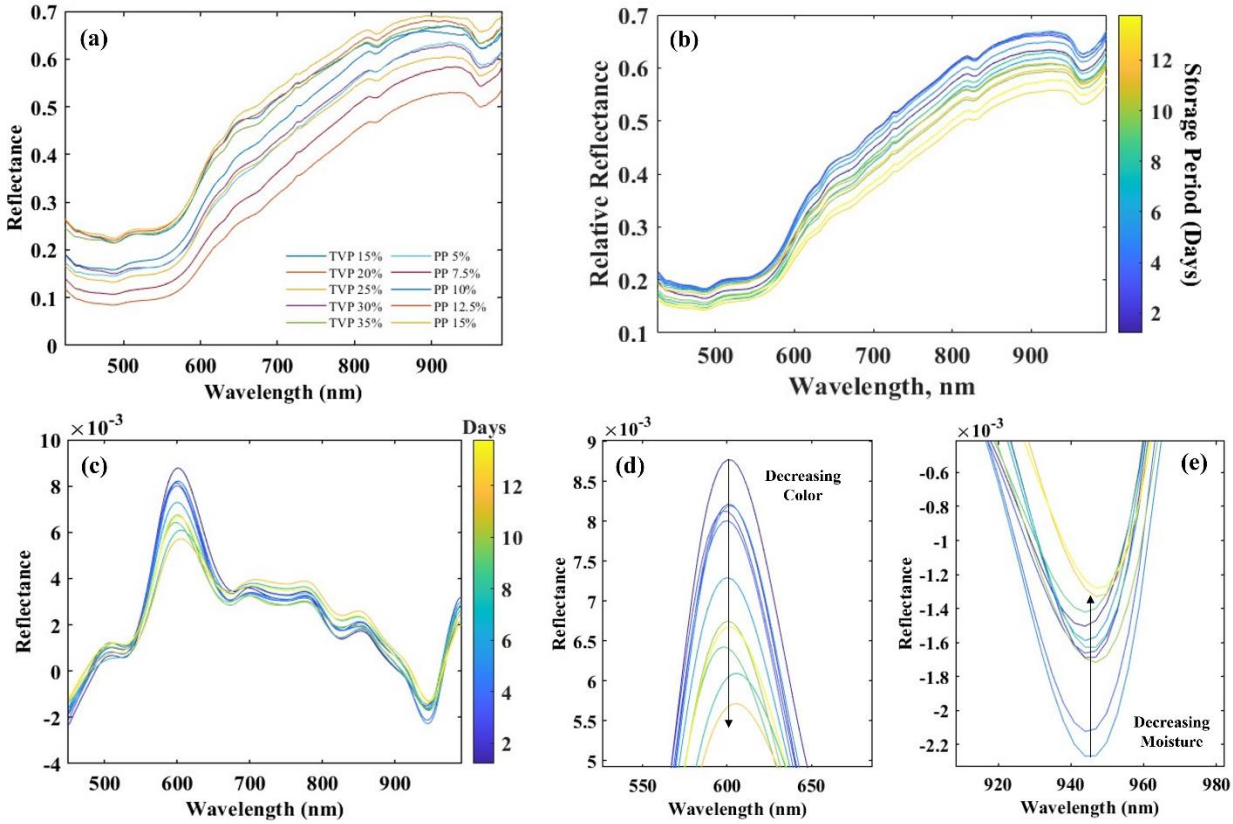

Figure 3.3 Overview of spectral changes in the VNIR range of plant-based meat burgers (PBMB): a) mean spectra extracted from samples of day 1, b) mean spectra extracted from day 1 to day 14 of the control PBMB, c) 1st derivative pre-processed spectra of control PBMB, d) spectra response in ~ 550 nm, e), spectra response ~ 920 nm. * Control PBMB – 25% Textured Vegetable Protein proportion.

The broad and overlapping absorption bands in the NIR range are a result of the intricate composition of food samples, arising from combinations of fundamental vibrations and overtones of functional groups (such as O-H, C-H, and N-H). Sierra et al. (Sierra et al., 2008) and De Marchi et al. (De Marchi et al., 2013) reported that 934–960 nm and 984–996 nm are related to moisture, whereas 962–968 nm are associated with fat. The observed distinct spectral variations among PBMBs highlight their potential for establishing reliable prediction models. Further, the reflectance measurements in the present study extend to the entire VNIR range and cover the entire sample surface, allowing for a more detailed investigation.

3.4.4 PCA-S based unsupervised classification

3.4.4.1 Discrimination based on the storage period

To understand the underlying patterns within the spectral responses, PCA applied on spectra is presented in **Fig. 3.4**. In **Fig. 3.4a,** it can be noted that **the** first two PC scores represented the pattern of increasing storage days i.e., sample freshness. The maximum variability of 52.15% was explained by PC1, followed by PC2 which accounted for only 25.70% of the total data variability. PC1 captured the main variability associated with sample freshness, with positive scores for fresh samples had positive scores and negative scores for those stored beyond day 8. The loading profile corresponding to these changes in the PC scores **(Fig. 3.5a)** indicated that the most key variables contributing to these variations were identified at approximately 500, 525, and 600 nm (related to beet pigments) and 820, and 950nm (related to O-H). This clear distinction indicates that the primary source of variance on PC1 is associated with the discoloration of samples, while PC2 is primarily related to the loss of moisture during the storage period.

The significant change in CIE-LAB color space on day 8 samples **(Table 3.2)** and the variation in spectra responses in the 500–700nm over the storage period **(Fig. 3.3)** validate the abovementioned statements. Sakai et al. (2022) reported a change in reflectance values at 500–700 nm due to the discoloration of PBMB made with beet during grilling. Based on previous research works, the discoloration of PBMBs could be primarily due to the oxidation of beet pigments during storage which results in a deep brownish color. Betacyanins and betaxanthin, the two groups of betalains (beet pigment), are absorbed in wavelengths of 535 and 580 nm and 420 and 480 nm, respectively. However, their absorption of light varies with their chemical structure. During the storage of PBMB, the alteration in pH significantly affects the chemical structures of betalains (Botella-Martínez et al., 2022), leading to changes in their stability and solubility thus changing the absorption peaks (Moss, 2002). Further, the breakdown of amino acids, change in temperature, pH, and influence of other ingredients in PBMBs produce xanthophylls (Dawson & Acton, 2018). Xanthophylls, a yellow pigment responsible for a change in yellowness of PBMB is attributed to the peak ranges from 470 to 530 nm. Accordingly, a significant increase in b^* from 11.9 to 14.46 ($p < 0.05$) was observed **(Table. 3.2.)**. Further, it can be noted that **(Fig. 3.2)** illustrates that pH is negatively correlated with b^*, thus loadings on PC1 from spectral data also explain the pH of PBMB samples.

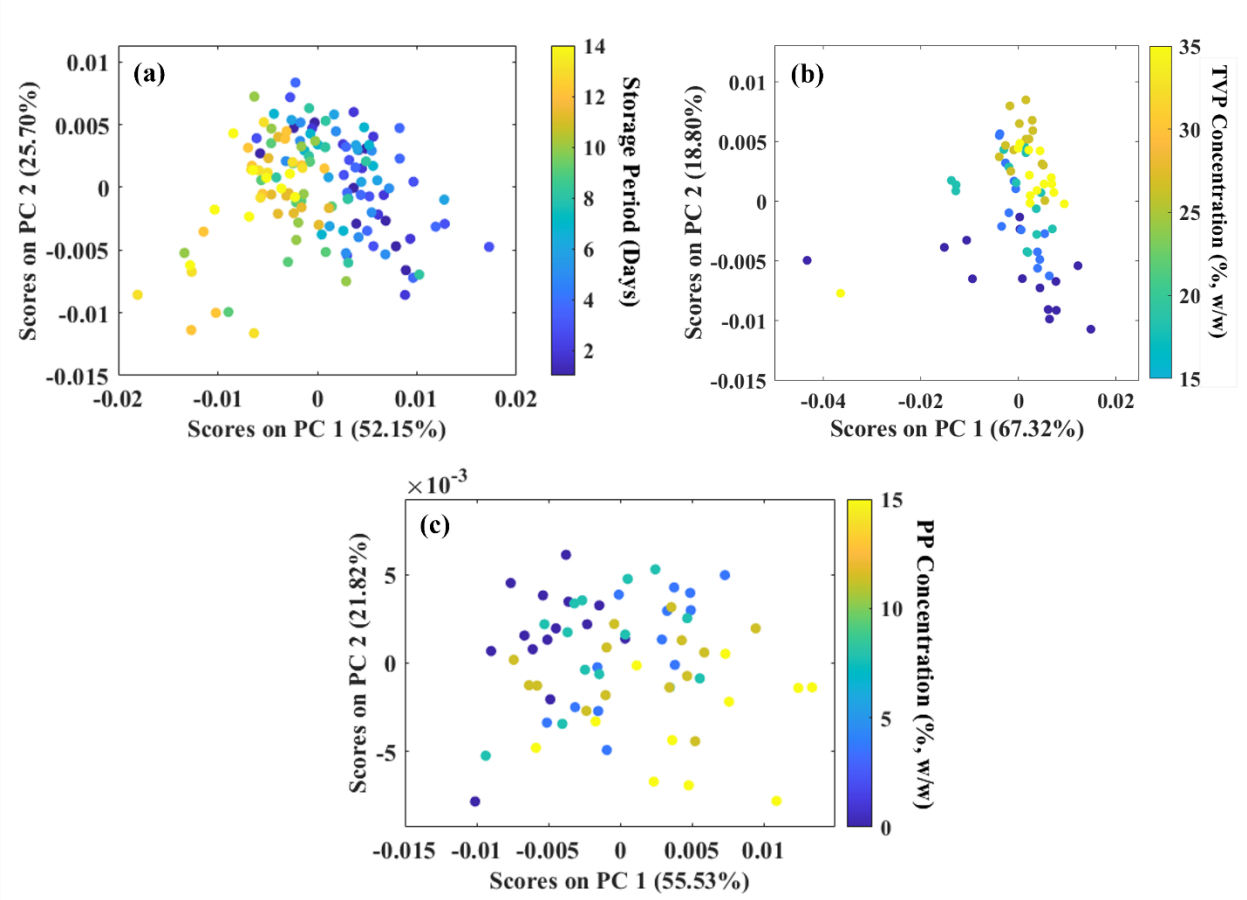

Figure 3.4 Principal component analysis scores plot: a) 140 PBMB samples during 14 days of the storage period, b) 70 Textured vegetable protein based PBMB samples; c) 70 Pea protein based PBMB samples. *PBMB- Plant-based meat burger

PC2 loadings indicated that the effect of moisture dominated the magnitude of the spectra concerning samples of different storage periods **(Fig. 3.5a)**, as the peak around 950 nm was attributed to the third overtone of O-H. Overall loss of moisture and free water evaporation during the storage and handling of PBMBs have been discussed in Section 3.1.3. **(Fig. 3.3b)** showed clear and distinctive lowering of reflectance with longer stored samples. The porous matrix of PBMB tissues, which contains starch, is primarily supported by a complex matrix of cellulose and water. As water is lost from this matrix during storage, a collapse of the matrix occurs, leading to a reduction in both cellulose pore size and starch granules. This, in turn, results in a decrease in scattered energy at the surface. The gradual decrease in moisture and free water ($p < 0.05$) **(Table 3.3)** with time supports the statement.

During storage, a change in pH affects the structure of proteins thereby increasing the exposure of hydrophobic regions in the protein molecules, which can form a hydration shell to stabilize the protein structure (Balcão & Vila, 2015), resulting in a decrease in the free water content of PBMB. Thus, the loadings on PC2 also explain pH which is positively correlated with moisture **(Fig. 3.2)**. (Wu et al., 2014) observed that alterations in dry matter and textural properties of meat samples are primarily reflected in the spectral profiles within the NIR region of 800 to 1000 nm. Sierra et al. (Sierra et al., 2008) and De Marchi et al. (De Marchi et al., 2013) indicated that 934–960 nm and 984–996 nm are related to moisture, whereas 962–968 are associated with fat. Loss of moisture content during storage increases the force required to disrupt the PBMBs. The effect of moisture and fat on texture has been discussed in Section 3.1.4. Thus, the loadings on PC2 also explain hardness which is negatively correlated with moisture **(Table 3.2)**. It can be noticed that in **(Fig. 3.4a)**, some data points are overlapping. This can be attributed to the minimal color change within a short duration and moisture migration causing similar internal absorption and scattering. (Chaudhry et al., 2021) reported that 2–8-day post-mortem beef samples didn't show clear discrimination when compared to 14–21-day post-mortem due to the minimal variations in the physiochemical properties of 2–8-day post-mortem samples.

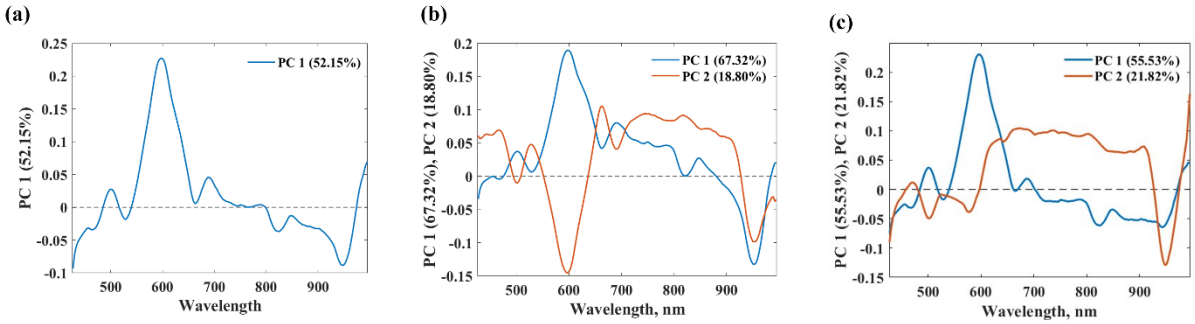

Figure 3.5 Principal component analysis loadings plot: a) 140 PBMB stored samples b) 70 Textured vegetable protein based PBMB samples, c)70 Pea protein based-PBMB samples PBMB samples. *PBMB- Plant-based meat burger

3.4.4.2 Discrimination based on plant-protein concentration

PCA-S was applied for SET 1 and SET 2 PBMB samples separately to understand the pattern of spectral responses with respect to protein type and concentration. It can be noted in **Fig. 3.4b**, that the main variability related to TVP concentration was captured by the PC2, where the

higher TVP concentration had positive scores, while samples with lower TVP concentration had negative scores. Observing the loadings plots, **(Fig. 3.5b)** variables responsible for classifications were those are 500, 525, 590–600, 680, 700, 800–850, and 950 nm. Notably, the impact of TVP on the spectral characteristics is attributed to its water-binding capacity and fibrous structure. The change in the amount of water bound with TVP's porous structure leads to a modified light absorption property, consequently resulting in changes in reflectance values. This observation aligns with the findings of (Bakhsh, Lee, Lee, Sabikun, et al., 2021), which reported that increased TVP concentration in PBMB enhances its water-absorbing capacity within the porous structure. An increase in TVP % in PBMB formulation affects the behavior of beet pigments by diluting their concentration, as it spreads the pigments over a larger protein matrix, potentially reducing their intensity. Betalains in beet powder are sensitive to changes in pH, and the rise in pH with TVP% **(Table 3.1)** affects the water activity influencing the solubility and dispersion of beet pigments. These factors collectively contribute to the observed color changes **(Table 3.1)** and spectral variations as depicted in **Fig 3.5b**.

Similarly, it is evident from **Fig. 3.4c** that PBMB samples with lower PP% exhibit relatively higher PC2 scores, and samples with higher PP content hold high positive scores on PC1. The associated loading profile **(Fig. 3.5c)** indicates that variations in pea protein (PP) concentration and its interactions with beet pigments led to alterations in light absorption and reflection within the VNIR range. In **Fig. 3.4c**, certain samples with low concentrations exhibit negative PC2 scores, overlapping with samples having higher PP%. These samples were identified through the PC2 score vs. samples plot. Subsequently, the quality attributes of the identified overlapping samples were compared, and there was no significant difference in their color intensity, moisture, and a_w ($p > 0.05$). The successful clustering of PBMBs shows the potential of VNIR-HSI to classify PBMBs based on their formulations and storage time. It is important to note that the PCA-S was performed on the pre-processed spectra. Therefore, when interpreting the loadings in relation to the original variables, it is important to consider the changes in signal profiles that arise from the derivation process.

3.4.5 PLSR Prediction models

To calibrate the portable hyperspectral imaging device with reference quality parameters measured through traditional wet-chemistry methods, PLSR regression was conducted, as pre-calibration is necessary for any spectral sensing approach. Following the approach of (Mishra et

al., 2022), a global PLSR model was developed from 140 PBMB samples (combining data from SET 1 and SET 2), aiming to enhance generalized solutions by capturing the chemical overtones unique to each sample variety.

The performance of PLSR models with various pre-processing techniques for predicting *a**, *b**, moisture, and hardness is presented in **Fig. 3.6**. In the case of redness prediction **(Fig. 3.6a)**, Model 1, which uses raw spectra, has a lower R^2_{CV} (0.88) and a higher RMSEP (0.38) compared to Models 3 and 4. This suggests that preprocessing methods can enhance prediction accuracy. Model 4 exhibits the highest R^2_{CV} (0.93) and the lowest RMSEP (0.28), which indicates a strong correlation between the predicted values and the reference data, and the model's ability to generalize well to new data, resulting in accurate predictions.

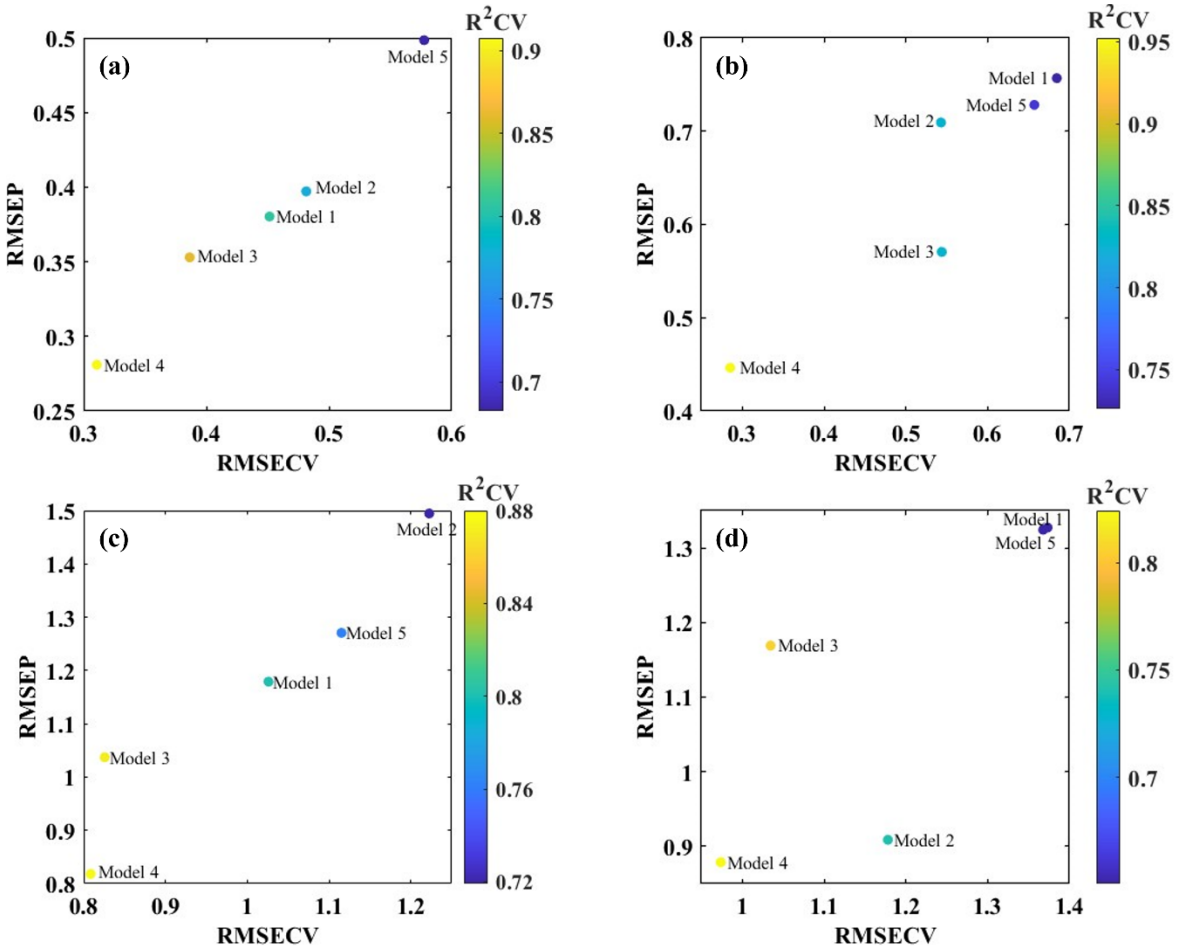

Figure 3.6 Comparison of the performance of prediction models based on preprocessing methods: a) redness (a*) value, b) yellowness (b* value), c) moisture content, d) hardness. Model 1 - raw spectra, Model 2 - 1st derivative, Model 3 – mean centering, Model 4 – 1st derivative mean centering, Model 5 – smoothing.

Whereas Model 5 displays the lowest R^2_{CV} (0.738) and the highest RMSEP (0.498), indicating that the smoothing may have removed valuable information from the spectra. Based on the R^2_{CV} and RMSEP, Model 4 (Mean Center, 1st Derivative) appears to be the best pre-processing for the prediction of redness, yellowness **(Fig 3.6b)**, moisture **(Fig 3.6c)**, and hardness **(Fig 3.6d)**. This can be attributed to mean centering's capability to eliminate constant offset in the data, thereby reducing the variations caused by instrument drift and variation in measurement or sample conditions. Additionally, the 1st Derivative differentiation process enhances subtle spectral features and patterns.

Table 3.4 Summary of full wavelength PLSR prediction modeling results

Parameters	Calibration		Cross Validation		Prediction		LV
	R^2_C	RMSEC	R^2_{CV}	RMSECV	R^2_P	RMSEP	
*L**	0.82	1.59	0.77	1.83	0.81	1.82	6
*a**	0.92	0.64	0.89	0.76	0.92	0.74	5
*b**	0.96	0.24	0.95	0.28	0.93	0.44	6
Moisture	0.90	0.71	0.87	0.80	0.90	0.81	4
Hardness	0.85	0.87	0.82	0.97	0.81	0.87	5
pH	0.81	0.06	0.71	0.08	0.71	0.08	7
a_w	0.82	0.01	0.77	0.01	0.72	0.02	6

LV = latent variables, R2 = coefficients of determination, RMSE = root mean square errors

The results of the PLS regression models built with Mean Center and 1st Derivative are presented in **Table 3.4** and predicted vs. measured plots are depicted in **Fig. 3.7**. Through cross-validation, the number of LVs was determined, yielding a range of 4 to 7 LVs for nearly all the analyzed parameters. In calibration, R^2_C exhibited a range of 0.81 (pH) to 0.96 (*b**), indicating a strong correlation between the predicted and actual values. Additionally, the obtained errors, as indicated by RMSECV and RMSEP were consistently low, supporting the accuracy and reliability of the models. Further, the small difference between the RMSECV and the RMSEP signifies the good stability of the obtained models. This finding suggests that the models possess reliable predictive capabilities and can produce accurate results beyond the training dataset. As this study

represents the first instance of simultaneously detecting quality parameters in PBMB using a completely non-invasive technique, the prediction models developed in this study are compared to previous relevant studies primarily focused on the VNIR wavelength range for assessing quality in red meats.

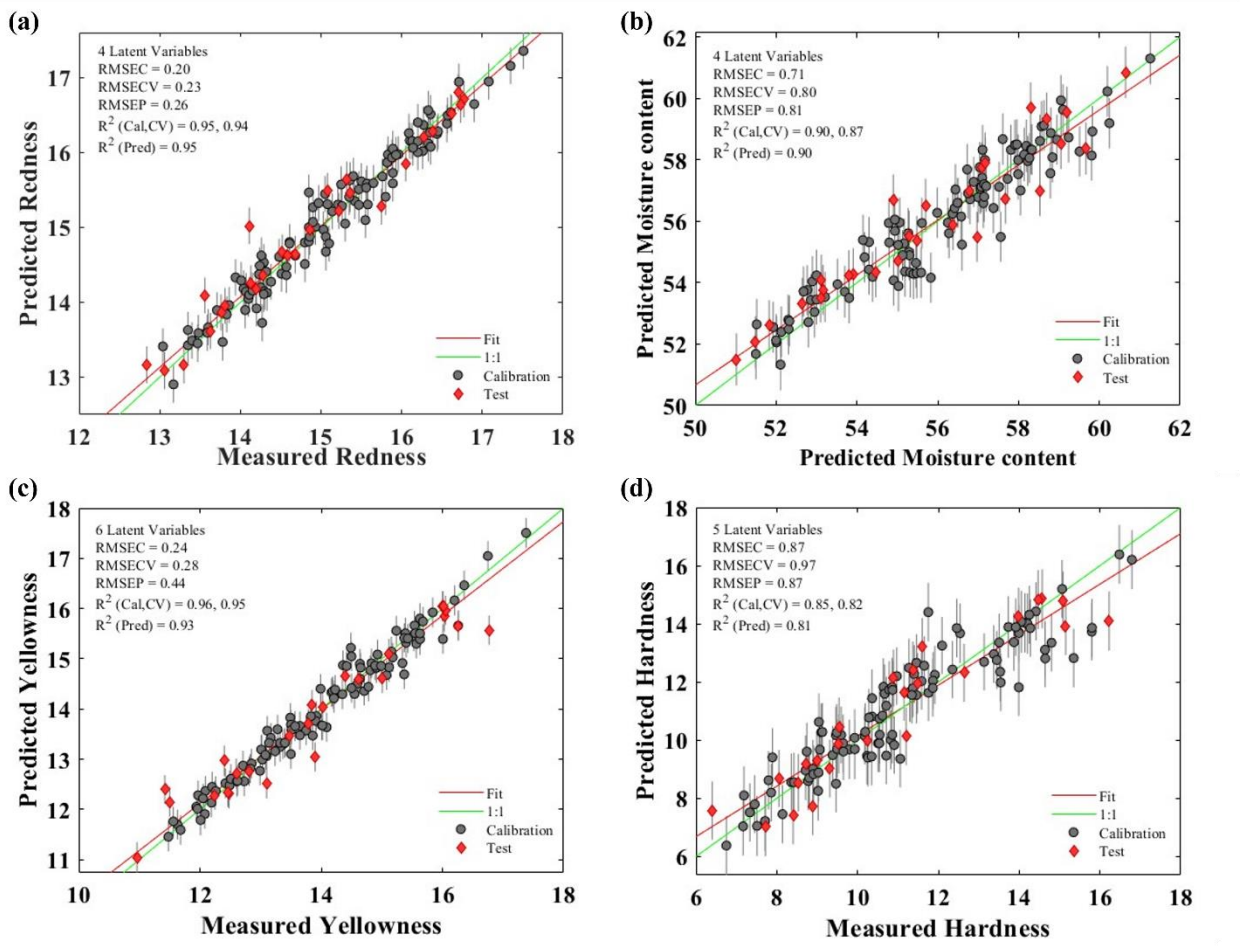

Figure 3.7 Calibration plots for the prediction of quality parameters: a) redness (a*) value), b) moisture content, c) yellowness (b* value), d) hardness

3.4.5.1 Prediction of color and hardness

The developed PLSR models on the full spectral range for redness with 5 LVs **(Fig. 3.7a)** and yellowness with 6 LVs **(Fig. 3.7b)**, yielded good accuracy in predicting as evidenced by strong correlations (R^2_P=0.92 for *a** and R^2_P=0.93 for *b**) and minimal prediction errors. In addition to the absorption due to pigments **(Section 3.4., Chapter 3)**, (Purslow et al., 2020) explained that the reflectance of meat samples is influenced by some achromatic factors like microstructures of meat tissues. A parallel concept could be drafted for PBMB, as the porous nature of TVP or solubility

of PP affects the microstructure changes with the formulation. In this regard, the information captured by the VNIR signal is limited to represent the L^* due to the huge variability in the microstructural properties caused by the interplay of multiple ingredients, thereby resulting in lower prediction accuracies for L^*. The increased deviation and reduced accuracy in predicting hardness were evident from the scattered data points of the hardness prediction model **(Fig. 3.7d).** The performance of prediction models is contingent upon the representativeness and variability of the reference data. Hence, the limited availability of instances with similar hardness values could be considered one of the reasons. Additionally, the prediction of internal moisture could have been limited due to the restricted penetration depth of VNIR waves. However, the predicting ability was comparable with (Kamruzzaman et al., 2013), who reported an R^2_{CV} of 0.83 and RMSECV of 5.88 N for tenderness prediction on 1st derivative NIR spectra, with 934 and 964 nm as one of the feature wavelengths.

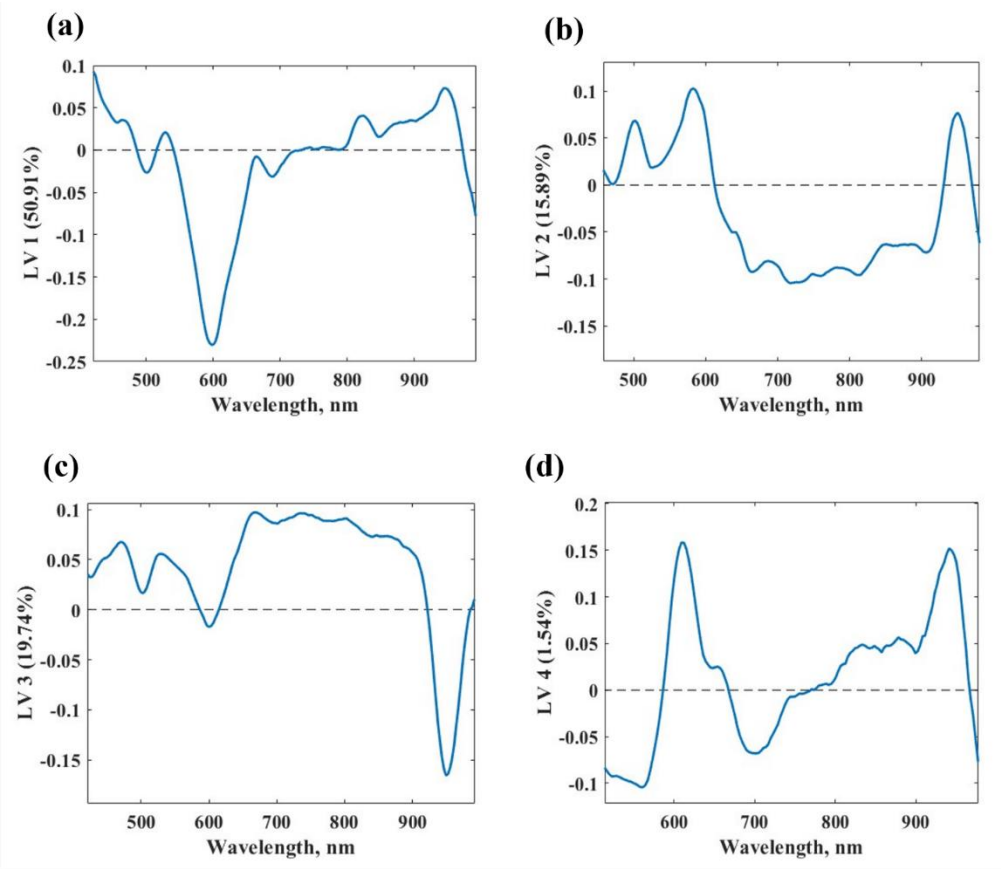

Figure 3.8 Significant data covariance explained by latent variables of PLSR models: a) LV1 of redness, b) LV2 for yellowness, c) LV3 of moisture, d) LV4 of hardness.

3.4.5.2 Prediction of moisture, pH, and water activity

With 4 LVs, moisture content was predicted with R^2_P of 0.90, and RMSEP of 0.81 %Wb as depicted in **Fig. 3.7c**. PLSR models on a_w did not produce acceptable prediction accuracies (**Table 3.5**). Though some significant differences can be noted among a_w with change in formulation (**Table 3.2**) and storage days (**Table 3.3**), variations were very minimal after two decimal points. (Ardila et al., 2023) reported that a_w did not show relevant differences between samples and characteristics of meat preparations. The accuracy of the developed PLSR model for pH prediction was lower (R^2_P = 0.78, RMSEP = 0.07). These discrepancies in accuracy compared to (Liu, Pu, et al., 2014), could potentially be attributed to variations in sample origin, spectral range, and the methods employed for feature extraction. The smaller change in pH values during storage in our study made the measurements vulnerable to experiment errors, which yielded models with lower prediction abilities. Further **Section 3.1. (Chapter 3)** explains the complex correlation between pH and other quality attributes, thus it is imperative to understand the role of pH in new food formulations from plant-derived ingredients as it depicts the color degradation, microbial load, and structural changes in PBMB. The aforementioned statements are substantiated by findings from (Ardila et al., 2023). Even though the HSI system does not have the capability to directly measure pH as H^+ sensitive electrodes, it is possible to understand how the acidity changes on the PBMB surface with respect to time/formulation using prediction maps.

3.4.6 Variables of importance and regression coefficients

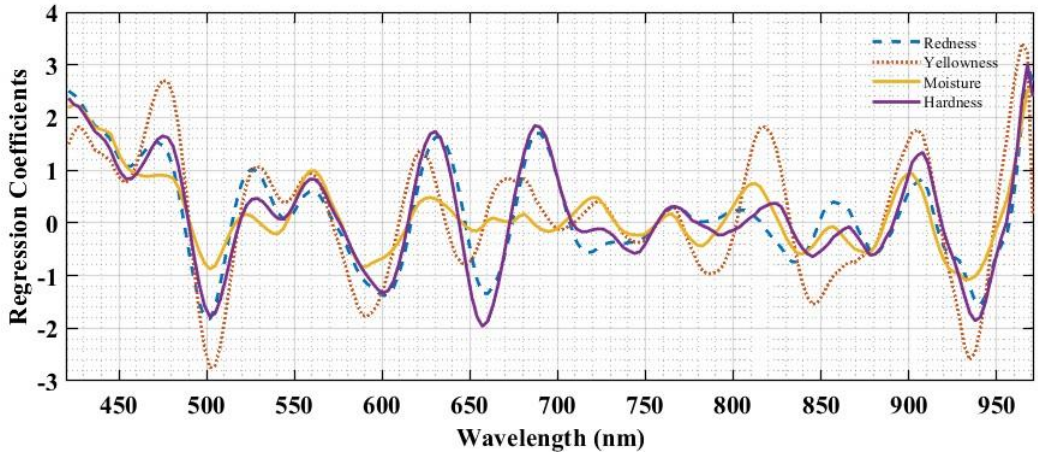

Figure 3.9 Regression coefficients of the PLSR models

Loading plots were used to assess the variables that contributed most to the PLSR models. It was evident that the wavelength range of 550-700 nm **(Fig. 3.8a)** greatly influenced *a**, while *b** was significantly impacted by variables within the ranges of 480-620 nm and 920-980 nm **(Fig. 3.8c)**. The peaks within the visible region predominantly corresponded to the pigments accountable for the color of PBMB (Sakai et al., 2022a), as elaborated in **Section 3.4.1. (Chapter 3)** Variations in the state of beet pigments due to the pH and moisture changes during storage, along with the changes in solubility and dispersibility of beet powders due to the changes in TVP% and PP%, contributed to alterations in the reflectance peaks at these specific wavelengths. Therefore, the LV plots of color prediction models effectively captured the spectral data set's covariance. In the LV3 plot for moisture prediction **(Fig. 3.8b)**, a prominent peak at 950-980 nm signifies a strong correlation with moisture content in PBMB, attributed to water absorption's O-H bonds. The peaks in the NIR range primarily originate from the overtones and combinations of O-H, C-H, and N-H. In specific, Sierra et al. (Sierra et al., 2008) and De Marchi et al. (De Marchi et al., 2013), indicated that 820 nm and 950 nm can be ascribed to the presence of the O-H bond, which is intrinsically linked to the water content within the samples. The pronounced peaks in **Fig. 3.8d** spanning the 800-980nm range, underscore the importance of this region in hardness prediction for PBMB. Hardness is a result of complex interaction among various components within PBMB, with moisture content playing a central role. The observed spectral features likely reflect the influence of moisture (Ma et al., 2017), as validated by the inverse relationship between moisture and hardness, as depicted in **Fig. 3.2** and **Table 3.2**. Essentially, the plots of LVs extracted indicate that the PLSR models were able to find meaningful patterns in the data that explain the relationships between the spectral features and the quality parameters.

Regression coefficients of the developed PLSR models are presented in **Fig. 3.9.** To build robust PLSR models with fewer variables for extending the method to pixel-by-pixel predictions, wavelength ranges with absolute regression coefficient values were selected while excluding the remaining variables (Ren & Sun, 2022). The performance of the newer PLSR models was lower than the full wavelength models but achieved acceptable accuracy with R^2_P of 0.825 and RMSEP of 0.490 with 7 LVs for *a**; R^2_P of 0.809 and RMSEP of 0.788 with 6 LVs for *b**; R^2_P of 0.825 and RMSEP of 1.154 %Wb with 7 LVs for moisture; and R^2_P 0.759 and RMSEP of 1.439 N for hardness with 8 LVs. (Liu, Sun, et al., 2014) reported that in situations where collinearity exists, the selection of feature variables based on regression coefficients might inadvertently exclude

important variables. The information loss due to the exclusion of variables that were relevant to the prediction but had low regression coefficients and the disruption of the balance of interdependencies among the wavelengths resulted in decreased precision accuracy. This highlights the importance of exploring advanced interval-based variable selection techniques, particularly when dealing with intricate and overlapping spectral features in complex food formulations, as demonstrated in this study. However, considering the covariance observed in the LV and regression plots, which reveal the selected wavelengths that effectively describe significant patterns in the data and explain the relations between spectral features and quality parameters, the potential for expanding the model with these selected variables for pixel-by-pixel predictions remains viable, even if it involves some reduction in prediction accuracy.

3.4.7 Pixel-by-pixel prediction

To visualize the spatial distribution of predicted quality parameters for PBMB, the calibration models with a reduced set of wavelengths were utilized to create concentration maps. **Fig. 3.10** depicts the prediction maps of selected parameters for day 1 samples. Distinct variations in quality parameters distribution were easily observable, as each pixel possessed unique spectra relevant to the target attributes. These distributions indicate localized variations in ingredient concentrations within specific regions of PBMB. An opposite relationship could be observed between the distribution of redness and moisture, hardness, and moisture. Further, the positive correlation between moisture and pH could be observed. These correlations are well aligned with the PCA biplot in **Fig. 3.2**.

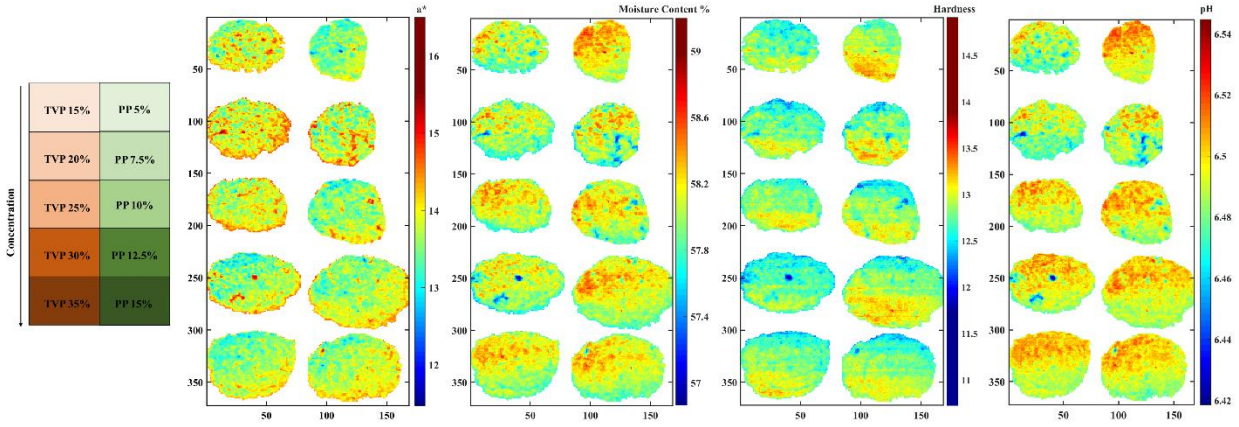

Figure 3.10 Pixel-by-pixel prediction quality distribution in plant-based meat burgers

The gradual reduction in concentration and distribution of redness with an increase in TVP% aligns with the ANOVA results of *a**. Though changes in *a** with PP% could be noticed, the change in distribution is lower compared to TVP-based samples which signifies the importance of textured protein ingredients as a key factor influencing the color characteristics of the PBMB. The slightly elevated redness values around the edges of the PBMB samples with TVP 20% and TVP 25% may be attributed to inherent structural variations within the samples affecting light interaction. Furthermore, the increase in pH and moisture with an increase in TVP% could be observed, which is in consistent with **Table 3.1**.

Moreover, the presence of surface pores or cracks in PBMB, which can occur during the mixing process may lead to certain pixels having predicted values out of the calibration range. This phenomenon can be attributed to the fact that PLSR model calibration is conducted using mean spectra, whereas prediction maps are generated on a pixel-by-pixel basis, as elucidated by (Squeo et al., 2022)(Chaudhry et al., 2021). In comparison to studies that conducted pixel-by-pixel prediction of quality attributes on muscle meat and processed foods such as (Hasan et al., 2022b; Feng & Makino, 2020a; Chaudhry et al., 2021), the results from this study showed lower accuracies. This can be attributed to several factors specific to plant-based meat, including the relative complexity in its formulation, high moisture content, and limited information regarding overtones and combination bands conveyed by the visible and near-infrared (VNIR) signal. Further, the prediction outcomes were influenced by the relatively small sample size, particularly in the case of hardness prediction, as well as the minimal changes in water activity, which were often observed at the second decimal places.

However, the results showed the non-uniform component distribution in PBMB leading to over or under-concentration in a specific area, which highlights the need for spectral fingerprinting techniques in evaluating meat alternative quality. Moreover, its conducive from **Fig. 3.10**, that the VNIR range holds great potential for mapping color distribution in meat alternatives. It also underscores the necessity of employing the NIR range to effectively map pH, a_w, and to provide comprehensive insights into macromolecule distributions and underlying factors in PBMB. Furthermore, the study highlights the inadequacy of comparing the visual appearance of plant-based meat with traditional meat products based on color values obtained from a colorimeter, which averages values from three spots, thus failing to represent the entire nature of the product.

Furthermore, these findings show the importance of conducting further investigations to monitor the dynamic evolution of quality and color during the storage period.

3.5 Conclusion

This study reported the first use of a hand-held and portable VNIR-HSI system coupled with multivariate data and image analysis for the prediction of quality traits in PBMB of different formulations during storage and mapping their distribution on each pixel. The outcome of the study reveals that VNIR-HSI could be used as a simple alternative or integrated with standardized methods for evaluating plant-based meat quality. Key findings from this study are summarized as follows:

I. ANOVA results highlighted the instability of PBMB quality even over a short storage period. PCA-M results showed the complex relationship between the textured, and non-textured protein, and quality parameters, underscoring the necessity for chemical mapping.

II. PCA-S model showed successful spatial separation of PBMB samples based on storage days, TVP %, and PP %. The principal variance in PCA-S is primarily from sample discoloration and moisture loss, attributed to the spectral variations at 500–650nm and 950–980 nm.

III. PLSR models on full spectral range possessed good prediction accuracies for a^* (R^2_P = 0.95, RMSEP = 0.27), b^* (R^2_P = 0.94, RMSEP = 0.45), moisture (R^2_P = 0.92, RMSEP = 0.74 %Wb), and hardness (R^2_P = 0.81, RMSEP = 0.88 N), respectively. Regression coefficients-based variable selection resulted in lower prediction accuracies due to high collinearity and intricate spectral features arising from the multiple ingredients in PBMB samples.

IV. Covariance observed in the LV and regression plots, reveal the selected wavelengths effectively describe significant patterns in the data and explain the relations between spectral features and quality parameters.

V. Pixel-by-pixel prediction maps unveiled the non-uniform surface distribution of the quality parameters. The distribution of quality parameters and their correlations were aligned with ANOVA and PCA-M results.

Overall, these results emphasize the need for spectral fingerprinting and suitability of VNIR for building a robust, and accurate multi-spectral system for real-time quality monitoring of

complex food formulations in plant-based food production. Further, this study highlights the potential of digital technologies in advancing sustainable food systems.

3.6 References

AOAC, 2006. (n.d.). *Official methods of analysis of AOAC International*. AOAC International.

Ardila, P., Honrado, A., Marquina, P., Beltrán, J. A., & Calanche, J. B. (2023). Innovative Plant-Based Burger Enriched with Tenebrio molitor Meal: Characterization and Shelf-Life. *Foods (Basel, Switzerland)*, *12*(18). https://doi.org/10.3390/foods12183460

Bakhsh, A., Lee, S.-J., Lee, E.-Y., Sabikun, N., Hwang, Y.-H., & Joo, S.-T. (2021). A Novel Approach for Tuning the Physicochemical, Textural, and Sensory Characteristics of Plant-Based Meat Analogs with Different Levels of Methylcellulose Concentration. *Foods*, *10*(3). https://doi.org/10.3390/foods10030560

Bakhsh Allah AND Lee, S.-J. A. N. D. L. E.-Y. A. N. D. H. Y.-H. A. N. D. J. S.-T. (2021). Evaluation of Rheological and Sensory Characteristics of Plant-Based Meat Analog with Comparison to Beef and Pork. *Food Science of Animal Resources*, *41*(6), 983–996. https://doi.org/10.5851/kosfa.2021.e50

Balcão, V. M., & Vila, M. M. D. C. (2015). Structural and functional stabilization of protein entities: state-of-the-art. *Advanced Drug Delivery Reviews*, *93*, 25–41. https://doi.org/https://doi.org/10.1016/j.addr.2014.10.005

Botella-Martínez, C., Viuda-Martos, M., Fernández-López, J. A., Pérez-Alvarez, J. A., & Fernández-López, J. (2022). Development of plant-based burgers using gelled emulsions as fat source and beetroot juice as colorant: Effects on chemical, physicochemical, appearance and sensory characteristics. *LWT*, *172*, 114193. https://doi.org/https://doi.org/10.1016/j.lwt.2022.114193

Chaudhry, M. M. A., Hasan, M. M., Erkinbaev, C., Paliwal, J., Suman, S., & Rodas-Gonzalez, A. (2021). Bison muscle discrimination and color stability prediction using near-infrared hyperspectral imaging. *Biosystems Engineering*, *209*, 1–13. https://doi.org/10.1016/j.biosystemseng.2021.06.010

Dawson, P. L., & Acton, J. C. (2018). 22 - Impact of proteins on food color. In R. Y. Yada (Ed.), *Proteins in Food Processing (Second Edition)* (Second Edi, pp. 599–638). Woodhead Publishing. https://doi.org/https://doi.org/10.1016/B978-0-08-100722-8.00023-1

De Marchi, M., Costa, A., Pozza, M., Goi, A., & Manuelian, C. L. (2021). Detailed characterization of plant-based burgers. *Scientific Reports*, *11*(1), 2049. https://doi.org/10.1038/s41598-021-81684-9

De Marchi, M., Penasa, M., Cecchinato, A., & Bittante, G. (2013). The relevance of different near infrared technologies and sample treatments for predicting meat quality traits in commercial beef cuts. *Meat Science*, *93*(2), 329–335. https://doi.org/https://doi.org/10.1016/j.meatsci.2012.09.013

Dreher, J., König, M., Herrmann, K., Terjung, N., Gibis, M., & Weiss, J. (2021). Varying the amount of solid fat in animal fat mimetics for plant-based salami analogues influences

texture, appearance and sensory characteristics. *LWT*, *143*, 111140. https://doi.org/https://doi.org/10.1016/j.lwt.2021.111140

Elmasry, G., Sun, D.-W., & Allen, P. (2013). Chemical-free assessment and mapping of major constituents in beef using hyperspectral imaging. *Journal of Food Engineering*, *117*, 235–246. https://doi.org/10.1016/j.jfoodeng.2013.02.016

Erkinbaev, C., Morrison, J., & Paliwal, J. (2017). *A Novel Exploratory Shape Analysis Method to Identify Spatial Variation of Fungi Infection Level on Wheat Kernels*. 71–79. https://doi.org/10.1142/9789813225701_0004

Erkinbaev, C., Nadimi, M., & Paliwal, J. (2022). A unified heuristic approach to simultaneously detect fusarium and ergot damage in wheat. *Measurement: Food*, *7*, 100043. https://doi.org/https://doi.org/10.1016/j.meafoo.2022.100043

Feng, C. H., & Makino, Y. (2020). Colour analysis in sausages stuffed in modified casings with different storage days using hyperspectral imaging – A feasibility study. *Food Control*, *111*, 107047. https://doi.org/10.1016/j.foodcont.2019.107047

FMI. (2023). *Plant-based burger market*. https://www.futuremarketinsights.com/reports/plant-based-burger-market

Hasan, M. M., Chaudhry, M. M. A., Erkinbaev, C., Paliwal, J., Suman, S. P., & Rodas-Gonzalez, A. (2022). Application of Vis-NIR and SWIR spectroscopy for the segregation of bison muscles based on their color stability. *Meat Science*, *188*(February), 108774. https://doi.org/10.1016/j.meatsci.2022.108774

Kamruzzaman, M., ElMasry, G., Sun, D.-W., & Allen, P. (2013). Non-destructive assessment of instrumental and sensory tenderness of lamb meat using NIR hyperspectral imaging. *Food Chemistry*, *141*(1), 389–396. https://doi.org/https://doi.org/10.1016/j.foodchem.2013.02.094

Liu, D., Pu, H., Sun, D.-W., Wang, L., & Zeng, X.-A. (2014). Combination of spectra and texture data of hyperspectral imaging for prediction of pH in salted meat. *Food Chemistry*, *160*, 330–337. https://doi.org/https://doi.org/10.1016/j.foodchem.2014.03.096

Liu, D., Sun, D.-W., & Zeng, X.-A. (2014). Recent Advances in Wavelength Selection Techniques for Hyperspectral Image Processing in the Food Industry. *Food and Bioprocess Technology*, *7*. https://doi.org/10.1007/s11947-013-1193-6

Ma, J., Sun, D.-W., Qu, J.-H., & Pu, H. (2017). Prediction of textural changes in grass carp fillets as affected by vacuum freeze drying using hyperspectral imaging based on integrated group wavelengths. *LWT - Food Science and Technology*, *82*, 377–385. https://doi.org/https://doi.org/10.1016/j.lwt.2017.04.040

McClements, D. J., Weiss, J., Kinchla, A. J., Nolden, A. A., & Grossmann, L. (2021). Methods for Testing the Quality Attributes of Plant-Based Foods: Meat- and Processed-Meat Analogs. *Foods*, *10*(2). https://doi.org/10.3390/foods10020260

Mishra, P., van Dijk, M., Wintermeyer, C., Sabater, C., Bot, A., Verkleij, T., & Broeze, J. (2022). At-line and inline prediction of droplet size in mayonnaise with near-infrared spectroscopy. *Infrared Physics & Technology*, *123*, 104155. https://doi.org/https://doi.org/10.1016/j.infrared.2022.104155

Moss, B. W. (2002). *The chemistry of food colour* (pp. 145–178). https://doi.org/10.1533/9781855736672.2.145

Mundhada, S., Chaudhry, M., Erkinbaev, C., & Paliwal, J. (2022). Non-Destructive Quality Monitoring of Flaxseed During Storage. *Journal of Food Measurement and Characterization*, *16*, 1–11. https://doi.org/10.1007/s11694-022-01464-5

Purslow, P. P., Warner, R. D., Clarke, F. M., & Hughes, J. M. (2020). Variations in meat colour due to factors other than myoglobin chemistry; a synthesis of recent findings (invited review). *Meat Science*, *159*, 107941. https://doi.org/https://doi.org/10.1016/j.meatsci.2019.107941

Ren, Y., & Sun, D.-W. (2022). Monitoring of moisture contents and rehydration rates of microwave vacuum and hot air dehydrated beef slices and splits using hyperspectral imaging. *Food Chemistry*, *382*, 132346. https://doi.org/https://doi.org/10.1016/j.foodchem.2022.132346

Ryu, K. K., Kang, Y. K., Jeong, E. W., Baek, Y., Lee, K. Y., & Lee, H. G. (2023). Applications of various natural pigments to a plant-based meat analog. *LWT*, *174*, 114431. https://doi.org/https://doi.org/10.1016/j.lwt.2023.114431

Sakai, K., Sato, Y., Okada, M., & Yamaguchi, S. (2022). Synergistic effects of laccase and pectin on the color changes and functional properties of meat analogs containing beet red pigment. *Scientific Reports*, *12*(1), 1168. https://doi.org/10.1038/s41598-022-05091-4

Schreuders, F. K. G., Schlangen, M., Kyriakopoulou, K., Boom, R. M., & van der Goot, A. J. (2021). Texture methods for evaluating meat and meat analogue structures: A review. *Food Control*, *127*, 108103. https://doi.org/https://doi.org/10.1016/j.foodcont.2021.108103

Sierra, V., Aldai, N., Castro, P., Osoro, K., Coto-Montes, A., & Oliván, M. (2008). Prediction of the fatty acid composition of beef by near infrared transmittance spectroscopy. *Meat Science*, *78*(3), 248–255. https://doi.org/https://doi.org/10.1016/j.meatsci.2007.06.006

Squeo, G., De Angelis, D., Summo, C., Pasqualone, A., Caponio, F., & Amigo, J. M. (2022). Assessment of macronutrients and alpha-galactosides of texturized vegetable proteins by near infrared hyperspectral imaging. *Journal of Food Composition and Analysis*, *108*, 104459. https://doi.org/https://doi.org/10.1016/j.jfca.2022.104459

Tóth, A. J., Dunay, A., Battay, M., Illés, C. B., Bittsánszky, A., & Süth, M. (2021). Microbial Spoilage of Plant-Based Meat Analogues. *Applied Sciences*, *11*(18). https://doi.org/10.3390/app11188309

Vallikkadan, M. S., Dhanapal, L., Dutta, S., Sivakamasundari, S. K., Moses, J. A., & Anandharamakrishnan, C. (2023). Meat Alternatives: Evolution, Structuring Techniques, Trends, and Challenges. *Food Engineering Reviews*. https://doi.org/10.1007/s12393-023-09332-8

Wu, D., Sun, D.-W., & He, Y. (2014). Novel non-invasive distribution measurement of texture profile analysis (TPA) in salmon fillet by using visible and near infrared hyperspectral imaging. *Food Chemistry*, *145*, 417–426.

Zhou, H., Vu, G., Gong, X., & McClements, D. J. (2022). Comparison of the Cooking Behaviors of Meat and Plant-Based Meat Analogues: Appearance, Texture, and Fluid Holding

Properties. *ACS Food Science \& Technology*, *2*(5), 844–851. https://doi.org/10.1021/acsfoodscitech.2c00016

CHAPTER 4

NON-INVASIVE CHARACTERIZATION OF COLOR VARIATION IN PLANT-BASED MEAT BURGERS USING PORTABLE HYPERSPECTRAL IMAGING DEVICE AND MULTIVARIATE IMAGE ANALYSIS

Logesh Dhanapal and Chyngyz Erkinbaev*

4.1 Abstract

The excessive color variation in plant-based meat burgers (PB) during storage, arising from the interplay of multiple ingredients, suggests the acute need for real-time color monitoring techniques. This study reports the use of a smart-portable hyperspectral imaging device in the visible-near-infrared coupled with multivariate data and image analysis for the prediction of color in PB samples of different formulations during storage. Principal Components Analysis (PCA) and Partial Least Squares Regression (PLSR) were applied to explore the spectral features and predict the CIE- *L**, *a**, *b**. PCA on spectral data showed successful spatial separation of PB samples based on color stability. The PLSR models in the full spectral range possessed good prediction accuracies for *L** (R^2_P = 0.88, RMSEP = 0.94), *a** (R^2_P = 0.98, RMSEP = 0.15), *b** (R^2_P = 0.92, RMSEP = 0.31). Prediction capabilities of simplified PLSR models were improved for *a** (R^2_P = 0.99, RMSEP = 0.09) with B-iPLS, *b** (R^2_P = 0.95, RMSEP = 0.23) with B-iPLS. Pixel-by-pixel prediction maps unveiled the pattern of color deterioration concerning individual base ingredients in the PB samples. The results unravel the feasibility of developing a real-time multi-spectral technique for quantification and visualization of color evolution in plant-based meat analogs.

Keywords: Plant-based meat color, Plant proteins, Non-destructive food testing, Hyperspectral imaging, Chemometrics, Plant-based meat quality

4.2 Introduction

Plant-based meat analogs (PBMA), engineered to replicate the characteristics of conventional meat products, gained substantial attention among researchers, consumers, product developers, and investors, driven by concerns for environmental sustainability, animal welfare, and health (Vallikkadan et al., 2023b). Driven by the application of structuring techniques like extrusion, the total retail sales of PBMA within the U.S. escalated to $5 billion in 2019, showcasing a notable 29% increase over a span of two years (Good Food Institute,

2020). Upon exiting the extruder, the sudden drop in pressure causes rapid moisture evaporation from the viscous melt, giving rise to voids within the agglomerated structure, creating the typical fibrillar-like structures. Such extrudates as texturized vegetable protein (TVP) with traditional meat processing technologies are easily further processed into plant-based meat burger patties (PB) (Saerens et al., 2021). According to (Future Market Insights, 2023), the PB market is expected to experience exponential growth with an estimated Compound Annual Growth Rate exceeding 22% between 2020 and 2030. Life Cycle Assessment (LCA) studies consistently find PB has a lower environmental impact (Smetana et al., 2021), whereas Saerens et al., (Saerens et al. 2021) reported the impact of PB was ten-fold lower than meat burger patties. Consumer acceptance of PB relates to factors including cost, appearance, texture, flavor, mouthfeel, and nutrition (Li et al., 2023). As outlined in the literatures, concerns persist regarding visual similarity to meat and color stability, which could deter their adoption. Despite the widespread availability of PB products across various countries, their visual characteristics, specifically color, still differ from that of conventional meat products, presenting an unresolved challenge.

Color is a primary factor that indicates wholesomeness and determines purchase intention for meat products. Any variation from visually appealing color can signal quality issues. The inherent color of meat products (uncooked) alters due to chemical changes in proteins, particularly myoglobin, during storage and handling (Chaudhry et al., 2021). This shift from oxymyoglobin to metmyoglobin results in a brown color, which consumers associate with meat being stale and unsuitable for consumption. A parallel concept can be illustrated for the significance of color and its alteration during storage in meat analog products (Sakai et al., 2022a). In general, uncooked plant-based proteins exhibit a yellow or beige color, and to achieve the distinct meat color, a few natural colorants have been used, including beet extract, soy leghemoglobin, and carrot juice extract (Botella-Martínez et al., 2022) (Sakai et al., 2022a). (Ryu et al. 2023) investigated the effect of red beet, monascus red, oleoresin paprika, sorghum, and cacao. (Bakhsh et al. 2022) used lactoferrin and red yeast rice. In commercial PB products, The Beyond Burger™ uses beet juice extract and Impossible™ Burger uses soy leghemoglobin (Vallikkadan et al., 2023b).

The characteristic color of uncooked PB products is generally unstable, such as early browning happens even within retail packaging conditions. The presence of over 20 ingredients, each possessing distinct physicochemical properties, combined with the distinct structure-function relationships of specific plant proteins in terms of hydration and solubility, collectively gives rise to variations in color stability (De Marchi et al., 2021). Thus, the

excessive variation in color stability and shelf life within PB products poses challenges in providing a stable product. Substantial studies has been reported on the effect of new raw materials and novel structuring techniques on the nutritional properties (Smetana et al., 2021), physicochemical properties (Bakhsh, Lee, Lee, Hwang, et al., 2021), microbial attributes (Tóth et al., 2021), and volatile composition changes of PB products (De Marchi et al., 2021). However, there are limited studies focusing on color variations in plant-based meat analogs and there is a lack of study on visualization of how the color of PB responds to different ingredients during storage time.

Existing research in the field of PB color analysis has primarily relied on contact-based single-point colorimeters, as evidenced by studies conducted by (Ardila et al. 2023), (Sakai et al. 2022), and (Bakhsh et al. 2021). However, the practice of averaging color values obtained from only three discrete points, without considering the entire surface area, results in a limited ability to capture information about non-uniform or non-homogeneous surfaces. Accordingly, (McClements et al. 2021) highlighted that the lack of standardized methods for analyzing, and evaluating the visual appearance or color of emerging food structures such as meat analogs, could hinder the acceptance of research outcomes and their comparability to traditional meat products. . From an industrial perspective, color evaluation using colorimeters or trained panelists in lab settings is a limited-scale analysis, is time-consuming, and is unsuitable for integration in processing and packaging facilities. In this context, the demand for accurate, rapid, and non-contact photonics-based quality assessment techniques has risen. The extensively studied non-destructive technique of visible-near infrared (VNIR) spectroscopy is employed to rapidly assess color values in various food matrices for online or at-line applications. However, it is difficult to examine the entire color distribution of a non-homogenous food sample spot by spot. Consequently, hyperspectral imaging overcomes numerous limitations posed by these approaches by capturing spatial and spectral information, that aids in visualizing the color distribution for the entire surface area, pixel by pixel.

Hyperspectral imaging (HSI), a non-destructive and non-targeted process analytical tool (PAT) that integrates spectroscopy and computer vision technologies in a single system has been extensively studied to provide qualitative and quantitative information on food products. VNIR-HSI has been profoundly utilized in predicting and visualizing the color attributes of various fibrous products such as fresh and processed meat. (Hasan et al. 2022) classified different muscle types based on their color stability using PLSDA. (Kamruzzaman et al. 2012) predicted lamb meat redness using PLSR with a high R^2_{CV} = 0.91. (Feng and Makino 2020) applied VNIR-HSI to cylindrical food structures and monitored the color

evolution of sausage by using PLSR-reported R^2_{CV} up to 0.78. HSI has also been applied to evaluate the chemical composition (Mundhada et al., 2022), defects (Erkinbaev et al., 2022), and quality (Erkinbaev, Henderson, et al., 2017) of cereal grains and products. The collective findings from these studies demonstrate the potential of extending VNIR-HSI to the analysis of plant-based meat that constitutes the physiochemical attributes of processed meat (high moisture content, fat marbling, non-uniform surface) and the functional nature of plant-derived ingredients.

While numerous studies have been reported on meat color, these have largely remained exploratory, exemplifying proof of concept through lab setups with slow acquisition rates. Such setups necessitate fast computers, sensitive detectors, extensive data storage, and complex data analysis, rendering them unsuitable for high-throughput commercial applications. On the other hand, accelerated digitalization in the food sector has brought the concept of "Food Quality 4.0", where spectral fingerprinting techniques meet and need Industry 4.0 capabilities, resulting in their evolution towards miniaturized and smart field devices (Hassoun, Jagtap, et al., 2023). Portable, miniaturized, and hand-held hyperspectral imaging devices could be conveniently employed for real-time analysis by translating the results obtained from multivariate prediction models (Hassoun, Aït-Kaddour, et al., 2023). This real-time data can aid in decision-making processes related to grading, labeling, storage, and processing.

However, the reduced predictive ability due to the high dimensional and co-linear nature of hyperspectral images remains a main limitation for this real-time application. The rapid development of new algorithms for feature wavelength extraction including interval-PLS (iPLS), recursive PLS (rPLS), and genetic algorithm (GAs), has suggested the potential of simplified models in devising multispectral imaging sensors for a fast, robust, and real-time prediction with less computational resource requirement (Dai et al., 2015). Our thorough literature review indicates that the feasibility of using portable HSI devices for monitoring the plant-based meat analogs' color remains to be fully investigated.

Considering the ultra-processed nature of PB with refined ingredients from protein in textured and non-textured form, fat mimetics, flavorings, oils, binding, thickening, and coloring agents, to a significant amount of water, it is imperative to understand the role of each ingredient and the effect of their interplay with color stability during the storage period. The prediction and distribution maps of color scores generated by HSI may potentially meet this requirement. Therefore, this study aimed to investigate the feasibility of portable and hand-held hyperspectral imaging technique in the VNIR (400–1000 nm) range, coupled with multivariate analysis for the prediction of color values, visualize the color evolution during the

storage period and understand each ingredient effect on color stability in PB. In this context, the aim of this study was (i) to develop plant-based meat burger patty formulations and characterize the effect of major ingredients and storage time on their color values, (ii) to extract spectral and spatial information from the hypercube images and develop full wavelength prediction models, (iii) to extract the feature wavelengths and develop simplified prediction models, (iv) to visualize the changes occurring from pixel to pixel via prediction maps.

4.3 Materials and Methods

4.3.1 Sample formulation and preparation

Granule-type commercial soy-based textured vegetable protein (TVP) was obtained from Bulk Barn Foods Ltd. (Winnipeg, Canada). Pea protein powder (PP) - 85 % protein from unflavored yellow pea (Pisum sativum) was purchased from SMOOV^{TM} (Canada). Fava bean protein powder (FP) was purchased from Green Boy Products, LLC (USA). Commercial potato starch, soy lecithin, nutritional yeast, and blackstrap molasses (unsulfured) were sourced from commercial ingredient suppliers (Bulk Barn Foods Ltd.). Beet powder, citrus extract, xanthan gum, cacao butter, and refined coconut oil were sourced from local commercial supermarkets (Winnipeg, Canada). 25% TVP, 10% PP, 15% FP, 2% xanthan gum, 30% fat emulsion (FE), 10% potato starch, 1% soy lecithin, and 8% soluble components including beetroot powder, nutritional yeast, blackstrap molasses, acetic acid, ascorbic acid, citrus extract was used to develop a control PB formulation on a mass basis (w/w). At room temperature, the protein constituents were initially hydrated at a 1:2 (m/v) ratio for 30 minutes. On hydration, the reformed and expandable structure of TVP results in a chewy, meat-like texture. Using a homogenizer (X 120, Ingenieurbüro CAT, M. Zipperer GmbH), the mixture containing cacao butter, coconut oil, water, and xanthan gum was homogenized at 28.00 rpm for 20 minutes to develop the fat emulsion. Subsequently, using a laboratory-scale mixer (KitchenAid®), the mixtures were combined with binders, thickeners, colorants, and flavor compounds, achieving a homogeneous blend. The obtained composite was moulded into 5×2 cm (diameter × thickness).

To study the interplay of each ingredient effect, four different treatments (T1-T4) were developed by modifying the ratios of major base components from the control formulation. This involved adjusting the proportions as follows: 35% TVP (T1), 15% PP (T2), 40% FE (T3), and 17.5% FP (T4). To stimulate retail packaging and storage conditions, the PB samples were packed in sealed plates using aluminium foil pan containers and food-grade commercial plastic stretch film, replicating North American retail conditions. The sealed trays were stored at a

temperature of 5°C, and consistent sealing thickness and tightness were maintained throughout the experiment. Samples from 5 formulations (Control, T1-T4) were stored for 10 days. During this period, the HSI-VNIR image acquisition and data collection (color values) were carried out at specific intervals, namely on day 1, day 3, day 5, day 7, and day 9 (D1, D3, D5, D7, and D9). Each sample underwent spectral measurements in 5 replicates, resulting in a total of 125 spectra. **Fig. 4.1** illustrates the visual difference among PB formulations.

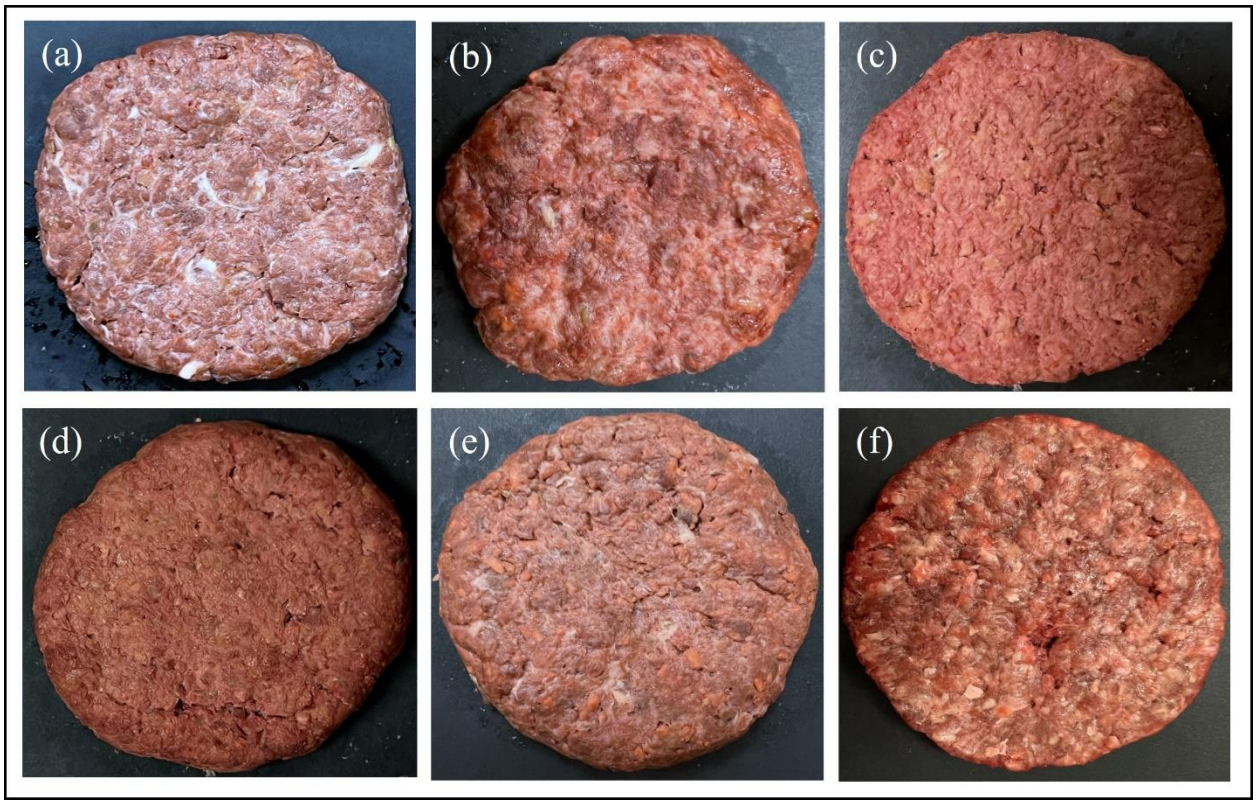

Figure 4.1 Digital images of plant-based meat burger samples – (a) Control, 15% textured vegetable protein (w/w); (b) T-3, 40% fat emulsion (w/w); (c) T-1, 35% textured vegetable protein (w/w); (d) T-2, 15% pea protein (w/w); (e) T-4, 17.5% fava bean protein (w/w); and (f) beef burger patty

4.3.2 Measurement and statistical analysis of color values

The surface color of the PB samples was measured using the tristimulus colorimeter (Chroma Meter CR–410, D65 illuminate, 2° observer; Konica Minolta, Japan). Following the calibration process, measurements of CIE - L^* (representing lightness), a^* (indicating redness), and b^* (reflecting yellowness) were obtained at three distinct locations across the surface of the samples. The values were then averaged for each color parameter. OriginPro Software, version 8.5 (OriginLab Corporation, Northampton, USA) was used to perform One-way

ANOVA to analyze the effects of different treatments and storage days on color. A significance level of p-value < 0.05 was used to indicate statistical significance.

4.3.3 Hyperspectral image acquisition

VNIR hyperspectral images were captured using a portable Specim IQ camera (Specim Inc., Finland), which utilizes a line scanning methodology. The camera offers a spectral range of 400–1000 nm with 204 spectral bands and a spectral resolution of 7 nm. The images were acquired in the diffuse reflectance mode with an optimized integration time of 5 ms. The imaging setup was arranged with a 575W halogen-based lighting system, which was augmented by barn doors to focus its illumination at an incident angle of roughly 40° onto a sample situated 22 cm away from the camera lens. The acquired images characterize data in a 3D hypercube at a resolution of 512 ×512 × 204 (spatial x spectral). For image calibration i.e., correction of variation in sample illumination was made by including a white reference panel within the image frame. The black reference is recorded as part of the data acquisition process of the camera. MATLAB (Mathworks Inc., Natick, MA) was used to organize, unfold, and analyze the 3D hypercubes. Regions of interest (ROI) of each image were selected, and corresponding mean reflectance spectra were derived using codes generated with MATLAB (Mathworks Inc., Natick, MA). Further, Specim IQ Studio (Specim Inc., Finland) was used to generate a library of spectra and develop models/applications for the camera. These applications enable the camera to perform real-time mapping of components within captured images.

4.3.4 Principal component analysis

Using the PLS Toolbox 8.6 (Eigenvector Technologies, Manson, MA), the VNIR spectra of PB samples were explored by the PCA model to investigate the variations between samples without referring to their color values. Projecting spectral data into principal components (PCs) i.e., orthogonal sub-spaces represent the entire variability present within the dataset. The scores of PC1, PC2, and PC3 for samples with different storage times were computed to examine the possible spatial separation. Further, the PCA loadings were evaluated to understand the spectral contributions to variance and identify the association between variables.

4.3.5 Spectral pre-processing

To reduce baseline drift (due to the light scattering), noise (due to instrumental drift), and undesired perturbations raw spectra were pre-treated. The lack of studies on spectral characteristics of meat analogs, necessitates a careful selection of pre-processing methods, as

incorrect selections may distort the useful information in spectra. The performance of seven pre-treatment methods, (i) Standard normal variate (SNV) was used to limit spectral intensity variation, by subtracting the mean and dividing by the standard deviation for each wavelength; (ii) Multiplicative scatter correction (MSC), was applied to correct baseline drifts in spectra, by fitting each spectrum to a reference spectrum **(Eq. 4.1)**, and then to correct them as shown in **Eq. 4.2**.

$$x_i = a * \bar{x} + b \qquad (4.1)$$

$$x_I^{MSC} = (x_i - b)/a \qquad (4.2)$$

where x_I^{MSC} the corrected spectrum is defined using measured spectrum (x), reference (or mean) spectrum ($\bar{\boldsymbol{x}}$), intercept (a), and slope (b); (iii) Mean centering (MC) was applied to remove the constant offset, by subtracting the mean of each point with its respective variable; (iv-vi) smoothing, first derivative (Sav-Gol-FD), second derivative (Sav-Gol-SD) was applied for denoising and baseline-correction, using Stavisky Golay (Sav-Gol) approach of stepwise fitting of local polynomial regressions to the spectral data within localized windows. Polynomial order 2 with an 11-point window was set for Sav-Gol-based treatments; and (vii) a combination of MC Sav-Gol-FD was evaluated using the PLS Toolbox 8.6 (Eigenvector Technologies, Manson, MA) in this research.

4.3.6 Partial least square regression modeling

Partial least square regression (PLSR) was performed in the PLS toolbox to establish regression fits between the VNIR spectral data and reference measurements (L^*, a^*, b^*). A data matrix (X) containing the spectral data of samples from all treatments (125 samples × 204 wavelengths), was split into a calibration set (80%) and a test set (20%) using the Kennard-Stone algorithm (KSA)(Zhang et al., 2022). KSA identifies a pair of samples with the highest Euclidean distance in the X matrix. These samples are then moved to the calibration set. This process is iterated for rest of the data points until the designated sample size is allocated to the calibration set. Test set is formed with the remaining samples. Venetian blinds cross-validation was executed, comprising 10 data splits where each split incorporated 1 sample per blind. Latent variables (LV), which explain the highest variation in X and define predictor variables (Y) in the best possible way, were evaluated by considering the lowest cross-validation error, aiming to prevent the issue of over-fitting.

4.3.7 Optimization of simplified PLSR models

Given the high collinearity and enormous nature of the acquired full-wavelength data, the feature wavelengths of the developed full-wavelength PLSR models were identified to build simplified PLSR models using three sequential variable selection techniques: interval-partial least squares (iPLS), recursive PLS (rPLS), and genetic algorithms (GAs). iPLS segments the spectrum into intervals, builds PLSR models for each interval, identifies intervals based on correlation with the response variable, selects spectral intervals with minimum RMSE in cross-validation, and constructs a simplified PLSR model. In this study, iPLS was carried out in forward mode (F-iPLS), where intervals are progressively included into the analysis, and reverse mode (B-iPLS), where intervals are progressively excluded from the analysis. Interval size (vars) was fixed to 10 in both cases. rPLS evaluates and eliminates wavelengths based on variable importance in projection (VIP) scores, iteratively refining the model by removing low-contributing variables. A total of 10 iterations were selected for the analysis. GAs, a population-based optimization approach, iteratively evolve candidate subsets of wavelengths from spectral data. By evaluating fitness scores based on PLSR model performance, GAs progressively refines the wavelength selection. Following GAs parameters were fixed the analysis: window width: 10, population size: 64, crossover: double, mutation rate: 0.005, % of convergence: 50, penalty slope: 10; Regression choice: PLS; and Cross-validation parameters: Random mode, 7 LVs, 10 splits, 1 iteration.

4.3.8 Evaluation of model performance

The performance of the PLSR models was evaluated in terms of the highest coefficients of determination (R^2) and lowest root mean square errors (RMSE) in calibration (R^2_C, RMSEC), cross-validation (R^2_{cv}, RMSECV), and prediction (R^2_P, RMSEP). It's defined using predicted values ($\hat{Y}$), measured values (Y), mean value of samples ($\bar{Y}$), and the number of sample spectra (n) as outlined in **Eq. 4.3** and **Eq. 4.4**.

$$R^2 = 1 - \frac{\sum_{i=1}^{n}(\hat{Y}_i - Y_i)^2}{\sum_{i=1}^{n}(\hat{Y}_i - \bar{Y}_i)^2} \qquad (4.3)$$

$$RMSE = \sqrt{\frac{1}{n}\sum_{i=1}^{n}(\hat{Y}_i - Y_i)^2} \qquad (4.4)$$

The RMSE of the developed models is reported with the respective units of the predicted parameters. Notably, the predicted parameters in this study are dimensionless values used to describe colors in the CIELAB color space.

4.3.9 Multivariate exploration of images

PCA analysis of hypercubes was performed in the PLS toolbox, to study the variability among the score surfaces of PB samples. To overview the main source of variance in both individual and set of samples, PCA models were built on hypercube images of (i) day 1 – Control sample; and (ii) day 1 - Control, T1, T2, T3, and T4 samples. The data were previously pre-processed (Sav-Gol-SD with a polynomial order 2 with an 11-point window) and mean-centered. To visualize the surface color distribution within a PB sample and color changes during storage stages, prediction maps were developed for each hyperspectral image. The simplified PLSR model was used to build a pixel-by-pixel prediction of color parameters on individual hyperspectral images. Distribution maps were generated using MATLAB (version 9.2; MathWorks Inc., USA) and HYPER-Tools (V3.0, available at www.hypertools.org).

4.4 Results and Discussion

4.4.1 Effect of treatments and storage stages on color

Table 1 presents the effects of treatments and different storage days on the color of the prepared PB samples. The addition of PP from 10% (control) to 15% (T2) increased the a^* and b^* values from 14.86 ± 0.14, 11.90 ± 0.11 to 15.91 ± 0.02, 13.45 ± 0.26, respectively ($p < 0.05$). The smaller particle size and uniform distribution of PP, due to its strong water-binding capacity, affect light absorption (Vatansever et al., 2020). Additionally, changes in PP concentration can lead to pH variations, influencing color, as reported by previous studies (Zhu et al., 2021). The a^* (14.06 ± 0.13) values of T1 samples were lower and b^* (13.15 ± 0.11) higher than that of the control formulation ($p < 0.05$). The higher hydration capacity of TVP, leading to the dilution of betalain pigments, may account for this phenomenon. The higher FE content (40%) in T3 samples significantly increased the L^* value (59.45 ± 0.37), indicating greater surface fat marbling, leading to increased light reflection.

Table 4.1 Colour evaluation across treatments and storage stages of plant-based meat burger patties

	L*	a*	b*
Treatments			
Control	58.84±0.63^{b}	14.86±0.14^{c}	11.91±0.11^{b}
T1	52.66±0.43^{c}	14.06±0.13^{d}	13.15±0.11^{a}
T2	52.43±0.62^{c}	15.91±0.02^{b}	13.45±0.26^{a}
T3	59.45±0.37^{b}	16.21±0.14^{a}	10.93±0.07^{c}
T4	61.69±0.65^{b}	16.57±0.17^{a}	13.51±0.02^{a}

Samples			
Control – D1	58.84±0.63^{a}	14.86±0.14^{a}	11.91±0.11^{c}
Control – D3	56.22±0.02^{b}	14.36±0.09^{b}	12.11±0.02^{c}
Control – D5	55.40±0.22^{b}	14.28±0.12^{bc}	12.90±0.43^{b}
Control – D7	55.36±1.77^{b}	14.12±0.23^{bc}	13.28±0.32^{b}
Control – D9	54.74±0.32^{b}	13.92±0.03^{c}	14.35±0.02^{a}
T1 - D1	52.66±0.43^{d}	14.06±0.13^{ab}	13.15 ±0.11^{ab}
T1 - D3	54.79±0.22^{c}	14.27±0.54^{a}	12.75±0.12^{b}
T1 - D5	56.09±0.29^{b}	13.86±0.03^{ab}	13.26±0.52^{ab}
T1 - D7	56.94±0.01^{a}	13.45±0.26^{b}	13.60±0.02^{a}
T1 - D9	57.46±0.01^{a}	13.56±0.04^{ab}	13.59±13.58^{a}
T2 - D1	52.43±0.32^{ab}	15.91±0.24^{a}	13.45±0.26^{b}
T2 - D3	53.22±1.86^{a}	15.94±0.46^{a}	13.76±0.13^{b}
T2 - D5	52.71±0.16^{ab}	15.10±0.35^{b}	14.64±0.32^{a}
T2 - D7	50.1±0.89^{b}	15.05±0.01^{b}	14.94±0.34^{a}
T2 - D9	53.69±1.14^{a}	14.88±0.15^{b}	14.86±0.32^{a}
T3 - D1	59.45±0.37^{a}	16.21±0.14^{a}	10.93±0.07^{d}
T3 - D3	59.23±0.05^{a}	15.89±0.07^{b}	11.71±0.00^{c}
T3 - D5	58.79±0.52^{a}	15.39±0.08^{c}	12.33±0.02^{b}
T3 - D7	57.56±0.02^{b}	14.71±0.09^{d}	12.44±0.01^{b}
T3 - D9	56.98±0.14^{b}	14.17±0.04^{e}	12.82±0.16^{a}
T4 - D1	61.69±0.35^{a}	16.57±0.17^{a}	13.51±0.02^{a}
T4 - D3	57.46±0.01^{b}	13.86±0.03^{bc}	12.75±0.12^{b}
T4 - D5	56.94±0.01^{bc}	13.29±0.04^{c}	13.26±0.52^{ab}
T4 - D7	56.09±0.29^{c}	13.56±0.04^{c}	13.59±0.03^{a}
T4 - D9	54.79±0.22^{d}	14.27±0.54^{b}	13.60±0.02^{a}

Data are presented as mean values (n = 3) and data that do not share a lowercase superscripted letter in the same column and within the same subsection are significantly different ($p < 0.05$).
* Control, 15% textured vegetable protein (w/w); T-3, 40% fat emulsion (w/w); T-1, 35% textured vegetable protein; (d) T-2, 15% pea protein (w/w); T-4, 17.5% fava bean protein (w/w)

Further, **Fig. 4.1** and prior research findings (Bakhsh, Lee, Lee, Hwang, et al., 2021)(Sakai et al., 2022a), confirmed the color values and visual similarity between the prepared PB formulations, commercial PB, and beef patty. There was a tendency for the color (L^*, a^*, b^*) to degrade with the storage days for all treatments. The overall color seems to be much unstable, with no linear increase or decrease with storage days. However, in the control formulation, T2, and T3, L^* and a^* decreased ($p < 0.05$), indicating a darker color with reduced redness. Further, these patterns were consistent with the previous observations for meat products (Hernández Salueña et al., 2019)(Chaudhry et al., 2021). The b^* value exhibited an increase in all treatments and this observation was in good agreement with the results of (C.-H. Feng & Makino, 2020). Despite the irregular trend with L^* in certain cases, the differences between D1 and D9 of all treatments were significant ($p < 0.05$). Overall, the results confirmed the rationality of complex correlations and represent minimum variability between treatments i.e., the effect of each ingredient on PB color is unclear, and maximum variability with storage days, i.e., degradation of color irrespective of treatment. Moreover, it should be noted that even though the fat marbling in T3 samples is higher due to 40% FE, the color values of T3 samples coincide with other treatments. This indicates that averaging the color scores obtained from single-point colorimeters neglects the effect of the non-uniform distribution of fat marbling. This outcome justifies the requirement for chemical mapping to ensure the color distribution of meat alternatives.

4.4.2 An overview of spectral characteristics of PB samples

The average raw and pre-processed spectra for PB with different treatments for wavelengths of 400–1000 nm is presented in **Fig. 4.2.** The variation in the type and amount of major chemical constituents, such as protein matrix, fat, and moisture, among different treatments caused changes in internal absorption and scattering properties, resulting in distinct reflectance magnitude (Zhang et al., 2022). While all raw spectra exhibited a similar trend **Fig. 4.2a**, sample-to-sample variations, noise, and baseline drift still existed, which were minimized through spectral preprocessing optimization. **Fig. 4.2b**, presents the results obtained after applying the SG-FD treatment to spectra. In the 420-600 nm range, spectral reflectance increased rapidly, featuring a prominent valley near 540 nm and a weaker one near 480 nm **Fig. 4.2b**. Between 600-1000 nm, spectral reflectance displayed a sharp peak at 600 nm, distinct reflection valleys near 680, 820, and 930-950 nm, and a weaker slope at 705 nm. These wavelengths correspond to vibrational and

combination overtones of C-H, O-H, and N-H bonds, which are essential structural elements in organic molecules.

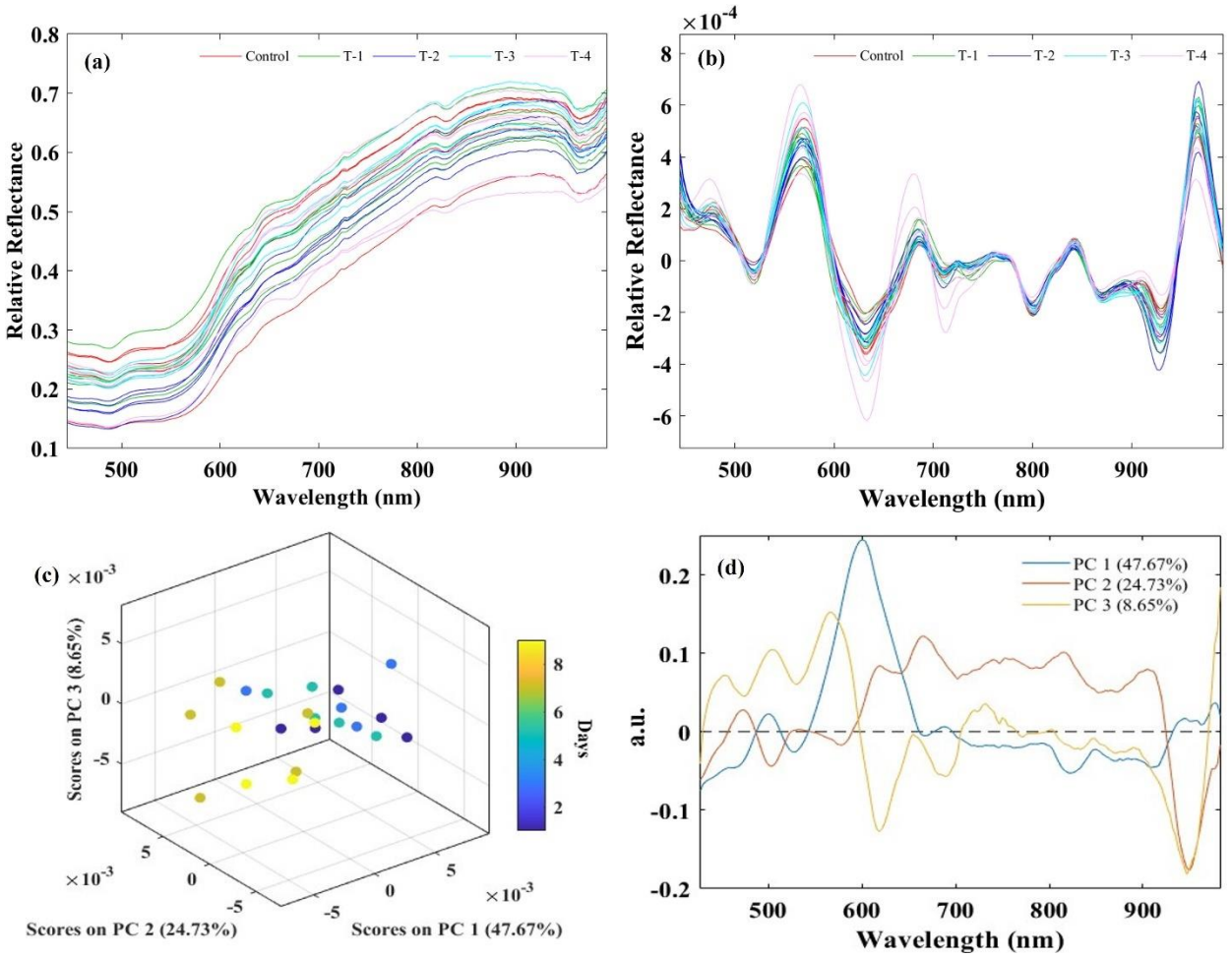

Figure 4.2 Spectral profiling of plant-based meat burgers in the VNIR range – (a) mean spectra and (b) Sav-Gol-SD pre-processed spectra of PB samples from 5 treatments; (c) PCA score plot and (d) loading plot for pre-processed meant spectra. *Sav-Gol-SD, second derivative; PCA, Principal Component Analysis

The PCA score plot **Fig. 4.2c** showed clear and distinctive spatial separation of fresh and stored samples in the VNIR range, with an overlapping of D5 and D7 samples observed. However, **Table 4.1** depicts that there was no significant change in the color scores for D5 and D7 for all treatments except T2. (Zhang et al., 2022) reported that PCA constructed from HSI-VNIR data of lamb samples revealed a notable overlap between fresh and sub-fresh lamb samples. The PC loadings were plotted in **Fig. 4.2d**, and the significant wavelengths were identified as 480, 500, 540, 600,

680, 820, and 950 nm. Existing literature on meat products (ElMasry et al., 2012)(Chaudhry et al., 2021)(Zhang et al., 2022)(L. Cheng et al., 2020), suggests that reflectance at 490 nm is linked to metmyoglobin, while 550 nm is associated with oxymyoglobin. According to (ElMasry et al. 2007), the 650 and 680 nm region represents anthocyanin and other pigments responsible for fruit color, while the spectral bands at 690–710 nm correspond to the total chlorophyll bands (Siedliska et al., 2018).

PCA loading plot highlighted wavebands responsible for the significant variances in the VNIR spectral data related to color changes in PB samples. The identified absorption bands around 450, 475, 500-650 nm **(Fig. 4.2d)** are attributed to derivatives of beet pigment (betalains), specifically betacyanins and betaxanthin (Sakai et al., 2022a). Changes in moisture and pH during PB storage impact the oxidation state of betalains group, altering their chemical structure, stability, and solubility (Esatbeyoglu et al., 2015). These alterations in betacyanins causes the absorption peaks among the PB samples to vary from 535 to 580 nm and the change of betacyanins state causes the absorption peaks among the PB samples to vary from 420 to 480 nm. The loading plot effectively captured these variations, emphasizing the importance of these wavelengths **(Fig. 4.2d)**. While other residual pigments from plant-derived ingredients that are less dominant than betalains in determining PB redness, may have contributed to the captured reflectance valleys.

The reflectance band around 960 nm is associated with the third overtone O-H stretching of water. Similar water absorption peaks at 962 nm were reported for beef (ElMasry et al., 2012) and bison (Chaudhry et al., 2021). Sierra et al. (2008) and De Marchi et al. (De Marchi et al. 2013) have reported that the spectral peaks at 934–960 nm and 984–996 nm are related to moisture. (Lambe et al., 2021) reported that the 930–950 nm corresponds to third overtone of C-H stretch, which is associated with the fat content. Thus, the variance captured in these wavelengths can be related to the changes in quantity, and location of water over the surface of PB samples that mark the freshness during storage. Further, according to (Gitelson et al. 2006), strong carbohydrate absorbance bands exist at 705 nm and 920 nm. The 995 nm band signifies the second vibration of NH bonds in proteins or amino acids (Seo et al., 2021). Additionally, the peak at 842 nm corresponds to the O-H stretching vibration of sugar (Baiano et al., 2012), and the mild peak at 790 nm is associated with the combination of the aromatic C-H and C=C stretching vibrations (Siedliska et al., 2018).

Based on the obtained results and reported literatures, it's conclusive that, the PB samples mimic the physical/color properties of meat while retaining the chemical/reflection/absorption characteristics associated with pigments (residual/related) of plant-derived ingredients. To definitively identify the exact compound or factor associated with the spectral shifts or valleys, absorption or reflection characteristics of individual components and mixtures at the specific wavelength of interest need to be studied. However, the spectral information of PBs in the VNIR range is a novel finding, and their distinct variation with different treatments and storage periods highlights their potential for establishing prediction models.

4.4.3 Full wavelength PLSR modeling for color prediction

PCA analysis revealed that the separation of PB samples was primarily due to the loss of reddish color resulting from the oxidation of beet pigments during storage **(Fig. 4.2c)**. Further, the loading plot **(Fig. 4.2d),** reveals prominent peaks in the wavelength range of 500-690 nm, signifying that pigments that are linked to PB redness (a^*) and yellowness (b^*) as significant factors contributing to the unsupervised classification. Therefore, PLSR models were developed using 204 variables (400-1000 nm) to establish correlations between spectral characteristics and a^*, b^*, and L^* values using the entire spectral data set, including all treatments and storage days. The report by (Mishra et al., 2022) indicated that the establishment of global models, rather than separate models for each treatment/variety, resulted in enhanced generalized solutions by acquiring additional insights into the unique chemical overtones specific to each sample variety. **Table 4.2** summarizes the performance of models for predicting L^*, a^*, and b^* using seven pre-processing techniques with the PLSR.

Most L^* prediction models showed appreciable prediction accuracy with R^2 of less than 0.85 and RMSE of >1 units. Scaling the spectral data in the calibration set using mean centering improved the R^2_C from 0.751 (raw) to 0.818. The improvement can be attributed to the effect of removing the constant offset in the data i.e., mitigating the impact of intensity variations caused by factors such as variations in sample presentation, or changes in measurement conditions. While SNV and MSC showed comparable performances with relatively lower R^2_P of 0.776 and 0.758 respectively. Despite the variance reduction, residual noise and unaccounted variations might still be influencing the predictive accuracy of these models, resulting in moderately lower R^2_P values. The lower performance of MSC could also be linked to the difficulty of identifying non-relevant baseline regions in VNIR spectra as reference spectrum (**Eqn. 4.2**).

Table 4.2 Comparison of the performance of prediction models based on full wavelengths.

Parameter	Modelling	Preprocessing		Calibration		Cross-validation		Prediction		LV
		Function	Method	R^2_C	RMSEC	R^2_{CV}	RMSECV	R^2_P	RMSEP	
*L**	PLSR	-	Raw	0.751	1.333	0.728	1.393	0.758	1.339	4
		Filtering	Sav-Gol-FD	0.849	1.038	0.827	1.112	0.854	1.038	5
			Sav-Gol-SD	0.874	0.949	0.843	1.058	0.869	0.983	5
			Smoothing	0.740	1.360	0.719	1.416	0.753	1.353	4
		Normalization	SNV	0.785	1.236	0.767	1.290	0.776	1.286	5
			MSC	0.769	1.282	0.744	1.352	0.758	1.337	4
		Scaling	MC	0.818	1.140	0.779	1.196	0.809	1.188	5
		Combination	**MC + Sav-Gol-FD**	**0.882**	**0.915**	**0.865**	**0.980**	**0.880**	**0.941**	**5**
*a**	PLSR	-	Raw	0.576	0.767	0.547	0.793	0.567	0.800	4
		Filtering	Sav-Gol-FD	0.748	0.59	0.706	0.639	0.744	0.615	6
			Sav-Gol-SD	**0.984**	**0.150**	**0.977**	**0.179**	**0.984**	**0.154**	**7**
			Smoothing	0.565	0.777	0.537	0.801	0.554	0.811	4
		Normalization	SNV	0.840	0.471	0.800	0.527	0.839	0.487	8
			MSC	0.790	0.539	0.739	0.602	0.790	0.557	7
		Scaling	MC	0.587	0.757	0.557	0.784	0.578	0.790	4
		Combination	MC + Sav-Gol-FD	0.814	0.516	0.780	0.552	0.821	0.516	7

b*	**PLSR**	**-**	Raw	0.794	0.613	0.767	0.652	0.768	0.575	4
		Filtering	Sav-Gol-FD	0.938	0.336	0.925	0.336	0.917	0.340	8
			Sav-Gol-SD	**0.948**	**0.307**	**0.934**	**0.346**	**0.929**	**0.314**	**7**
			Smoothing	0.850	0.523	0.827	0.562	0.799	0.529	4
		Normalization	SNV	0.796	0.610	0.774	0.642	0.723	0.624	4
			MSC	0.796	0.610	0.774	0.643	0.723	0.624	4
		Scaling	Mean Center	0.811	0.588	0.787	0.623	0.762	0.579	4
		Combination	MC + Sav-Gol-FD	0.860	0.506	0.845	0.532	0.813	0.512	4
			MC + Sav-Gol-SD	0.942	0.325	0.925	0.370	0.920	0.335	6

Sav-Gol-FD = first derivative, Sav-Gol-SD = second derivative, SNV = standard normal variate, MSC = multiplicative scatter correction, MC= mean centering, LV = latent variables, R2 = coefficients of determination, RMSE = root mean square errors (shares the unit of the respective color parameters, which are dimensionless)

The use of the entire spectrum as a reference, might introduce variations and correlations (Stark et al., 2017), that are chemically significant for the prediction of *L** values in PB samples. In contrast, the PLSR model on spectra treated with SG-SD showed relatively higher prediction R^2_P of 0.87 and RMSEP of 0.98, as the differentiation process in SG-SD enhances fine spectral features and patterns, bypassing the challenge of selecting a reference region for correction (Rinnan et al., 2009). The combination of SG-FD with MC was considered to as the best model for *L**, with R^2_C, R^2_{CV}, and R^2_P of 0.882, 0.865, and 0.880, while RMSEC, RMSECV, and RMSEP of 0.91, 0.98 and 0.94, respectively. The observed improvement in the combined model can be attributed to MC, as it reduces multicollinearity by focusing on the variations around the mean and aligns the data with the assumptions of the regression technique. The lightness prediction for PB using VNIR HSI in the full wavelength range was lower in comparison with other meat products. (Feng and Makino 2020) reported R^2_P = 0.96, RMSEP = 1.08 for sausage using SG-FD. (ElMasry et al. 2012) reported R^2_{CV} = 0.89, RMSECV = 1.21 for fresh beef. In addition to the surface moisture and absorption due to pigments, the differences in achromatic aspects like microstructures of PB, influence *L** (Purslow et al., 2020). The alteration in light refraction through the porous matrix of plant-based meat analogs, influenced by the concentration and distribution of various plant-derived ingredients contributes to the observed differences in *L** values compared to traditional meat products.

The PLSR model for *a** with raw spectra produced the lowest calibration performance among all tested models, yielding R^2_C and RMSEC values of 0.576 and 0.7, respectively **(Table 4.2)**. Increasing the number of LVs resulted in overfitting, where the model fits noise and irrelevant fluctuations in the training data. This was evident with the increased RMSECV, i.e., a reduction in the model's ability to generalize to new data. In contrast, the derivatives captured more accurate relationships between the spectral patterns and the *a** values, resulting in higher predictive performance, although the effect of SG-FD was relatively limited. The PLSR model with SG-SD was considered the best model with R^2_C, R^2_{CV}, and R^2_P of 0.984, 0.977, and 0.984 while RMSEP was 0.154. The second derivative transformation helped to emphasize fine details in the spectral data while minimizing uninformative variations. Besides, the prediction accuracies were generally improved by SNV (R^2_P: 0.839, RMSEP: 0.487) and MSC (R^2_P: 0.790, RMSEP: 0.487). As reported by (C.-H. Feng & Makino, 2020), MC degraded the model performance by magnifying certain variations around the mean that are not directly related to the *a** values, which disrupts the balance

of spectral information required for accurate predictions. Based on R^2 and RMSE, the findings after respective preprocessing were comparable to (Chaudhry et al. 2021), who reported R^2_{CV} = 0.882, RMSECV = 1.56, and (Hasan et al. 2022) who reported R^2_P = 0.91, RMSEP = 1.34 for *a** prediction of bison muscle using MC treated spectra from full spectral range.For *b**, the PLSR model derived from spectra pre-treated with SG-SD achieved the best results (R^2_C: 0.948, RMSEC: 0.307; R^2_P: 0.929, RMSEP: 0.314) with a small absolute difference between RMSEC and RMSECV (0.039) **(Table 4.2)**. The performance of PLSR models based on MC + SG-SD (R^2_C: 0.942) was nearly equal to SG-SD, but the test set yielded an RMSE of 0.335, indicating an overfitted calibration model. This underscores that the excessive model complexity captured noises and emphasized certain variations that are not relevant to the target *b** values. The predicting ability in this study was comparable with (Feng and Makino 2020), who reported an R^2_{CV} of 0.90 and RMSECV of 1.07 for *b** prediction on SG-SD spectra. These findings suggest that the first and second derivatives or their combination with MC had better performances in eliminating the redundant information in the VNIR range irrelevant to PB color values.

The developed PLSR models hold practical significance due to their ability to predict color values for new PB samples, irrespective of coloring agents that shall be used, as long as the samples fall within the minimum and maximum ranges (L*, a*, b*) that were used to build the prediction models. However, it is essential to note that the generalizability of the models may be affected if the calibration set lacks representative samples for a specific PB product type. In such instances, enhancing prediction accuracy can be achieved by incorporating relevant samples into the calibration sets (Mishra et al., 2022).

4.4.4 Feature wavelength extraction in simplified PLSR models

Due to the impracticality of processing thousands of HSI data points within a short timeframe, certain uncorrelated wavelengths were removed from the full wavelength range of PLSR models to enhance robustness and model simplicity. The feature wavelength selection was automatically determined by selecting wavelengths that have the least RMSECV with the interval added in F-iPLS, with the interval removed in B-iPLS, and iterations in rPLS. In most cases, identical regions are excluded; however, there is some variation in the intervals included. For instance, in the *L** model, intervals from 663-725 and 931-1000 nm were underrepresented in the F-iPLS model but seems to hold significant importance in the B-iPLS model. This variance can be attributed to the earlier elimination of certain regions in the B-iPLS process, which resulted in these intervals being

the sole source of some information. In contrast, the F-iPLS models discovered that a different combination of intervals could achieve a better RMSECV = 0.608 by discarding these intervals.

A summary of extracted feature wavelength models with prediction accuracies and model performance is listed in **Table 4.3**. The results of the simplified model in terms of R^2_C and RMSEP were heavily improved for all the color parameters. The B-iPLS model yielded the best results for predicting *a** values with high R^2 values indicating that the model captures a high degree of variation in the *a** values. By starting with the full set of wavelengths and iteratively removing the least informative ones, B-iPLS has ensured that only the most relevant features are retained **(Table 4.3)**. The low RMSEC (0.09), RMSECV (0.116), and RMSEP (0.096) values indicate that the model's predictions are close to the actual *a** values and generalize well to new data. In alignment with our findings, a study on meat classification based on freshness (Zhang et al., 2022), demonstrated the effectiveness of the B-iPLS approach in selecting relevant features. Further, the iterative elimination process in B-iPLS has prevented overfitting, which was noted with F-iPLS. The lower results observed in the rPLS model suggest that its approach of recursively eliminating variables might not have effectively captured the underlying spectral features relevant for predicting *a** values. The iterative updating process in rPLS might introduce noise, and the risk of omitting important wavelengths early in the iteration might result in instability and reduced model performance (Rinnan et al., 2014). On a similar note, feature selection based on iPLS has improved *a** prediction accuracies in beef (Hasan et al., 2022). Further, the *b** predictive ability using B-iPLS and F-iPLS models have similar predictive performance, achieving relatively high R^2_C, R^2_{CV}, and R^2_P values **(Table 4.3)**. The rPLS model, however, demonstrates lower results in terms of R^2 values, as well as higher RMSECV and RMSEP values.

The higher results observed in the GAs model highlight its effectiveness in selecting the optimal subset of wavelengths for predicting *L** values **(Table 4.3)**. The GAs iteratively refine the subset of wavelengths over multiple generations, converging towards a solution (both possible optimal and near-optimal subsets) that maximizes predictive accuracy (Jarvis & Goodacre, 2004). However, they tend to be extremely slow compared to the B-iPLS, F-iPLS, and rPLS and present a tremendous configuration challenge because of the numerous adjustable factors that affect the outcome of GAs. In contrast to full spectral PLSR models, the simplified PLSR models in predicting *a** (R^2_C = 0.75, RMSEC = 1.18), *L** (R^2_C = 0.63, RMSEC = 3.59) by (C.-H. Feng & Makino, 2020) and *a** (R^2_C = 0.75, RMSEC = 1.18), *L** (R^2_C = 0.63, RMSEC = 3.59) by (ElMasry

et al., 2012) were lower. The studies used weighted regression coefficients to extract the feature wavelengths which assigns weights to each wavelength based on how well it correlates with the target. This approach might not capture complex non-linear relationships i.e., present in spectral data of PB samples where the signals from different chemical components are strongly overlapping and correlated which could lead to missing important information when predicting color attributes. Thus, the result from the current study explores the feasibility of robust, advanced, and automated optimization-driven techniques that consider the interactions or combined effects of multiple wavelengths. While the VNIR-HSI studies by (Yuan et al., 2020) on metymyoglobin in cooked tan mutton and (L. Cheng et al., 2020) on myoglobins in fresh tan mutton, highlight the necessity for future research to explore comprehensive techniques, including successive projection algorithm, uninformative variable elimination, competitive adaptive reweighted sampling, interval random frog, and interval variable iterative space shrinkage for optimizing PB spectral profiles.The most obvious wavebands of the optimal models as mentioned in **Table 4.3**, contain the wavelengths that were also responsible for distinguishing PB samples in PCA based on freshness. As mentioned earlier, these bands within the visible region predominantly corresponded to the pigments accountable for the color of PB. Conversely, the peaks in the NIR range primarily originate from the overtones and combinations of O-H, C-H, and N-H. Summarily, the improved performance from fewer wavelengths suggested the potential of optimized simplified models for a fast, robust, and in-line estimation of color values of PB with less computational resource requirement. The simplified models with selected wavelengths were regarded as the optimized model to be used for the subsequent process of visualization of pixel-by-pixel prediction.

Table 4.3 Comparison of the performance of simplified prediction models based on feature wavelengths.

Parameters	Preprocessing	Variable selection and Feature Wavelengths (nm)	Calibration		CV		Prediction	
			R^2_C	RMSEC	R^2_{CV}	RMSECV	R^2_P	RMSEP
L*	**MC + Sav-Gol-FD**	Full Wavelength [400-1000]	0.882	0.915	0.865	0.980	0.880	0.941
		Forward iPLS [427-513,546-573, 606-663, 725-872, 905-931]	0.954	0.572	0.948	0.608	0.952	0.597
		Reverse iPLS [427-513, 546-573, 606-752, 785-872, 905-988]	0.947	0.612	0.935	0.628	0.948	0.619
		rPLS [424-430, 471, 477-531, 561-567, 600-609, 630-369, 687-701, 752, 794-830, 863-940, 958-976, 988]	0.937	0.667	0.922	0.743	0.936	0.689
		Genetic Algorithm [504-555, 639-663, 719-743, 773-797, 827-851, 908- 931]	**0.963**	**0.514**	**0.953**	**0.581**	**0.968**	**0.493**
a*	**Sav-Gol-SD**	PLSR-Full Wavelength [400-1000]	0.984	0.150	0.977	0.179	0.984	0.154
		Forward iPLS [427-555, 612-663, 719- 770, 827-982]	0.987	0.133	0.984	0.147	0.987	0.133
		Reverse iPLS [442-483, 531-573, 710-797, 845-982]	**0.993**	**0.09**	**0.990**	**0.116**	**0.993**	**0.096**
		rPLS [427-442, 463-471, 579-582, 588-600, 636-645, 678-687, 749-755, 848, 878, 887-902, 931-937, 958-964, 970-982]	0.980	0.166	0.976	0.182	0.980	0.166
		Genetic Algorithm [427-468, 516-558, 606-648, 740-782, 875-916, 964-982]	0.945	0.27	0.933	0.306	0.945	0.275

		PLSR-Full Wavelength [400-1000]	**0.948**	**0.307**	**0.934**	**0.346**	**0.929**	**0.314**
		Forward iPLS [457-513, 755-782, 845-961]	0.968	0.242	0.955	0.287	0.960	0.235
b*	**Sav-Gol-SD**	**Reverse iPLS [436-471, 552-588, 630-666, 707-821, 863-982]**	**0.972**	**0.226**	**0.967**	**0.238**	**0.959**	**0.238**
		rPLS [427, 543-549, 582-591, 633-645, 698, 743-746, 881-884, 916-919, 943, 961, 967, 979-982]	0.938	0.337	0.930	0.358	0.913	0.347
		Genetic Algorithm [439-513, 561-603, 740-782, 830-961]	0.958	0.315	0.946	0.315	0.941	0.284

Sav-Gol-FD = first derivative, Sav-Gol-SD = second derivative, MC= mean centering, LV = latent variables, R^2 = coefficients of determination, RMSE = root mean square errors (shares the unit of the respective color parameters, which are dimensionless)

4.4.5 Exploration of PCA Score Surface Images

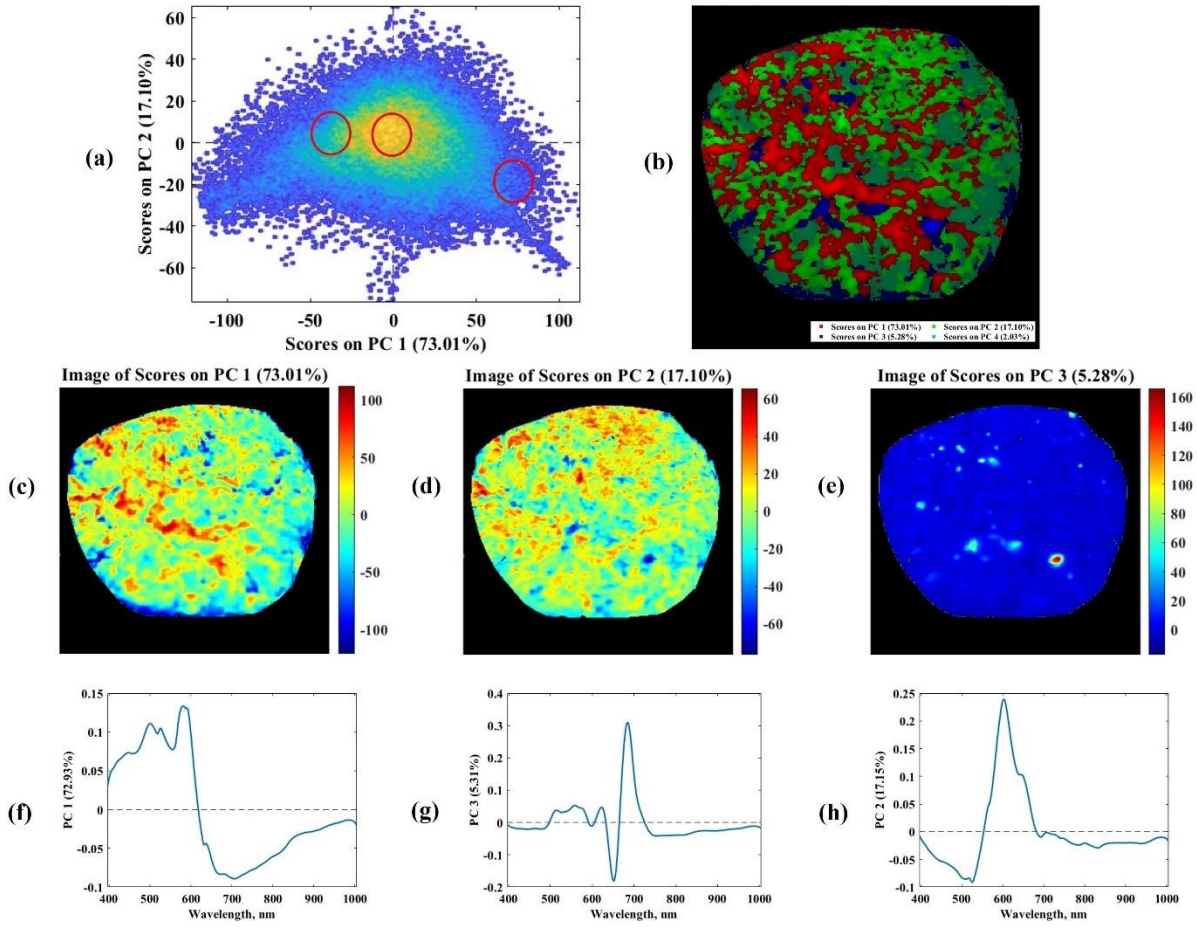

Figure 4.3 Principal Component Analysis carried out on hypercube image of Control PB sample – (a) PCA score plot of PC1 versus PC2 for all pixels in the hypercube image, (b) false color RGB image with scores of PC1-PC4 concinnated, (c-e) score-surfaces, and (f-h) loading plots. *Control, 15% textured vegetable protein (w/w)

PCA was used to identify key factors of variability and analyze the spatial distribution of constituents in a single image qualitatively. In **Fig. 4.3**, the distribution of chemical compounds and physical artifacts across the surface of a Control-D1 PB sample has been illustrated. PC1-PC3 accounted for over 95% of the variance. As observed in **Fig. 4.3(c-e)**, each score map corresponds to a distinct surface feature, as evidenced by the varying color in scale reflecting different sections of the PB sample in the different PCs. The loading vectors shown in **Fig. 4.3(f-h)** represent the key spectral bands associated with these changes in features of the PB sample. Based on the typical

wavebands discussed in **(Section 4.3.2., Chapter 4)**, the first PC primarily reflects the surface's yellowness and lightness, majorly concentrated on the left side. The second PC emphasizes the presence of redness distributed throughout the entire surface. The third PC is more difficult to assign, resulting from a combination of factors involving intense red spots and pores that formed due to shearing during blending.

Fig. 4.3a illustrates a 2-dimensional (2D) scatter plot of PC1 and PC2 scores, where each pixel in the entire image is represented. This plot shows that pixels with similar spectral characteristics are positioned in the same region of the PC space. **Fig. 4.3b** presents a false color red-green-blue (RGB) mapping, obtained by refolding the scores of these pixels into a 2D form so that each image pixel is assigned R, G, and B channel intensities based on their respective PC scores 1-3. This resulted in pixels with similar spectral signatures displaying matching color intensities. **Fig. 4.3b** highlights the surafce heterogeneity and/or compositional/physiochemical differences within the PB sample surface. These variations are linked to distinct absorption characteristics among regions like the marbling of fat mimic and non-fat portions (protein matrix).

In the context of fresh meat cuts or processed products, areas with comparable physiochemical properties and fiber orientation exhibit similar spectral features, leading to a distinct segmentation between meat constituents. For example, in studies using PCA score images from VNIR-HSI, (Barbin et al. 2012) identified distinctions between the loin eye, fat, and muscles adjacent to the loin eye, while (Kamruzzaman et al. 2011) identified various lamb muscle components. In the case of whole grains, (Williams et al. 2009) distinguished between glassy and floury endosperm in maize kernels. On the contrary, **Fig. 4.3b** illustrates a multitude of spectral feature variations within a single sample. In contrast to well-defined meat sections, these variations caused by the differential interactions of non-fat portions (protein matrix) with light, resulted in numerous segments. This may be attributed to factors including but not limited to hydrated textured protein-beet interactions, non-textured protein interactions with beets, and residual pigments from other plant-derived ingredients. These possibilities of multiple interactions/regions result in variations in physiochemical properties across the regions and non-uniform color distribution. This highlights the assessment of the visual appearance of novel or heterogeneous food formulations using a single-point spectrophotometer may not adequately represent the entire sample. The results obtained through pixel-by-pixel modeling demonstrate that chemical mapping from hyperspectral images when combined with the reflectance characteristics of individual plant-derived components

and mixtures at specific wavelengths of interest, can serve as a crucial tool for representing each portion and studying the interplay of each ingredient's effects in complex food formulations.

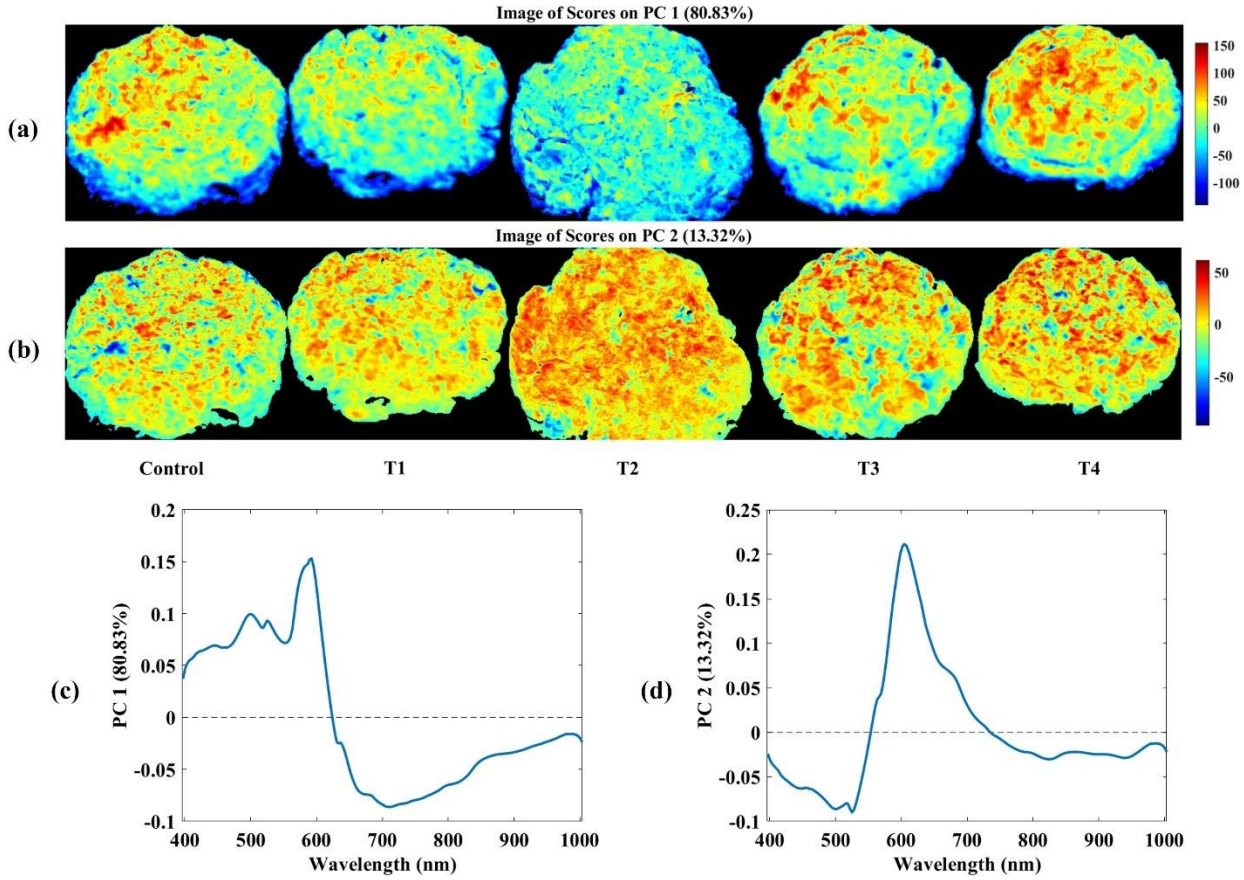

Figure 4.4 Principal Component Analysis carried out on hypercube images of D1-PB samples – (a-b) score-surfaces of PC1 and PC2, and (c-d) corresponding loading plots. *D1-day1

PCA of several samples together visualized both the distribution of various elements within the individual surfaces and the variance between different formulations. **Fig. 4.4.** displays the results for day 1 samples concerning PC1 and PC2. PC1 accounts for approximately 80.83% of the total data variance, while PC2 accounts for around 13.32%. The score surfaces indicate that pixels with higher positive scores on PC1 are associated with PB samples having higher L^* values, specifically the control, T1, and T4 samples **(Table 4.1)**. The corresponding loading profile revealed that the key variables responsible for these differences were concentrated in the spectral range of 480-520 nm and 560-610 nm. The score surface of PC2 was linked to redness, primarily influenced by variables in the spectral range around 600 nm. Pixels displaying higher positive

scores on PC2 are indicative of samples with higher *a** values, specifically T2, T3, and T4 **(Table 4.1)**. The results from PCA provide a qualitative understanding of differences among the five formulations, surface heterogeneity in PB samples, and the basic variance structure of sample data. This information is valuable for constructing regression models aimed at quantifying color parameters on the PB surface.

4.4.6 Visualization of pixel-by-pixel prediction using PLSR

The simplified PLSR models were used for pixel-by-pixel predictions of the PB samples' color. The distribution and concentration of *a** value for T2, and T3 PB samples and ***b**** values for T1, and T4 samples during days 1, 5, and 9 are reported in **Fig. 4.5**. Differences in the surface color distribution of the PBs are readily noticeable. During PB production, the raw ingredients may not mix evenly due to the intense forces applied during blending, leading to non-uniform distribution and the concentration of some ingredients in specific spots. In this context, single-spot colorimetry would fail to account for the complexity and may not represent the whole color of the PB surface. to visually depict this non-uniform distribution. However, it was possible to visualize this non-order distribution of color concentration across various PB formulations. But one important note is that PLSR was carried out for individual images. Therefore, the interpretation of the color values and distribution concerning the individual images should consider the modifications of the ranges in the respective color scales.

The *a** values of the T3-D1 PB sample were higher than the T2-D1 sample, which was consistent with **Table 4.1** ($p < 0.05$). The range of *b** values within the T1-D1 PB sample was roughly comparable to that of the T2-D1 sample. Likewise, no significant difference was observed in their reference measurements, as shown in **Table 4.2**. Similarly, most of the predicted values for other PB samples fell within the anticipated theoretical calibration range. Nonetheless, in specific images, some pixels' predicted values fall outside the calibration range. For instance, in the T3-D9 sample, a few spots on the surface registered negative values, significantly lower than the lower calibration range. Typically, PLSR model calibration is carried out by averaging the spectra of ROI's pixels within an individual sample and repeating this process for all samples. However, during prediction, the analysis is performed on a pixel-by-pixel basis, leading to the observed discrepancies. (Squeo et al. 2022) emphasized that using mean sample spectra for predicting macromolecules in TVP didn't fully account for the variability of individual pixels, leading to extreme predictions in certain images. Similar observations on concentration mapping

in red meat were made by (Chaudhry et al., 2021) who noted that using average spectra to create concentration maps can lead to pixels falling outside the calibration range. Additionally, it could be argued that the *a** value at T1-D9 **(Fig. 4.5)** might appear higher towards the edges, possibly due to shadow effects during the measurement. Despite these irregularities, the results presented here were consistent with several other studies on the estimation of *a** and *b** values in red meats (C.-H. Feng & Makino, 2020)(W. Cheng et al., 2017)(Kamruzzaman et al., 2012).

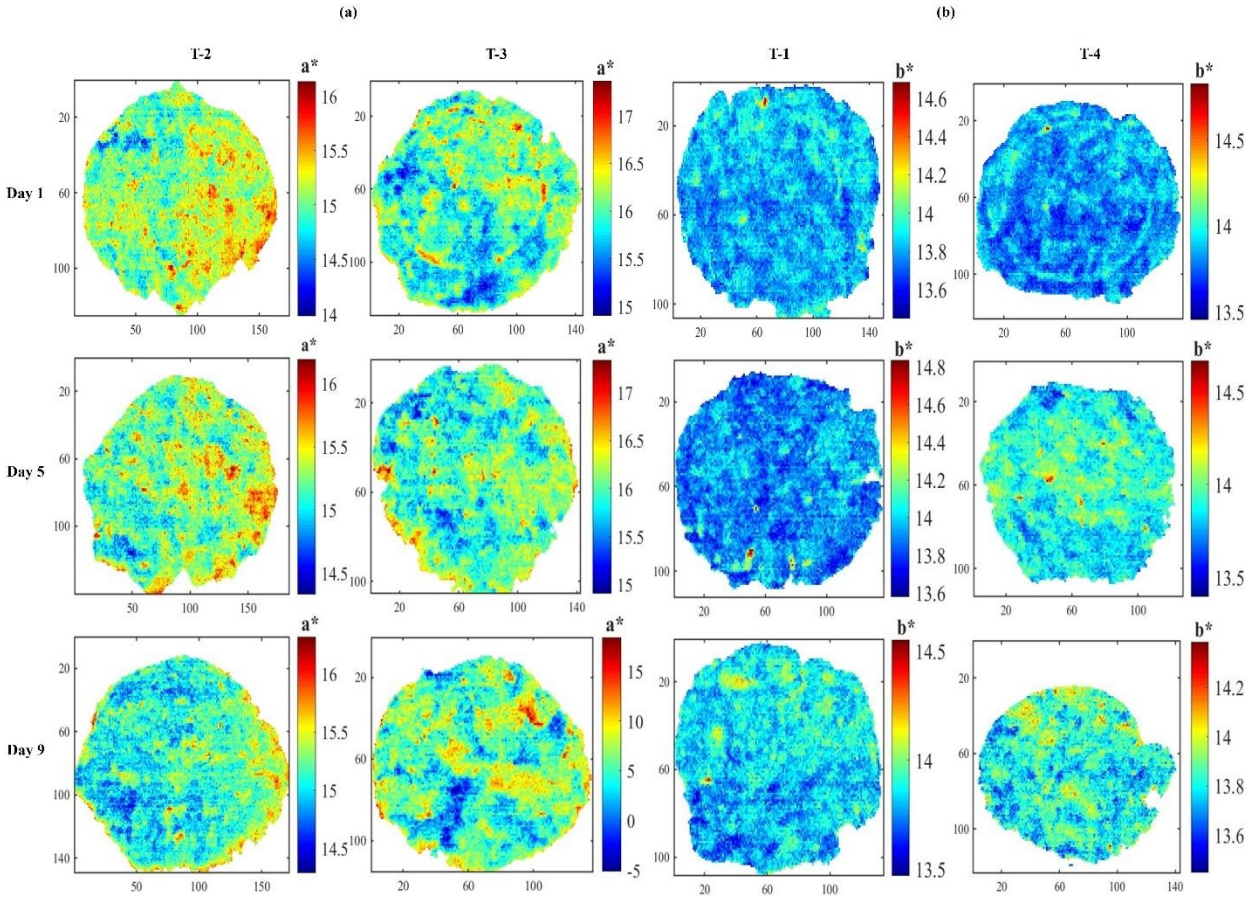

Figure 4.5 Color distribution maps of (a) redness evolution in plant-based meat burgers of T-2 and T-3 treatments, (b) yellowness evolution in plant-based meat burgers of T-1 and T-4 PB treatments. *T-1, 35% textured vegetable protein (w/w); T-2, 15% pea protein (w/w); T-3, 40% fat emulsion (w/w); T-4, 17.5% fava bean protein

Furthermore, the individual prediction images reveal the evolving color changes over storage days, with PB samples from various treatments displaying distinct patterns of color degradation. **Table 4.1** shows a significant reduction in the redness between d1, d5, and d7. The

redness in the central areas of T-2 samples decreased uniformly. T-2 samples were formulated using PP as the primary ingredient, due to its smaller particle size and strong water-binding capacity, which facilitated a uniform distribution of PP throughout the sample. In contrast, the redness in T-3 samples reduced irregularly. This can be attributed to the higher fat marbling in T3 samples, resulting from a 40% FE inclusion in the formulation, which randomly covers most of the surface. Regarding the prediction maps for *b** **(Fig. 4.5b)**, there was an increase in *b** values with storage time observed in both T1 and T4 samples. This trend aligns with the findings in **Table 4.1**, where T-4 displayed a comparatively higher rate of *b** increase. However, these effects could be thoroughly investigated by predicting moisture and other macronutrients on the PB surface using NIR-HSI.

Based on the findings of this study and the insights presented by (Squeo et al. 2022) and (McClements et al. 2021), hyperspectral imaging emerges as a potential option for integration or as a simplified alternative to recent approaches like NMR, cryo-imaging, or X-ray measurements for monitoring the quality of meat alternatives. Considering practical implications, gaining insights into the spatial distribution of color enables more effective monitoring and definition of plant-based meat quality, improves evaluation of new product formulations, and enhances the control and optimization of various processing stages, including mixing. Additionally, it provides valuable insights into post-processing aspects like selecting suitable packaging materials, optimizing storage conditions, and considering cooking characteristics.

4.5 Conclusion

The study reveals that color evaluation of heterogenous plant-based food formulations using single-point colorimeters is insufficient to represent the whole sample. The developed multivariate models using VNIR data from smart-miniaturized hyperspectral imaging device predicted the color changes occurring from pixel to pixel. Key findings include: PCA highlights the effectiveness of 500-650 nm in capturing color variations. Sequential variable selection algorithms improved the prediction accuracies of full wavelength PLSR models in the following order: For a*, B-iPLS (R^2_P = 0.98) > F-iPLS > rPLS > GAs; For b*, B-iPLS (R^2_P = 0.95) > F-iPLS > GAs > rPLS; and for L*, GAs * (R^2_P = 0.96) > F-iPLS > B-iPLS > rPLS. PCA score surface images showed spectral feature variations within single samples, aiding in understanding the physical artifacts and component distribution. PLSR prediction maps show the color deterioration pattern

related to base ingredients. In summary, pixel-by-pixel mapping of plant-based meats enables researchers optimize formulations and comprehend ingredient interactions. Simplified models indicate the potential of low-complexity hyperspectral sensors for real-time quality monitoring; however, in-line image acquisition and prediction need further investigation. Future studies should explore non-linear models to address the spectral data non-linear effects without additional variable selection steps. Crucially, the impact of packaging materials on PB quality, considering O_2 and CO_2 permeability require attentions. Additionally, exploring HSI on packaged PB patties aids in making informed decisions about grading, labeling, and developing real-time shelf-life prediction models.

4.6 References

Ardila, P., A. Honrado, P. Marquina, J.A. Beltrán and J.B. Calanche. 2023. Innovative Plant-Based Burger Enriched with Tenebrio molitor Meal: Characterization and Shelf-Life. Foods (Basel, Switzerland) 12(18). https://doi.org/10.3390/foods12183460.

Baiano, A., C. Terracone, G. Peri and R. Romaniello. 2012. Application of hyperspectral imaging for prediction of physico-chemical and sensory characteristics of table grapes. Computers and Electronics in Agriculture 87: 142–151. https://api.semanticscholar.org/CorpusID:108507206.

Bakhsh, A., E.-Y. Lee, A.M. Bakry, D. Rathnayake, Y.-M. Son, S.-W. Kim, Y.-H. Hwang and S.-T. Joo. 2022. Synergistic effect of lactoferrin and red yeast rice on the quality characteristics of novel plant-based meat analog patties. LWT 171: 114095. https://doi.org/https://doi.org/10.1016/j.lwt.2022.114095.

Bakhsh, A., S.-J. Lee, E.-Y. Lee, Y.-H. Hwang and S.-T. Joo. 2021. Evaluation of Rheological and Sensory Characteristics of Plant-Based Meat Analog with Comparison to Beef and Pork. Food Science of Animal Resources 41(6): 983–996. https://doi.org/10.5851/kosfa.2021.e50.

Barbin, D., G. Elmasry, D.-W. Sun and P. Allen. 2012. Near-infrared hyperspectral imaging for grading and classification of pork. Meat Science 90(1): 259–268. https://doi.org/https://doi.org/10.1016/j.meatsci.2011.07.011.

Botella-Martínez, C., M. Viuda-Martos, J.A. Fernández-López, J.A. Pérez-Alvarez and J. Fernández-López. 2022. Development of plant-based burgers using gelled emulsions as fat source and beetroot juice as colorant: Effects on chemical, physicochemical, appearance and sensory characteristics. LWT 172: 114193. https://doi.org/https://doi.org/10.1016/j.lwt.2022.114193.

Chaudhry, M.M.A., M.M. Hasan, C. Erkinbaev, J. Paliwal, S. Suman and A. Rodas-Gonzalez. 2021. Bison muscle discrimination and color stability prediction using near-infrared hyperspectral imaging. Biosystems Engineering 209: 1–13. https://doi.org/10.1016/j.biosystemseng.2021.06.010.

Cheng, L., G. Liu, J. He, G. Wan, C. Ma, J. Ban and L. Ma. 2020. Non-destructive assessment of the myoglobin content of Tan sheep using hyperspectral imaging. Meat Science 167: 107988. https://doi.org/https://doi.org/10.1016/j.meatsci.2019.107988.

Cheng, W., D.-W. Sun, H. Pu and Q. Wei. 2017. Chemical spoilage extent traceability of two kinds of processed pork meats using one multispectral system developed by hyperspectral imaging combined with effective variable selection methods. Food Chemistry 221: 1989–1996. https://doi.org/https://doi.org/10.1016/j.foodchem.2016.11.093.

Dai, Q., J.-H. Cheng, D.-W. Sun and X.-A. Zeng. 2015. Advances in Feature Selection Methods for Hyperspectral Image Processing in Food Industry Applications: A Review. Critical Reviews in Food Science and Nutrition 55(10): 1368–1382. https://doi.org/10.1080/10408398.2013.871692.

ElMasry, G., D.-W. Sun and P. Allen. 2012. Near-infrared hyperspectral imaging for predicting colour, pH and tenderness of fresh beef. Journal of Food Engineering 110(1): 127–140. https://doi.org/https://doi.org/10.1016/j.jfoodeng.2011.11.028.

ElMasry, G., N. Wang, A. ElSayed and M. Ngadi. 2007. Hyperspectral imaging for nondestructive determination of some quality attributes for strawberry. Journal of Food Engineering 81(1): 98–107. https://doi.org/https://doi.org/10.1016/j.jfoodeng.2006.10.016.

Erkinbaev, C., K. Henderson and J. Paliwal. 2017. Discrimination of gluten-free oats from contaminants using near infrared hyperspectral imaging technique. Food Control 80: 197–203. https://doi.org/https://doi.org/10.1016/j.foodcont.2017.04.036.

Erkinbaev, C., M. Nadimi and J. Paliwal. 2022. A unified heuristic approach to simultaneously detect fusarium and ergot damage in wheat. Measurement: Food 7: 100043. https://doi.org/https://doi.org/10.1016/j.meafoo.2022.100043.

Esatbeyoglu, T., A.E. Wagner, V.B. Schini-Kerth and G. Rimbach. 2015. Betanin--a food colorant with biological activity. Molecular Nutrition & Food Research 59(1): 36–47. https://doi.org/10.1002/mnfr.201400484.

Feng, C.-H. and Y. Makino. 2020. Colour analysis in sausages stuffed in modified casings with different storage days using hyperspectral imaging – A feasibility study. Food Control 111: 107047. https://doi.org/https://doi.org/10.1016/j.foodcont.2019.107047.

Future Market Insights. 2023. Plant-based burger market. https://www.futuremarketinsights.com/reports/plant-based-burger-market (2023 /9/19)

Gitelson, A., G. Keydan, M. Merzlyak and C. Gitelson. 2006. Three-Band Model for Noninvasive Estimation of Chlorophyll Carotenoids and Anthocyanin Contents in Higher Plant Leaves. Geophysical Research Letters - GEOPHYS RES LETT 33. https://doi.org/10.1029/2006GL026457.

Good Food Institute. 2020. Good Food Retail Report: Benchmarking the Top U.S. Retailers on Plant-Based Sales Strategies. GFI. https://www.gfi.org/retail-report (2023 /7/20)

Hasan, M.M., M.M.A. Chaudhry, C. Erkinbaev, J. Paliwal, S.P. Suman and A. Rodas-Gonzalez. 2022. Application of Vis-NIR and SWIR spectroscopy for the segregation of bison muscles based on their color stability. Meat Science 188(February): 108774. https://doi.org/10.1016/j.meatsci.2022.108774.

Hassoun, A., A. Aït-Kaddour, A.M. Abu-Mahfouz, N.B. Rathod, F. Bader, F.J. Barba, A. Biancolillo, J. Cropotova, C.M. Galanakis, A.R. Jambrak, J.M. Lorenzo, I. Måge, F. Ozogul and J. Regenstein. 2023a. The fourth industrial revolution in the food industry—Part I: Industry 4.0 technologies. Critical Reviews in Food Science and Nutrition 63(23): 6547–6563. https://doi.org/10.1080/10408398.2022.2034735.

Hassoun, A., S. Jagtap, G. Garcia-Garcia, H. Trollman, M. Pateiro, J.M. Lorenzo, M. Trif, A.V. Rusu, R.M. Aadil, V. Šimat, J. Cropotova and J.S. Câmara. 2023b. Food quality 4.0: From traditional approaches to digitalized automated analysis. Journal of Food Engineering 337: 111216. https://doi.org/https://doi.org/10.1016/j.jfoodeng.2022.111216.

Hernández Salueña, B., C. Sáenz Gamasa, J.M. Diñeiro Rubial and C. Alberdi Odriozola. 2019. CIELAB color paths during meat shelf life. Meat Science 157: 107889. https://doi.org/10.1016/j.meatsci.2019.107889.

Jarvis, R.M. and R. Goodacre. 2004. Genetic algorithm optimization for pre-processing and variable selection of spectroscopic data. Bioinformatics 21(7): 860–868. https://doi.org/10.1093/bioinformatics/bti102.

Kamruzzaman, M., G. ElMasry, D.-W. Sun and P. Allen. 2011. Application of NIR hyperspectral imaging for discrimination of lamb muscles. Journal of Food Engineering 104(3): 332–340. https://doi.org/https://doi.org/10.1016/j.jfoodeng.2010.12.024.

Kamruzzaman, M., G. ElMasry, D.-W. Sun and P. Allen. 2012. Prediction of some quality attributes of lamb meat using near-infrared hyperspectral imaging and multivariate analysis. Analytica Chimica Acta 714: 57–67. https://doi.org/https://doi.org/10.1016/j.aca.2011.11.037.

Lambe, N.R., N. Clelland, J. Draper, E.M. Smith, J. Yates and L. Bunger. 2021. Prediction of intramuscular fat in lamb by visible and near-infrared spectroscopy in an abattoir environment. Meat Science 171: 108286. https://doi.org/https://doi.org/10.1016/j.meatsci.2020.108286.

Li, J., C. Silver, M.I. Gómez, M. Milstein and G. Sogari. 2023. Factors influencing consumer purchase intent for meat and meat substitutes. Future Foods 7: 100236. https://doi.org/https://doi.org/10.1016/j.fufo.2023.100236.

De Marchi, M., A. Costa, M. Pozza, A. Goi and C.L. Manuelian. 2021. Detailed characterization of plant-based burgers. Scientific Reports 11(1): 2049. https://doi.org/10.1038/s41598-021-81684-9.

De Marchi, M., M. Penasa, A. Cecchinato and G. Bittante. 2013. The relevance of different near infrared technologies and sample treatments for predicting meat quality traits in commercial beef cuts. Meat Science 93(2): 329–335. https://doi.org/https://doi.org/10.1016/j.meatsci.2012.09.013.

McClements, D.J., J. Weiss, A.J. Kinchla, A.A. Nolden and L. Grossmann. 2021. Methods for Testing the Quality Attributes of Plant-Based Foods: Meat- and Processed-Meat Analogs. Foods 10(2). https://doi.org/10.3390/foods10020260.

Mishra, P., M. van Dijk, C. Wintermeyer, C. Sabater, A. Bot, T. Verkleij and J. Broeze. 2022. At-line and inline prediction of droplet size in mayonnaise with near-infrared spectroscopy. Infrared Physics & Technology 123: 104155. https://doi.org/https://doi.org/10.1016/j.infrared.2022.104155.

Mundhada, S., M. Chaudhry, C. Erkinbaev and J. Paliwal. 2022. Non-Destructive Quality Monitoring of Flaxseed During Storage. Journal of Food Measurement and Characterization 16: 1–11. https://doi.org/10.1007/s11694-022-01464-5.

Purslow, P.P., R.D. Warner, F.M. Clarke and J.M. Hughes. 2020. Variations in meat colour due to factors other than myoglobin chemistry; a synthesis of recent findings (invited review). Meat Science 159: 107941. https://doi.org/https://doi.org/10.1016/j.meatsci.2019.107941.

Rinnan, Å., M. Andersson, C. Ridder and S.B. Engelsen. 2014. Recursive weighted partial least squares (rPLS): an efficient variable selection method using PLS. Journal of Chemometrics 28(5): 439–447. https://doi.org/https://doi.org/10.1002/cem.2582.

Rinnan, Å., F. van den Berg and S.B. Engelsen. 2009. Review of the most common pre-processing techniques for near-infrared spectra. TrAC Trends in Analytical Chemistry 28(10): 1201–1222. https://doi.org/https://doi.org/10.1016/j.trac.2009.07.007.

Ryu, K.K., Y.K. Kang, E.W. Jeong, Y. Baek, K.Y. Lee and H.G. Lee. 2023. Applications of various natural pigments to a plant-based meat analog. LWT 174: 114431. https://doi.org/https://doi.org/10.1016/j.lwt.2023.114431.

Saerens, W., S. Smetana, L. Van Campenhout, V. Lammers and V. Heinz. 2021. Life cycle assessment of burger patties produced with extruded meat substitutes. Journal of Cleaner Production 306: 127177. https://doi.org/https://doi.org/10.1016/j.jclepro.2021.127177.

Sakai, K., Y. Sato, M. Okada and S. Yamaguchi. 2022. Synergistic effects of laccase and pectin on the color changes and functional properties of meat analogs containing beet red pigment. Scientific Reports 12(1): 1168. https://doi.org/10.1038/s41598-022-05091-4.

Seo, Y., G. Kim, J. Lim, A. Lee, B. Kim, J. Jang, C. Mo and M.S. Kim. 2021. Non-Destructive Detection Pilot Study of Vegetable Organic Residues Using VNIR Hyperspectral Imaging and Deep Learning Techniques. Sensors 21(9). https://doi.org/10.3390/s21092899.

Siedliska, A., P. Baranowski, M. Zubik, W. Mazurek and B. Sosnowska. 2018. Detection of fungal infections in strawberry fruit by VNIR/SWIR hyperspectral imaging. Postharvest Biology and Technology 139: 115–126. https://doi.org/https://doi.org/10.1016/j.postharvbio.2018.01.018.

Smetana, S., A. Profeta, R. Voigt, C. Kircher and V. Heinz. 2021. Meat substitution in burgers: nutritional scoring, sensorial testing, and Life Cycle Assessment. Future Foods 4: 100042. https://doi.org/https://doi.org/10.1016/j.fufo.2021.100042.

Squeo, G., D. De Angelis, C. Summo, A. Pasqualone, F. Caponio and J.M. Amigo. 2022. Assessment of macronutrients and alpha-galactosides of texturized vegetable proteins by near infrared hyperspectral imaging. Journal of Food Composition and Analysis 108: 104459. https://doi.org/https://doi.org/10.1016/j.jfca.2022.104459.

Stark, E.W., H. Martens, G. Vegen, M. G., Hieftje, T. Hirschfeld, S.H. Åge and Jensen. 2017. Multivariate Linearity Transformations for Near-Infrared Reflectance Spectrometry -. https://api.semanticscholar.org/CorpusID:157062830.

Tóth, A.J., A. Dunay, M. Battay, C.B. Illés, A. Bittsánszky and M. Süth. 2021. Microbial Spoilage of Plant-Based Meat Analogues. Applied Sciences 11(18). https://doi.org/10.3390/app11188309.

Vallikkadan, M.S., L. Dhanapal, S. Dutta, S.K. Sivakamasundari, J.A. Moses and C. Anandharamakrishnan. 2023. Meat Alternatives: Evolution, Structuring Techniques, Trends, and Challenges. Food Engineering Reviews. https://doi.org/10.1007/s12393-023-09332-8.

Vatansever, S., M. Tulbek and M. Riaz. 2020. Low- and High-Moisture Extrusion of Pulse Proteins as Plant-Based Meat Ingredients: A Review. Cereal Foods World 65. https://doi.org/10.1094/CFW-65-4-0038.

Williams, P., P. Geladi, G. Fox and M. Manley. 2009. Maize kernel hardness classification by near infrared (NIR) hyperspectral imaging and multivariate data analysis. Analytica Chimica Acta 653(2): 121–130. https://doi.org/https://doi.org/10.1016/j.aca.2009.09.005.

Yuan, R., G. Liu, J. He, C. Ma, L. Cheng, N. Fan, J. Ban, Y. Li and Y. Sun. 2020. Determination of metmyoglobin in cooked tan mutton using Vis/NIR hyperspectral imaging system. Journal of Food Science 85(5): 1403–1410. https://doi.org/10.1111/1750-3841.15137.

Zhang, J., G. Liu, Y. Li, M. Guo, F. Pu and H. Wang. 2022. Rapid identification of lamb freshness grades using visible and near-infrared spectroscopy (Vis-NIR). Journal of Food Composition and Analysis 111: 104590. https://doi.org/https://doi.org/10.1016/j.jfca.2022.104590.

Zhu, H.-G., H.-Q. Tang, Y.-Q. Cheng, Z.-G. Li and L.-T. Tong. 2021. Potential of preparing meat analogue by functional dry and wet pea (Pisum sativum) protein isolate. LWT 148:

CHAPTER 5

THESIS SUMMARY AND OVERALL CONCLUSION

5.1 General conclusions

This study introduced a completely non-invasive technique using spectral fingerprints to estimate quality parameters and map surface distribution of PBMB patties. ANOVA and PCA results on reference quality measurements revealed variations in quality parameters among TVP-based, PP-based PBMB, and different concentrations. Overall, PBMB quality showed instability, with discoloration and moisture loss becoming prominent after day 8 of storage.

The PCA model clustered samples based on storage days, TVP %, and PP%, highlighting the feasibility of VNIR spectra in qualitatively explaining PBMB characteristics. Changes in reflectance spectra primarily occurred in spectral ranges of 500–650nm (related to beet pigments) and 950–980 nm (third overtone of O-H), indicative of discoloration and moisture loss during storage. While some data points overlapped, ANOVA results showed non-significant differences in quality variables, validating the PCA's accuracy.

Prediction models developed for a*, b*, moisture, and hardness on the full spectral range exhibited good prediction accuracies, supported by low RMSE and high covariance observed in LV and regression plots. The pixel-by-pixel prediction models, employing variables selected via regression coefficients, exhibited lower prediction accuracies, yet showed regions of under/over concentration of the quality parameters. High moisture areas exhibited lower hardness, redness, and higher pH. These results aid in understanding individual ingredient effects. For instance, redness distribution with PP % remained stable compared to TVP-based samples.

Further, B-iPLS and GAs improved color prediction models, accurately depicting color distribution and deterioration patterns. Additionally, PCA on hypercube images identified surface pores or cracks, indicating uneven blending and non-uniform ingredient distribution. These findings challenge the efficiency of single-point colorimeters to represent overall surface color.

Overall, the outcomes of this study emphasize the suitability of HSI for real-time non-invasive quality monitoring and shelf-life predictions of ultra-processed plant-based meat patties. The findings highlight the significance of spectral fingerprinting and chemical mapping in

comprehending the effects of multiple ingredients, optimizing mixing processes, and advancing new product development in complex plant-based meat formulations. Moreover, this study takes a significant step towards enhancing smart sensing technologies for sustainable food systems.

5.2 Future recommendations

- Spectral-based kinetic modeling to predict the real-time shelf-life of packaged meat analogs.
- On-package visualization of quality deterioration through vacuum-packed and retail-packed plant-based meat prototypes using hyperspectral imaging and variable alignment techniques.
- Coupling finite-element analysis with hyperspectral imaging to evaluate the diffusion behavior of beet pigments in plant-based meat patty for 3D space simulation.
- Rapid detection of bulking agents in plant proteins/pulse flours and adulterants in plant-based meat products using hyperspectral imaging
- Monitoring hydration and rehydration dynamics to understand the freeze-thaw stability of high moisture meat analogs through NIR hyperspectral imaging and chemometrics.
- Chemical mapping of high-moisture meat analogs to investigate the effect of extrusion parameters on texturization index.

APPENDIX

Table A Color evaluation of plant-based meat burger patties with 4-treatments and 10-day storage period

Labels	*L**	*a**	*b**
Treatments			
Control – D1	58.11	14.69	11.77
Control – D1	59.21	14.94	11.96
Control – D1	59.2	14.94	11.99
T1 - D1	52.69	14.08	13.03
T1 - D1	53.08	13.91	13.26
T1 - D1	52.22	14.18	13.16
T2 - D1	52	17.64	13.34
T2 - D1	52.14	17.38	13.26
T2 - D1	53.15	18.28	13.75
T3 - D1	59.42	16.06	10.88
T3 - D1	59.1	16.23	10.9
T3 - D1	59.84	16.35	11.02
T4 - D1	61.34	16.38	10.75
T4 - D1	61.28	16.72	10.73
T4 - D1	62.44	16.45	10.99
Samples			
Control – D1	58.11	14.69	11.77
Control – D1	59.21	14.94	11.96
Control – D1	59.2	14.94	11.99
Control – D3	56.25	14.45	12.14
Control – D3	56.2	14.27	12.09
Control – D3	56.22	14.37	12.1
Control – D5	55.22	14.3	12.42
Control – D5	55.55	14.39	13.03
Control – D5	55.66	14.15	13.26
Control – D7	56.36	14.37	13.02
Control – D7	53.31	14.08	13.65
Control – D7	56.41	13.91	13.17
Control – D9	54.41	13.89	14.37
Control – D9	55.06	13.95	14.34
Control – D9	54.74	13.93	14.33
T1 - D1	52.69	14.08	13.03
T1 - D1	53.08	13.91	13.26
T1 - D1	52.22	14.18	13.16

T1 - D3	54.53	13.99	12.79
T1 - D3	54.86	13.92	12.84
T1 - D3	54.97	14.89	12.61
T1 - D5	55.76	13.88	12.89
T1 - D5	56.22	13.89	13.04
T1 - D5	56.3	13.82	13.86
T1 - D7	56.95	13.34	13.63
T1 - D7	56.93	13.26	13.58
T1 - D7	56.93	13.75	13.58
T1 - D9	57.47	13.54	13.62
T1 - D9	57.45	13.54	13.58
T1 - D9	57.46	13.61	13.56
T2 - D1	52	17.64	13.34
T2 - D1	52.14	17.38	13.26
T2 - D1	53.15	18.28	13.75
T2 - D3	54.97	16.47	13.69
T2 - D3	53.44	15.61	13.67
T2 - D3	51.26	15.75	13.92
T2 - D5	52.52	14.73	15.007
T2 - D5	52.81	14.87	14.5
T2 - D5	52.8	15.03	14.4
T2 - D7	49.42	14.69	14.61
T2 - D7	51.11	15.33	15.29
T2 - D7	49.77	15.27	14.91
T2 - D9	55	17.76	15.24
T2 - D9	52.94	16.46	14.69
T2 - D9	53.12	15.42	14.65
T3 - D1	59.42	16.06	10.88
T3 - D1	59.1	16.23	10.9
T3 - D1	59.84	16.35	11.02
T3 - D3	59.17	15.84	11.71
T3 - D3	59.28	15.98	11.71
T3 - D3	59.23	15.85	11.71
T3 - D5	59.39	15.31	12.36
T3 - D5	58.42	15.38	12.33
T3 - D5	58.57	15.47	12.31
T3 - D7	57.57	14.61	12.44
T3 - D7	57.53	14.8	12.43
T3 - D7	57.57	14.72	12.46
T3 - D9	56.84	14.15	12.81
T3 - D9	56.97	14.1	12.66
T3 - D9	57.12	14.07	12.98

T4 - D1	61.34	16.38	13.5
T4 - D1	61.28	16.72	13.5
T4 - D1	62.44	16.45	13.53
T4 - D3	57.47	13.88	12.79
T4 - D3	57.45	13.89	12.84
T4 - D3	57.46	13.82	12.61
T4 - D5	56.95	13.26	12.89
T4 - D5	56.93	13.34	13.04
T4 - D5	56.93	13.26	13.86
T4 - D7	55.76	13.54	13.62
T4 - D7	56.22	13.54	13.58
T4 - D7	56.3	13.61	13.56
T4 - D9	54.53	13.99	13.63
T4 - D9	54.86	13.92	13.58
T4 - D9	54.97	14.89	13.58

Control, 15% textured vegetable protein (w/w); T-3, 40% fat emulsion (w/w); T-1, 35% textured vegetable protein; (d) T-2, 15% pea protein (w/w); T-4, 17.5% fava bean protein (w/w)

Table B Effect of different protein type and concentration on the quality traits of plant-based meat burgers on Day 1

Ingredient	*L**	*a**	*b**	*ΔE*	pH	Cohesiveness (N)	Hardness (N)	Stringiness (mm)
TVP 15%	61.34	16.38	10.75	-	6.41	-0.44068	15.28214	-32.6408
TVP 15%	61.28	16.72	10.73	-	6.4	-0.51618	9.0628	-33.3667
TVP 15%	62.44	16.45	10.99	-	6.38	-1.66149	8.2301	-32.8427
TVP 20%	59.42	16.06	10.88	1.95082	6.42	-0.24353	15.1589	-33.0708
TVP 20%	59.1	16.23	10.9	2.25002	6.42	-0.37031	8.27878	-33.5266
TVP 20%	59.84	16.35	11.02	1.5244	6.43	-0.27236	2.16966	-33.372
TVP 25%	58.11	14.69	11.77	3.78542	6.54	-0.30594	11.04355	-33.3772
TVP 25%	59.21	14.94	11.96	2.84158	6.53	-0.3171	7.82984	-33.3772
TVP 25%	59.2	14.94	11.99	2.86196	6.54	-1.92603	7.54208	-32.9752
TVP 30%	56.25	14.45	12.32	5.6655	6.57	-0.44061	7.86196	-36.9087
TVP 30%	56.2	14.27	12.55	5.84052	6.56	-0.44061	7.86196	-36.9087
TVP 30%	56.22	14.37	12.42	5.74834	6.54	-0.44061	7.86196	-36.9087
TVP 35%	52.69	14.08	13.03	9.23639	6.64	-0.35172	8.24481	-31.5865
TVP 35%	53.08	13.91	13.26	8.97934	6.66	-0.40695	7.29999	-32.0663
TVP 35%	52.22	14.18	13.16	9.6862	6.64	-0.43807	17.17545	-32.0663
PP 5%	45.71	14	15.01	-	6	-4.38881	18.42697	-120.965
PP 5%	47.1	15.36	15.27	-	5.96	-4.97233	13.60688	-120.965
PP 5%	45.84	15.94	15.84	-	5.98	-0.30519	13.80697	-119.468
PP 7.5%	49.06	15.46	15.44	3.67954	6	-1.45835	15.28146	-72.1075
PP 7.5%	49.21	15.52	15.27	3.82466	5.99	-1.45835	16.59768	-55.8274
PP 7.5%	49.67	16.29	16.11	4.70486	6.02	-0.98538	22.95393	-37.1863
PP 10%	52.42	15.37	14.35	6.88016	6.22	-0.3586	11.40122	-45.0783
PP 10%	49.85	15.75	14.75	4.50219	6.17	-3.92435	10.83421	-45.0783
PP 10%	50.34	15.89	14.76	5.00714	6.16	-2.61191	19.40051	-52.3202
PP 12.5%	50.89	15.09	14.31	5.33952	6.43	-0.37063	9.9046	-68.886

PP 12.5%	50.98	15.51	14.42	5.51372	6.41	-2.99373	12.0947	-68.886
PP 12.5%	51.37	16.07	14.75	6.03225	6.41	-3.09631	11.82244	-68.886
PP 15%	52	17.64	13.34	7.45672	6.53	-0.88864	19.38607	-78.6464
PP 15%	52.14	17.38	13.26	7.47207	6.45	-0.4368	22.86196	-78.6464
PP 15%	53.15	18.28	13.75	8.67523	6.52	-0.4368	22.86196	-78.6464

TVP - textured vegetable protein; PP - pea protein

AUTHOR CONTRIBUTIONS

Chapter 3: The contents of this chapter are reproduced with permission from the self-work of the published article in a peer-reviewed journal.

Dhanapal, L., & Erkinbaev, C. **(2024)**. Portable hyperspectral imaging coupled with multivariate analysis for real-time prediction of plant-based meat analogues quality. Journal of Food Composition and Analysis, 126, 105840. https://doi.org/10.1016/j.jfca.2023.105840.

- **Logesh Dhanapal** (Thesis Author)
  Methodology [Lead], Data collection [Lead], Formal analysis [Lead], Software [Lead], Project administration [Lead], Figures & Tables Preparation [Lead], First draft preparation [Lead], Writing - review & editing [Equal].
- **Chyngyz Erkinbaev**
  Conceptualization [Lead], Supervision [Lead], Funding acquisition [Lead], Resources [Lead], Writing - review & editing [Equal].

Chapter 4: The contents of this chapter are reproduced with permission from the self-work of the published article in a peer-reviewed journal.

Dhanapal, L., & Erkinbaev, C. **(2024)**. Non-invasive characterization of color variation in plant-based meat burgers using portable hyperspectral imaging device and multivariate image analysis. Future Foods, 9, 100293. https://doi.org/10.1016/j.fufo.2023.100293

- **Logesh Dhanapal** (Thesis Author)
  Methodology [Lead], Data collection [Lead], Formal analysis [Lead], Software [Lead], Project administration [Lead], Figures & Tables Preparation [Lead], First draft preparation [Lead], Writing - review & editing [Equal].
- **Chyngyz Erkinbaev**
  Conceptualization [Lead], Supervision [Lead], Funding acquisition [Lead], Resources [Lead], Writing - review & editing [Equal].